Intensity Adaptation in the Cricket Auditory System

D I S S E R T A T I O N

zur Erlangung des akademischen Grades

doctor rerum naturalium (Dr. rer. nat.)
im Fach Biologie

eingereicht an der
Mathematisch-Naturwissenschaftlichen Fakultät I
Humboldt-Universität zu Berlin

von
Dipl.-Biol. Ulrike Ziehm

Präsident der Humboldt-Universität zu Berlin:
Prof. Dr. Jan-Hendrik Olbertz

Dekan der Mathematisch-Naturwissenschaftlichen Fakultät I:
Prof. Dr. Stefan Hecht

Gutachter:
1. Prof. Dr. Jan Benda
2. Prof. Dr. Matthias Hennig
3. Prof. Dr. Jutta Kretzberg

eingereicht am: 18.07.2013
Tag der mündlichen Prüfung: 22.01.2014

Contents

List of Figures

List of Tables

List of Abbreviations

AN1	ascending interneuron 1 (cricket auditory system)
AN2	ascending interneuron 2 (cricket auditory system)
AN	auditory nerve (mammals)
IC	inferior colliculus
LF	low frequency
HF	high frequency
SFA	spike frequency adaptation
pdf	probability density function
$\text{cdf}^{(-1)}$	(inverse) cumulative probability distribution function
STD	standard deviation
RMSE	root mean squared error

1 Introduction

1.1 Sensory systems

All living organisms need to sense environmental parameters to react appropriately to their environment. Animals have developed a large variability of specialized sensory organs and have adapted to almost all thinkable sensory environments.

In spite of the the diversity of sensory modalities and the diverse complexity of nervous systems, the basic steps of sensory processing are always to capture the stimulus energy and translate it into a change of membrane potential. From the membrane potential of sensory receptors, the nervous system has to infer everything the animal needs to know about its environment. The modality of a stimulus – e.g. sound, light, pressure – is encoded by the type of receptor that is stimulated and the central target area, while the signal quality – e.g. the sound frequency, or the wavelength (color) of light – is encoded in the tuning of individual receptors of one type. The intensity of a stimulus is usually reflected in the amplitude of membrane potential deflections and in the frequency of action potentials (spike frequency, firing rate) generated in response to the stimulus (Kandel et al., 2000; Reichert, 2000).

1.2 Intensity coding

The intensity coding scheme of a neuron can be characterized by the intensity response curve of a neuron, i.e. the strength of neural response (e.g. membrane potential or spike frequency) as a function of stimulus intensity. Intensity response curves are typically monotone functions with a flat subthreshold and a flat saturated region flanking the dynamic range, i.e. the range of intensities for which the neural response changes substantially with intensity (fig. 1.1).

The intensity ranges relevant for an animal can span several orders of magnitude. The response range of neurons is limited as firing rates cannot be negative or arbitrarily high, and membrane potentials are limited by the reversal potentials and eventually the number of ion channels available. One phenomenon associated with the need to represent large intensity ranges in limited response ranges is the non-linear (often approximately logarithmic) intensity response characteristics of many sensory neurons (see e.g. Burns and Baylor (2001); Reichert (2000)), a property reflected on the perceptional level (Stevens, 1975; Krueger, 1989).

Because neural responses are limited, an increase in the dynamic range of a neuron will come at the expense of a reduced sensitivity to small intensity differences. High sensitivity to intensity differences is reflected in a large slope of the intensity response curve, that is if the response changes strongly with small changes in intensity (fig. 1.1 B). I n spite of logarithmic response characteristics, the representation of large intensity ranges conflicts with the demand for high intensity discrimination. One of the fundamental challenges in

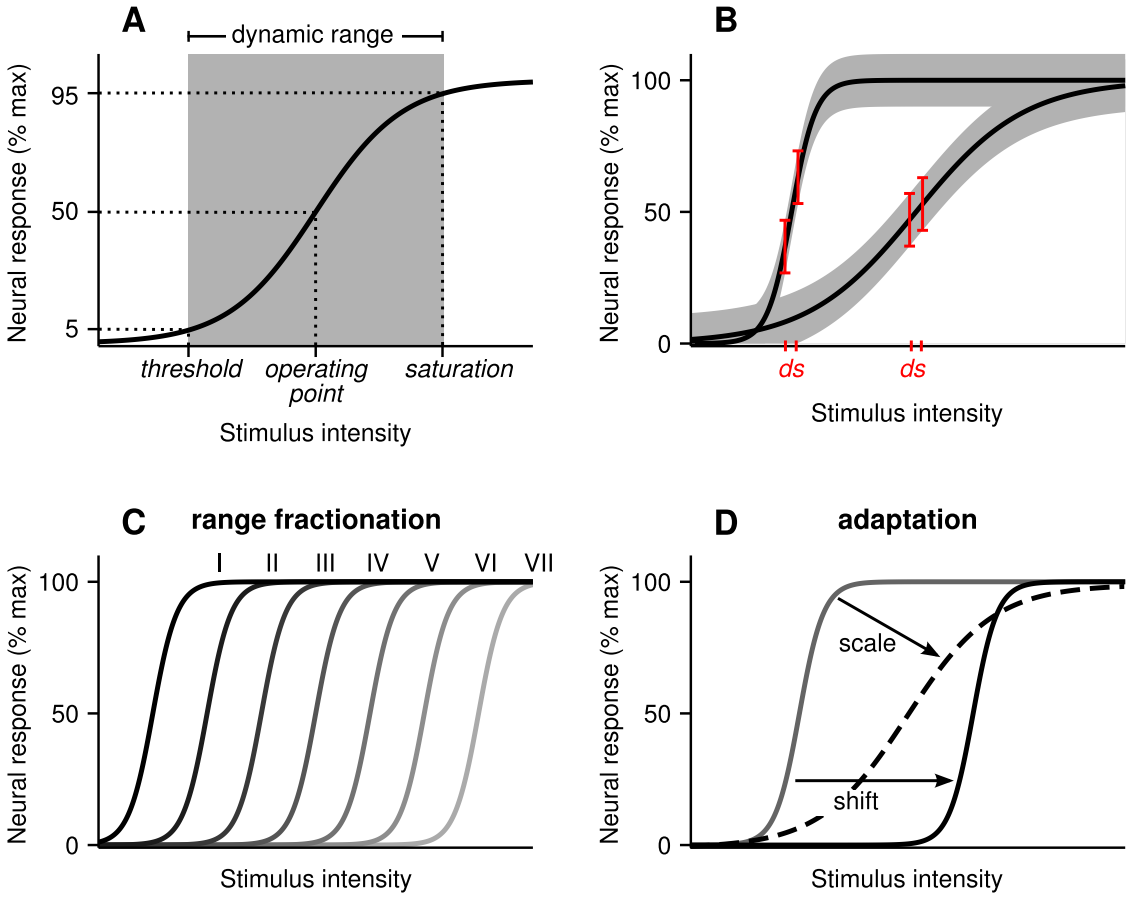

Figure 1.1: Principles of intensity coding. **A** Illustration of basic features of intensity response curves. **B** Illustration of the influence of slope and neural response variability on the discrimination ability of a neuron. The same intensity difference *ds* indicated by red bars on the intensity axis mapped to response difference in a shallow and a steep response curve with identical amount of additive noise. The interval of 2 standard deviations around the mean response is indicated in red for the two respective intensities. The response intervals overlap strongly in the shallow response curve while they are clearly separated in the steep response curve, illustrating the better discrimination performance with steep response curves. **C** Scheme of intensity range fractionation by receptor neurons. **D** Two possible effects of neural adaptation on response curves – scaling and horizontal shift.

intensity coding is therefore to ensure high sensitivity to small intensity differences over a large range of absolute intensities.

In a noise free system with a continuous response variable intensities could be discriminated with arbitrary precision with a shallow response curve, as long as it is strictly monotone. However, neural responses will generally vary between presentations of the same stimulus, and this response variability would inevitably lead to a high amount of misclassifications if the response curve is shallow (fig. 1.1 B). There has been considerable theoretical work on how the optimal response curve should be shaped given the probability distribution of the

stimulus intensity (Laughlin, 1981; McDonnell and Stocks, 2008).

The response variability can be reduced by averaging over the responses of a population of neurons with similar coding properties that converge on higher order neurons. Alternatively, neurons within a population may differ in their response thresholds, each neuron using its full response range to encode a subrange of relevant intensities with high precision (*intensity range fractionation*, e.g. Eckert (2002), fig. 1.1 C). While intensity range fractionation is believed to increase the dynamic range of higher order neurons (e.g. Hennig et al. 2004), it is poorly understood how populations of neurons with stacked response thresholds are integrated along the sensory pathway.

1.3 Neural adaptation

So far, the intensity response curve of a neuron was implicitly regarded as static. However, throughout the nervous system neurons are observed to change their coding schemes if the statistics of the stimulus, e.g. the mean or variance of stimulus intensity, changes. While the total intensity range relevant for the animal might be huge, the variations around a slowly varying mean typically encountered by the animal could be considerably smaller. Exploiting the temporal structure of the stimulus, the nervous system could adapt its coding scheme to match the current stimulus statistics by adjusting its operating point or slope to optimally encode the fast changing stimulus components.

The effect of changes in the stimulus mean on the coding scheme has been assessed for example by studying the intensity response curves constructed from the initial responses to intensity steps after letting the neuron adapt to different background intensities (Laughlin and Hardie, 1978; Benda and Hennig, 2008; Hildebrandt et al., 2011), or to a noise background (Rees and Palmer, 1988; May and Sachs, 1992). Alternatively, response curves were constructed from responses to noise stimuli with different intensity distributions (Dean et al., 2005; Wen et al., 2009). All these response curves represent the input output relation for the fast changing components of the stimulus.

In several sensory systems response functions of neurons were found to shift along the intensity axis with changes in mean intensity, e.g. at various stages in the visual system of vertebrates and invertebrates (Albrecht et al., 1984; Shapley and Enroth-Cugell, 1984; Ohzawa et al., 1982, 1985; Barlow and Földiák, 1989; Carandini and Ferster, 1997; Solomon et al., 2004; Laughlin and Hardie, 1978), in the auditory system of vertebrates and invertebrates (Dean et al., 2005; Benda and Hennig, 2008; Hildebrandt et al., 2011), in the electrosensory system of weakly electric fish (Benda et al., 2005), and in the vertebrate olfactory system (Reisert and Matthews, 1999; Boccaccio et al., 2006). These shifts may result in responses that are invariant with the mean intensity of the respective stimulus (Laughlin, 1989; Benda and Hennig, 2008), that is variations around the mean lead to the same changes in response independent of the actual mean intensity.

Also changes in slope of response curves with changes in stimulus variance have been described for the visual motion sensitive neuron H1 of the blowfly (Borst et al., 2005), yielding responses that are invariant under changes in the stimulus motion variance (Brenner et al., 2000; Fairhall et al., 2001).

Often, what underlies the adaptive effects on response curves observed on some level of sensory processing is poorly understood. A phenomenon generally believed to be associated with the maintenance of sensitivity is spike frequency adaptation (SFA , also referred to as firing rate adaptation). Almost all neurons adapt to sustained stimuli in the sense that the neural response to a constant stimulus is vigorous at onset but decays as the stimulus goes on, eventually settling to a steady state value. SFA has been described for almost all types of neurons, e.g. in hippocampal pyramidal cells (Gustafsson and Wigström, 1981; Madison and Nicoll, 1984; Lanthorn et al., 1984), neocortical neurons (Connors et al., 1982; McCormick et al., 1985), vertebrate motoneurons (Granit et al., 1963; Sawczuk et al., 1995), auditory nerve (AN), cochlear nucleus, inferior colliculus (IC), and auditory cortex of mammals (Westerman, Larry A and Smith, Robert L, 1984; Javel, 1996; Wen et al., 2009; May and Sachs, 1992; Ingham and McAlpine, 2004; Dean et al., 2005; Ulanovsky et al., 2004), auditory receptors and interneurons of locusts and crickets (Benda et al., 2001; Farris et al., 2004; Benda and Hennig, 2008; Hildebrandt et al., 2011) vertebrate photoreceptors, retinal ganglion cells, and visual cortex (Burkhardt, 1994; Schneeweis and Schnapf, 1999; Enroth-Cugell and Shapley, 1973; O'Brien et al., 2004; Mason and Larkman, 1990), motion sensitive neurons of the blowfly visual system (Maddess and Laughlin, 1985), and insect mechanoreceptors (French, 1984, 1989; Juusola and French, 1998; Clague et al., 1997), and many more.

The biophysical mechanisms underlying the change in response to a sustained stimulus are manifold. The accessory structures of a sensory organ might already contribute to the degree of adaptation observed in receptors and higher order neurons, like the iris muscle adjusts the pupil diameter in order to constrict the amount of light entering the eye. The threshold of vertebrate photoreceptors is shifted over a considerable range of background illumination strengths by several calcium dependent modifications of the phototransduction chain (Burns and Baylor, 2001). In mechano-sensory hair cells, transducer adaptation occurs by modification of the mechanical properties of the hair bundle (Hudspeth and Gillespie, 1994; Gillespie and Corey, 1997; Gillespie and Walker, 2001; Holt and Corey, 2000; Eatock, 2000). Neural adaptation will also occur as a result of synaptic depression (Finlayson and Cynader, 1995; Todorov et al., 1997; Chance et al., 1998; Chung et al., 2002; Rothman et al., 2009), or due to inhibitory inputs (Finlayson and Adam, 1997; Ingham and McAlpine, 2005).

Many neurons possess spike driven adaptation currents like calcium dependent potassium currents (Madison and Nicoll, 1984; Lancaster and Adams, 1986; Constanti and Sim, 1987), sodium dependent potassium currents (Schwindt et al., 1989; Sanchez-Vives et al., 2000), voltage dependent potassium currents (Brown and Adams, 1980; Storm, 1990; Weckström et al., 1991; Kang et al., 2000), and inactivation of sodium currents (Fleidervish et al., 1996; Torkkeli et al., 2001). These slow adaptation currents act subtractively on the input current (Benda and Herz, 2003; Benda, 2002), that is they cause a horizontal shift of the neuron's f-I-curve (spike frequency as a function of input current). SFA that shifts f-I-curves along the current axis will be referred as subtractive SFA or subtractive adaptation throughout this thesis independent of the biophysical mechanisms underlying it in order to distinguish it from SFA with different effect on f-I-curves. Subtractive adaptation acts as a high-pass filter (Nelson et al., 1997; French et al., 2001; Benda et al., 2005) that attenuates slow stimulus

components like the mean intensity, yielding a possible mechanism for intensity invariance.

Neural adaptation is generally thought to adjust the neurons coding scheme to the actual sensory environment, and indeed, adaptation has been found to match the highest discrimination ability to the current signal mean (Dean et al., 2005) and to enhance information transmission in sensory networks (Brenner et al., 2000; Fairhall et al., 2001; Sharpee et al., 2006). In the context of intensity coding, neural adaptation provides a means to maintain high sensitivity over large intensity ranges, for example by realizing invariance to the slow changing stimulus components thus saving the full response range for the fast changing fluctuations.

The adaptation observed in an individual neuron will usually result from a combination of adaptation mechanisms in the neuron itself and the network it is part of. Isolating the mechanisms that contribute to the adaptation at a higher stage of neural processing is challenging, because the neurons displaying high degrees of adaptive capacity are typically part of large networks with complex connectivity, and with adaptive mechanisms and nonlinearities at numerous sites.

1.4 The cricket auditory system as a model system

The ascending interneuron 1 (AN1) of the cricket's auditory pathway provides an excellent model system to study intensity coding in general and adaptive properties in particular. The AN1 shows a pattern of adaptive shift with changes in background intensities that is very similar to that observed at intermediate processing levels (inferior colliculus) in the auditory system of mammals (Benda and Hennig, 2008; Dean et al., 2005). It is part of a very simple and well described network, as it gets direct feed forward input from auditory receptors and there is little feedback connectivity (Hill, 1974; Rheinländer et al., 1976; Esch et al., 1980; Schildberger, 1984; Hennig, 1988; Huber et al., 1989; Horseman and Huber, 1994). The AN1 integrates the responses of approximately 30-40 ipsilateral receptors that are tuned to the carrier frequency of the calling songs. That is, the frequency tuning of the receptors converging to the AN1 is relatively homogeneous. Receptors within this subpopulation show an almost textbook like intensity range fractionation. And eventually, the receptors adapt to sustained stimulation (Farris et al., 2004) presumably in a way that acts subtractive on the input, similar to that observed for locust receptors (Benda et al., 2001). Therefore, the AN1 is ideally suited to explore how adaptive shifts and intensity invariance arise in a sensory pathway, and how range fractioning receptor populations with sigmoid response curves may be integrated by higher order neurons.

1.5 Thesis outline

This thesis aims at a better understanding of how populations of sensory neurons with sigmoid intensity response functions are integrated by higher order neurons to give rise to adaptive shifts of response curves.

In chapter 2 a neural network inspired by the cricket AN1 is used to develop different scenarios of how the receptor responses can be integrated to generate adaptive shifts in the

response curves of the output neuron. It turned out that a static saturating non-linearity in the output neuron together with subtractive adaptation in the receptor and output neuron as basic computational elements are sufficient to explain the adaptive shift as it is observed in the AN1 and other sensory neurons. The position of the saturation with respect to the adaptation mechanism in the output neuron affects the shape of adapted response curves in detail. However, the extent of differences between the two models depends on the applied model parameters. With the saturating non-linearity and subtractive adaptation, response curves are shifted towards the background intensity over a range fairly exceeding the original dynamic range, yet the model neurons are not strictly invariant with mean intensity, which is in accordance with the findings of Dean et al. (2005) and Benda and Hennig (2008). Interestingly, seemingly complex pattern of the adaptive shift in mammals and crickets are generated as a consequence of the saturating non-linearity.

The first part of chapter 3 analyses the discrimination performance for the different models and for different stages in the network tracing the stepwise approximation of intensity invariance. The discrimination accuracy is quantified by the Fisher information functions estimated for each response curve. In the models featuring a saturation step the discrimination accuracy is largest around the background intensity with a bias to intensities larger than the background. These models reach comparably high values of Fisher information as a model specifically designed to generate intensity invariant responses.

In the second part of chapter 3 the models' coding accuracy for noise stimuli as a function of stimulus mean and variance is assessed by noise response curves and estimation of the mutual information between firing rate response and stimulus. It is found that adaptation in the receptor layer together with the saturating non-linearity generates a decrease in the slope of the response curves as the stimulus variance increases. Furthermore, for the fluctuating stimuli, response driven adaptation as implemented for the individual neurons in the network, serves as a source of response variability.

In chapter 4 the models from chapter 2 are fitted to experimental data from the AN1 of two cricket species, that show some characteristic differences in the pattern of adaptive shift, and to a the second ascending interneuron (AN2) of one cricket species, which receives input from another receptor population. The models with a combination of adaptation in receptors and output neuron and a static saturation in the output neuron are able to fit the experimental data from both species and both neuron types well. The fitting process revealed that the distribution of receptor thresholds has a key role in shaping the response curves.

2 Shifting Intensity Response Curves in a Convergent Network

The aim of this thesis is to enhance the understanding on the mechanisms and interactions that underlie the emergence of adaptive shifts in sensory neurons that center the response curves at the current background or mean intensity. In the following chapter a model framework is derived which is based on the auditory system of the cricket, in which shifting adaptation and intensity invariance are realized with a minimal number of neurons in a convergent feed forward network.

Acoustic communication in crickets is well explored and the underlying neural circuitry well described. Crickets are sensitive to the carrier frequency and the temporal pattern of acoustic signals (Moiseff et al., 1978; Nolen and Hoy, 1986, 1987; Oldfield, 1980; Pollack and Hoy, 1979; Thorson et al., 1982; Pollack and El-Feghaly, 1993; Ehret et al., 1982; Schildberger, 1984), and show distinct phonotactic behaviour (Moiseff et al., 1978; Oldfield, 1980; Nolen and Hoy, 1986; Schildberger and Hörner, 1988).

Female crickets of the species *Teleogryllus oceanicus* turn towards sound sources that simulated the temporal pattern of the calling songs of conspecific males when the carrier frequency is low (between 3 and 9 kHz, depending on the species), and turn away from the sound source for carrier frequencies in the ultrasound range, demonstrating spectral and temporal sensitivity (Moiseff et al., 1978). Ultrasound signals arouse negative phonotaxis and, at high intensities, an evasive response in males and females of *Gryllus campestris*, *Gryllus bimaculatus*, and *Teleogryllus oceanicus* (Nolen and Hoy, 1986).

The underlying auditory neural circuitry has been shown to be extraordinarily simple, consisting of a small number of neurons, many of which are characterized in detail (e.g. Hill 1974; Esch et al. 1980; Popov and Markovich 1982; Wohlers and Huber 1982; Hennig 1988; Nolen and Hoy 1987). The two behavioural contexts – conspecific communication and predator avoidance – are reflected in the tuning of auditory receptors neurons and preserved on the level of prothoracic ascending interneurons. The majority of auditory receptors (30–40 per ear) have their peak sensitivity at the carrier frequency of calling songs (referred to as low frequency or LF receptors in the following), a smaller fraction is most sensitive to ultrasound frequencies, i.e. associated with the detection of echolocation calls (referred to as HF receptors in the following, Nocke 1972; Imaizumi and Pollack 1999, 2001). While the frequency tuning within a subpopulation is fairly homogeneous, the response thresholds are distributed over an intensity range exceeding the dynamic range width of individual receptors, i.e. they show classic intensity range fractionation (Imaizumi and Pollack, 2001).

The ascending interneurons AN1 and AN2 receive direct input from the respective ipsilateral auditory receptors (Esch et al., 1980; Schildberger, 1984; Hennig, 1988). The AN1 integrates the responses of the LF receptors and is assumed to participate in recognition and

localization of conspecific songs (Hill, 1974; Rheinländer et al., 1976; Wohlers and Huber, 1978, 1982). The AN2 gets input from LF and HF receptors with higher impact of the HF receptors and is considered to mediate predator avoidance via detection and localization of bat echolocation calls (Popov and Markovich, 1982; Moiseff and Konishi, 1983; Nolen and Hoy, 1984, 1987).

The cricket auditory system has received attention in the context of adaptation and intensity invariance (Benda and Hennig, 2008; Benda, 2002). In the cricket species *T. oceanicus* adaptation to a background intensity above threshold shifts the intensity response curves of the AN1 towards the background intensity, and the responses are intensity invariant for mean intensities above 60 dB (Benda and Hennig, 2008). The pattern of the adaptive shift is surprisingly similar to that observed in neurons of the inferior colliculus (IC) in guinea pigs (Dean et al., 2005): response curves are shifted to the right with increasing background or mean intensity over a certain range, however, the shift is accompanied by a reduction in the maximum response, and for large shifts the slope of response curves decreases.

Similarities along the auditory pathways of mammals and crickets are found in spite of overall differences: On low processing levels, the capacity for adaptive shifts of response curves is limited. Auditory nerve fibres in mammals show adaptation and also a shift of response curves with changes in mean intensity, however, they are not able to shift the neurons operating points far enough to match background intensities outside of the original dynamic range (Gibson et al., 1985; Wen et al., 2009). The behaviour of neurons in the cochlear nucleus to adapting background resembles strongly that of auditory nerve fibres in the same animal (Gibson et al., 1985). The same holds for auditory receptors of grasshoppers (Benda et al., 2001), and presumably for those of crickets.

On intermediate processing levels – the prothoracic interneurons in the cricket and IC in mammals – the response curves shift over a range that well exceeds the dynamic range of the unadapted response (Benda and Hennig, 2008; Dean et al., 2005). Schildberger (1984) described a decrease in the dependence of responses on the intensity for increasing processing levels in the cricket, where the responses of brain neurons were almost intensity invariant, reflected in steady state response curves with a slope near zero. Dean et al. (2005) argues that the responses in the IC are not perfectly invariant and that higher degrees of invariance might be found at higher processing levels.

The mechanisms and interactions leading to this stepwise increase in intensity invariance are poorly understood. The parallels between the auditory systems of mammals and crickets may indicate the existence of general computational principles in auditory processing interacting to achieve the adaptive shift of response curves, while the precise biophysical implementation could be different. Finding such basic computational elements and understanding how their interaction might generate adaptive shifts or intensity invariance is the aim of the following chapter.

To this end a convergent feed forward network is used as a basic framework to model scenarios that give rise to adaptive shifts in the output neuron. The organization of the network are motivated by the organization of the cricket AN1 as a specific example.

2.1 Methods

Network Inspired by the AN1 of the cricket the considered neural network is a 2 layer feed forward network, in which a population of 30 receptors converges to a single output neuron. The receptors have identical properties except for their response thresholds. Receptor response thresholds are uniformly distributed in the range of 0 to 100 dB.

2.1.1 Model equations

Receptor Model Individual receptors were modelled in two steps, the first one describing the mechano-electrical transduction of the physical stimulus into a receptor current and the second one describing the resulting firing rate and the adaptation driven by it.

The normalized receptor current I_j of the j$^{\text{th}}$ receptor resulting from stimulus intensity s was modelled as a Boltzmann-function

$$I_j(t) = \left[1 + \exp\left(-c\left(s(t) - s_j^o\right)\right)\right]^{-1} - I^o \tag{2.1}$$

j indicates the j$^{\text{th}}$ receptor in the population, s_j^o determines the position of the receptor response curve on the intensity axis (i.e. approximately its operating point), c sets the slope and I^o the offset on the current axis. The values of c and I^o were fixed at $c = 0.2\,\text{dB}^{-1}$ and $I^o = 0.16$, so that the receptor current I_j ranged between 0 and 0.84.

The firing rate response $r_{R,j}$ of the j$^{\text{th}}$ receptor is given by

$$r_{R,j}(t) = \frac{r_R^{max}}{\sqrt{1 - I^o}} \sqrt{\left[I_j(t) - A_{R,j}(t)\right]_+} \tag{2.2}$$

r_R^{max} is the maximum firing rate, $[\cdot]_+$ symbolizes rectification to non-zero current values, and $A_{R,j}$ is the adaptation current in the receptor, following

$$\tau_R \frac{dA_{R,j}(t)}{dt} = -A_{R,j}(t) + \alpha_R \cdot r_{R,j}(t) \tag{2.3}$$

with adaptation time constant τ_R, and adaptation strength α_R, both assumed to be identical for all receptors.

The maximum firing rate r_R^{max} was set to 350 Hz and the adaptation time constant to 40 ms, both values borrowed from auditory receptors of grasshoppers (Benda and Herz, 2003) since respective data are missing for cricket receptors. Their exact values do not matter, however, since only onset and steady state responses are regarded, not the time course of adaptation. The adaptation strength of receptors α_R was 3.75, 9, and 23.75 kHz^{-1}, respectively, corresponding to 50, 75, and 90 % reduction in the firing rate from onset to steady state. For the individual receptor, the operating point was $s^o = 25\,\text{dB}$.

Sum of Receptor Responses The starting point and reference case is given by a neuron that computes the sum of receptor responses

$$r_{\sum}(t) = \frac{1}{N}\sum_{i=1}^{N} r_{R,i}(t) \tag{2.4}$$

$r_{\sum}$ and $r_{R,i}$ are the firing rates of the output neuron and of the i$^{\text{th}}$ receptor, respectively, and N is the number of receptors.

Additionally, adaptation in the output neuron is considered. The complete sum-model reads

$$r_{sum}(t) = r_{\sum} - A_{sum} \tag{2.5}$$

with adaptation variable A_{sum} following

$$\tau_A \frac{dA_{sum}(t)}{dt} = -A_{sum}(t) + \alpha_{sum} \cdot r_{sum}(t) \tag{2.6}$$

where τ_A (here as in the following models) is the time constant of adaptation in the output neuron, and α_{sum} the (dimensionless) adaptation strength of the sum-model with output neuron adaptation.

τ_A, was fixed at 40 ms for all models based on data on the AN1 of the cricket *Teleogryllus oceanicus* (Benda and Hennig, 2008). Three cases of adaptation in the sum model were considered: adaptation in receptors ($\alpha_R = 3.75\,\text{kHz}^{-1}$, $\alpha_{sum} = 0$), adaptation in the output neuron ($\alpha_R = 0\,\text{kHz}^{-1}$, $\alpha_{sum} = 1$), and a combination of adaptation in receptors and output neuron ($\alpha_R = 3.75\,\text{kHz}^{-1}$, $\alpha_{sum} = 1$).

NL-A-Model The second output neuron model contains a saturating non-linearity acting on the collective input of receptors and subtractive adaptation in the output neuron. If saturation precedes the adaptation in the output neuron, the model is referred to as the NL-A-model.

The saturating non-linearity Θ is given by the sigmoid function

$$\Theta(x) = 2 \cdot \left(\frac{1}{1 + \exp(-x)} - 0.5 \right). \tag{2.7}$$

The output neuron's response according to the NL-A-model is given by:

$$r_{NLA}(t) = \left[r_{NLA}^{max} \Theta\left(w \cdot r_{\sum}(t) \right) - A_{NLA}(t) \right]_+ \tag{2.8}$$

where $r_{\sum}$ is the sum of receptor responses as in eq. 2.4, r_{NLA}^{max} the maximum firing rate, w weights the receptor input (all receptors are equally weighted), and A_{NLA} is the adaptation variable (in Hz) in the output neuron which, in the NL-A-model, follows

$$\tau_A \frac{dA_{NLA}(t)}{dt} = -A_{NLA}(t) + \alpha_{NLA} \cdot r_{NLA}(t) \tag{2.9}$$

with the adaptation time constantτ_A, and the adaptation strength of the NL-A-model α_{NLA}.

The maximum firing rate r_{NLA}^{max} was set to 350 Hz. Three combinations of receptor adap-

tation strength α_R and weight w were considered, and the adaptation strength of the output neuron adjusted so as to produce equal total adaptation in all cases: weak receptor adaptation and small weight ($\alpha_R = 3.75\,\mathrm{kHz}^{-1}$, $w = 12.5\,\mathrm{kHz}^{-1}$, $\alpha_{NLA} = 0.62$), strong receptor adaptation and large weight ($\alpha_R = 23.75\,\mathrm{kHz}^{-1}$, $w = 62.0\,\mathrm{kHz}^{-1}$, $\alpha_{NLA} = 0.6$), and weak receptor adaptation and large weight ($\alpha_R = 3.75\,\mathrm{kHz}^{-1}$, $w = 62.0\,\mathrm{kHz}^{-1}$, $\alpha_{NLA} = 1$).

A-NL-Model Because the order of saturation and adaptation in the output neuron matters, the case of adaptation in the output neuron followed by adaptation is considered as well (referred to as the A-NL-model). In this case the output neuron's response is given by

$$r_{ANL}(t) = r_{ANL}^{max}\Theta\left(\left[w \cdot r_{\sum}(t) - A_{ANL}(t)\right]_+\right) \tag{2.10}$$

where $r_{ANL}^{max} = 350\,\mathrm{Hz}$ is the maximum firing rate of the output neuron, and A_{ANL} (dimensionless) is the adaptation current in the output neuron, which in this model follows

$$\tau_A \frac{dA_{ANL}(t)}{dt} = -A_{ANL}(t) + \alpha_{ANL} \cdot w \cdot r_{\sum}(t) \tag{2.11}$$

with α_{ANL} being the adaptation strength of the A-NL-model (dimensionless).

Weak receptor adaptation and low weight ($\alpha_R = 3.75\,\mathrm{kHz}^{-1}$, $w = 12.5\,\mathrm{kHz}^{-1}$, $\alpha_{NLA} = 0.5$), strong receptor adaptation and large weight ($\alpha_R = 23.75\,\mathrm{kHz}^{-1}$, $w = 62.0\,\mathrm{kHz}^{-1}$, $\alpha_{NLA} = 0.5$), and no receptor adaptation, large weight and strong adaptation in the output neuron ($\alpha_R = 0\,\mathrm{kHz}^{-1}$, $w = 62.0\,\mathrm{kHz}^{-1}$, $\alpha_{NLA} = 0.96$) were considered.

Invariance Model At one particular mean intensity most receptors are either fully saturated or below threshold and hence not available to encode the structure of the stimulus, only a fraction of receptors is stimulated within their dynamic range. Based on this observation, the model output neuron was constructed to focus only on the responses of receptors with operating points close to the actual intensity, and to ignore the responses of saturated and subthreshold receptors. The assignment of high weights to appropriate receptors follows slow components of the stimulus (i.e. the mean intensity).

The output neuron's response is given by a weighted sum of receptor responses

$$r_I(t) = \sum_{i=1}^{N} w_i(t) r_{R,i}(t) \tag{2.12}$$

where w_i is the weight factor for the connection between the i^{th} receptor and the output neuron, which is defined at any time as

$$w_i(t) = e^{\frac{(i-g(t))^2}{2\sigma_w^2}} \tag{2.13}$$

where $i = 1, 2, ...N$ refers to the receptor indices in order of increasing response threshold, and g is the center of the weight function on the receptor grid. It underlies a slow dynamics with time constant τ_g

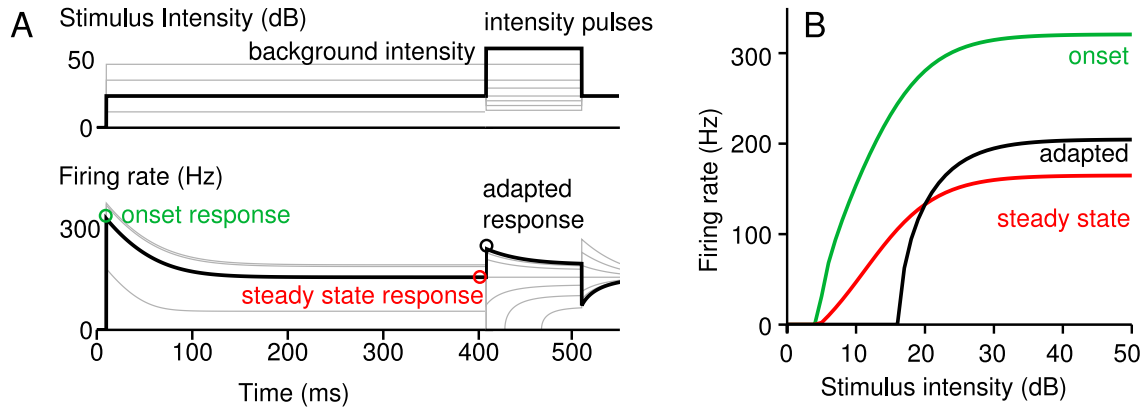

Figure 2.1: Adaptation stimuli and construction of different intensity response curves. **A** Exemplary stimuli (*upper panel*) used to test the effect of adaptation and corresponding firing rate responses (*lower panel*). The green, red, and black circle mark the times at which the response was evaluated to construct the onset (*green*), steady state (*red*), and adapted (*black*) response curves, respectively. **B** Onset, steady state and adapted response curves constructed from this stimulation paradigm.

$$\tau_g \frac{dg(t)}{dt} = -g(t) + \bar{g}(s(t)) \tag{2.14}$$

where the steady state value of g $\bar{g}$ is the index of the receptor with its operating point closest to the actual stimulus intensity, or formally

$$\bar{g} = \mathrm{cdf}^{-1}(s(t)) \tag{2.15}$$

where $\mathrm{cdf}^{-1}(\cdot)$ denotes the inverse cumulative distribution function of receptor thresholds. The weights are normalized to the total weight $w_i \to \frac{w_i}{\sum_{j=1}^{N} w_j}$.

The invariance model was considered for different widths of the weight distribution, σ_w, of 500, 30 and 1.

2.1.2 Stimulation and data analysis

In this study the effects of adaptation on the coding scheme of the neuron models is evaluated by regarding intensity response curves (response curves in the following) constructed under different conditions on the stimulus. The stimulation paradigm is illustrated in fig. 2.1.

To measure the onset and steady state response curves, the models were driven by constant intensity input of duration long enough to allow the neuron models to settle to steady state (400 ms). Input intensities ranged from 0 to 150 dB, in steps of 2 dB. The onset response curve is generated from the response at stimulus onset (since the models did not feature any response latency), the steady state responses curves are generated from the neural response

at 400 ms after onset.

Adapted response curves are constructed from the onset responses to intensities pulses after the model neuron had been adapted to a (constant) background intensity. To save computation time, the models were driven for 400 ms by background intensity s_B, and the value of the firing rate and adaptation variables were stored and in a next step used as starting conditions when the models were stimulated by short test pulses (20 ms). The intensities of test pulses were 0 to 150 dB in steps of 2 dB, and background intensities ranged from 10 to 110 dB in steps of 10 dB in output neuron models, and from 5 to 50 dB in steps of 5 dB.

All simulations and analyses were done in Matlab (c). The models were integrated using Euler's method with time steps of 0.1 ms. A table listing the parameter combinations used in this chapter is found in the appendix A1.6.

2.1.3 Data analysis

To quantify the adaptive shift of the model neurons, the thresholds of adapted response curves were estimated. For the receptor, linear sum, NL-A-model and A-NL-model, the thresholds were defined as the intensity of first non-zero response and plotted versus the background intensity. For the invariant model the operating point was determined instead (the intensity, at which the response curve reaches 50 % of the maximum response), because the shape of response curves in the threshold region depended strongly on the width of the weight distribution.

2.2 Results

To understand how intensity invariance may arise in neural networks, a model network with basic properties of the cricket auditory system was set up. The contributions of convergence, subtractive adaptation, and non-linearites were studied on successive levels.

2.2.1 Receptors

The model receptor qualitatively reproduces basic features of the response curves of auditory receptors of grasshoppers (Benda et al., 2001). The parameters of the receptor model were chosen to yield tuning curves with a dynamic range of 20 dB (roughly a fifth of the total relevant intensity range represented by the population). The width of the onset and steady state response curves is approximately identical. Adaptation to a constant intensity background shifts the operating point of the receptor to larger intensities (fig. 2.2 A and B) without a change in the slope of the response curves. The shift of response curves is accompanied by a reduction in the maximum response and limited to the dynamic range of the steady state response curve. Only for very large values of the adaptation strength α_R, the adapted response curves shift their threshold to intensities beyond the saturation point of the onset and steady state response curve, and at these adaptation strengths, the maximum responses of the adapted response curve become very small (fig. 2.2 B).

There is only one adaptation mechanism in individual receptors, which acts subtractive to the receptor current and is responsible for the shift. The reduction in the maximum

response of adapted response curves is a result of the saturating non-linearity used to describe the transduction mechanism (fig. 2.2 D). The adaptation acts subtractive on the receptor current, i.e. it shifts the f-I-curve (the response as a function of the current) to the right. Because the current saturates, a shift along the current axis will lead to successively smaller responses to one respective current value (fig. 2.2 E) so that adapted response curves reach successively smaller firing rates with increasing shift.

2.2.2 Sum of receptor responses

As a first reference for all further models of output neurons the sum of receptor responses was considered (sum-model). The onset and steady state response curve of this model neuron rise essentially linearly over the intensity range covered by the receptor population. Saturation occurs due to the finiteness of the receptor population.

If adaptation acts in the receptor layer only, the adapted tuning curves start to rise with the slope of the stationary tuning curve, then change their slope to that of the onset response curve just below the background intensity, and cross the stationary tuning curve at background intensity (fig. 2.3 A). For intensities below the background intensities most of the receptors that contribute to the sum (those that have their thresholds at intensities below the background intensity) are fully adapted and contribute only their adapted responses to the sum. For test intensities larger than the background intensity, the receptors that contribute to the sum are not adapted and contribute larger firing rates. The strength of adaptation in receptors determines the reduction of firing rate between onset and steady state, and the maximum shift of the thresholds of adapted response curves is limited by the threshold of the most sensitive receptor in maximally adapted state.

If adaptation acts only in the output neuron, the thresholds of adapted response curves are shifted to the right, while their saturation point and slope remains identical to that of the onset response curve (fig. 2.3 B).

In both cases, and for a combination of adaptation in receptors and the output neuron (fig. 2.3 C), onset, steady state and adapted response curves saturate at the same intensity. Consequently, the widths of adapted response curves and their saturated responses decrease as their thresholds are shifted to higher intensities. It is important to note, that the latter is a result of the non-linearity in the input imposed by the finite receptor population. The adaptation mechanism shifts response curves along the intensity axis not along the response axis.

The sum of receptor responses can obviously represent the full range of intensities that is covered by receptors. If the relevant intensity range is small, this is a feasible method. However, as the range of relevant intensities increases, the sensitivity of the cell to intensity differences decreases, making it an unsatisfactory solution for large intensity ranges.

2.2.3 Models with a saturating non-linearity

Using a static non-linearity that imposes a sharp saturation on the summed receptor responses, the output neuron could use its full response range on a clipped input range, thus increasing the slope of the response curve.

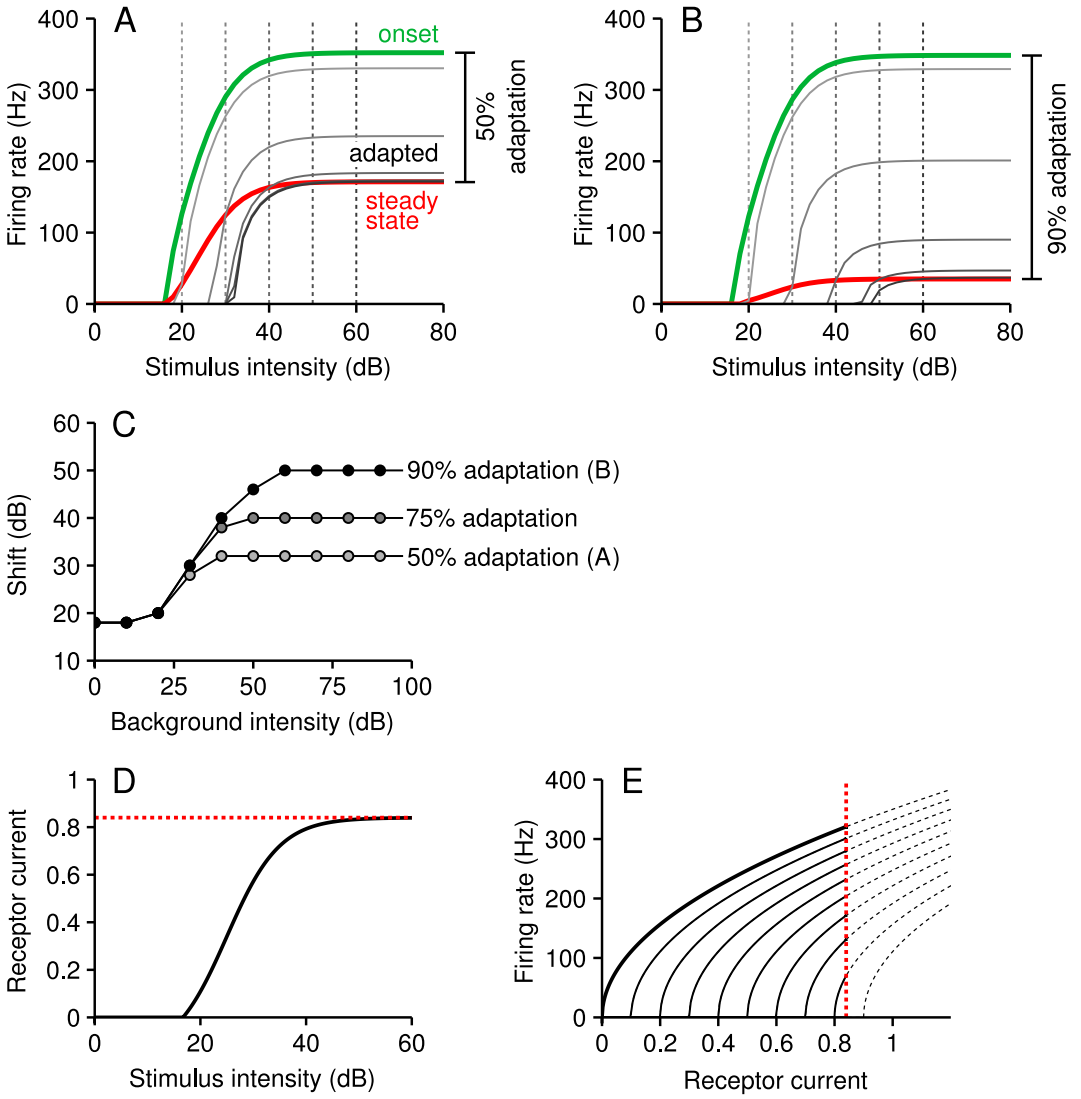

Figure 2.2: Receptor model. **A** and **B** show the response curves of an individual model receptor for 50 and 90 % adaptation, respectively. The onset and steady state response curves are indicated in green and red, respectively, adapted response curves to different background intensities are indicated in grey scales, dotted vertical lines of respective color mark the corresponding background intensity. **C** Shift of threshold of adapted response curves for 50, 75 and 90 % adaptation. **D** The non-linearity used to model the transduction of the physical stimulus into the receptor current. **E** Onset and adapted firing rate response as a function of receptor current, showing the subtractive effect of adaptation on the input current. The red dotted lines in **D** and **E** indicate the maximum receptor current approached by the model. Parameters: **A** $\alpha_R = 3.75\,\mathrm{kHZ}^{-1}$ (50%); **B** $\alpha_R = 23.75\,\mathrm{kHZ}^{-1}$ (90%); **C** $\alpha_R = 9.0\,\mathrm{kHZ}^{-1}$(75%)

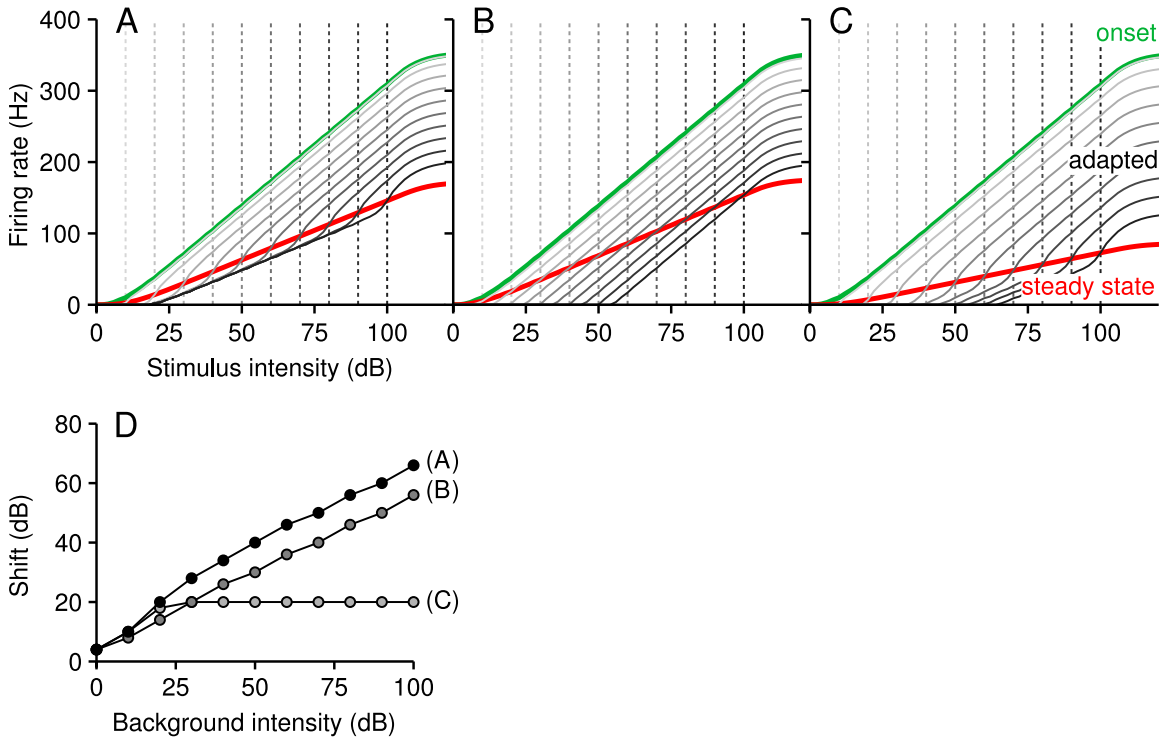

Figure 2.3: Linear sum of receptor responses. **A**–**C** show response curves resulting from a linear summation of receptor responses. **A** Adaptation in receptors, **B** adaptation in the output neuron, and **C** adaptation in receptors and in the output neuron. The onset and steady state response curves are indicated in green and red, respectively, adapted response curves to different background intensities are indicated in grey, dotted vertical lines of respective color mark the corresponding background intensity. **D** Shift of the thresholds of adapted response curves as a function of the background intensity for the response curves shown above. Parameters: **A** $\alpha_R = 3.75\,\mathrm{kHZ}^{-1}$ (50%), α_{sum}=0; **B** $\alpha_R = 0\,\mathrm{kHZ}^{-1}$, α_{sum}=1; **C** $\alpha_R = 3.75\,\mathrm{kHZ}^{-1}$(50%), α_{sum}=1

The first case considered is that in which the saturation precedes the adaptation in the output neuron (NL-A-model). The parameters of the saturating non-linearity and the maximum firing rate were fixed, thus the width and slope of the onset and adapted response curves are determined by the synaptic weight, larger synaptic weight leading to smaller width and larger slope. Figure 2.4 A to C shows the response curves of the NL-A-model for different parameters of weight and adaptation strengths.

Adapted response curves are shifted towards the intensity to which the neuron had been adapted, and as in individual receptors their maximum responses are reduced with increasing shift (see also fig. 2.4 E). The adapted response curves can only shift towards intensities within the dynamic range of the steady state response curve, i.e. they cannot be shifted to intensities at which the steady state response curve is saturated (see also fig. 2.4 D). The width of the steady state response curve is determined by the combination of the synaptic

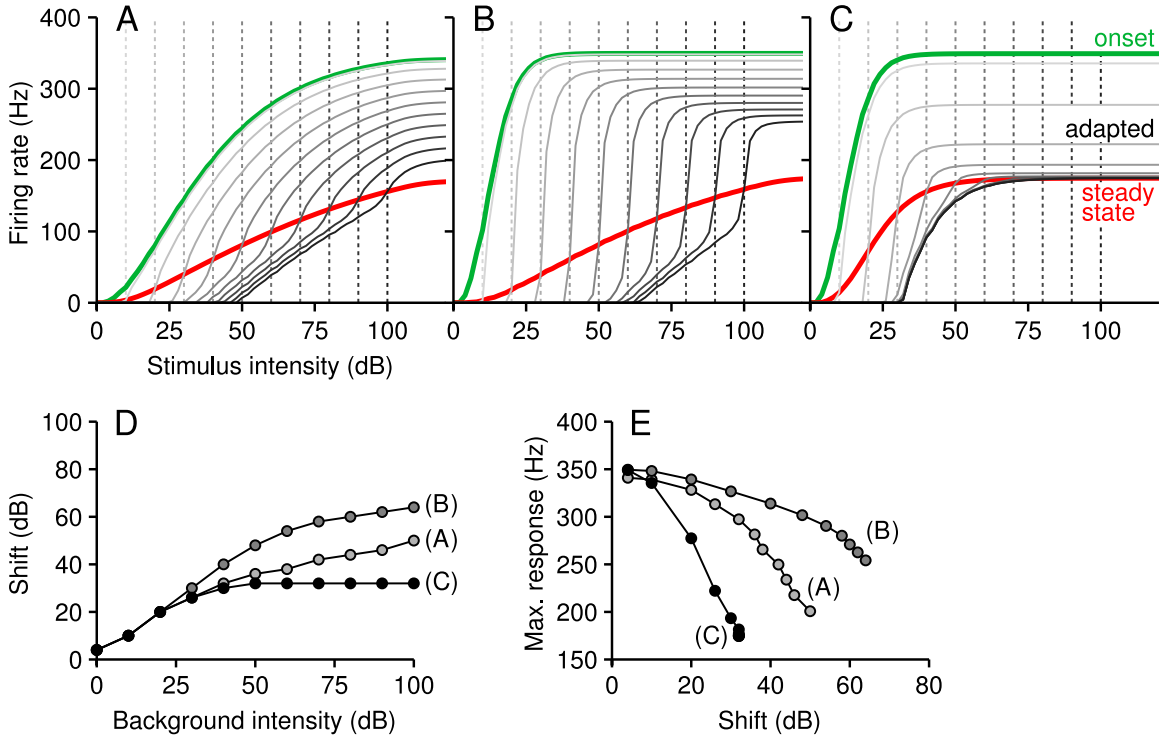

Figure 2.4: NL-A-model (saturation followed by adaptation). **A**–**C** response curves for different combinations of adaptation strengths and weight factor. The onset and steady state response curves are indicated in green and red, respectively, adapted response curves to several background intensities are indicated in grey, dotted vertical lines of respective color mark the corresponding background intensity. **D** Threshold shift of adapted response curves for the models in **A**–**C**. **E** Maximum responses of adapted response curves for the models in **A**–**C**. Parameters: **A** $\alpha_R = 3.75\,\mathrm{kHZ}^{-1}$ (50%), α_{NLA}=0.62, $w = 12.5\,\mathrm{kHZ}^{-1}$; **B** $\alpha_R = 23.75\,\mathrm{kHZ}^{-1}$ (90%), α_{NLA}=0.6, $w = 62.0\,\mathrm{kHZ}^{-1}$; **C** $\alpha_R = 3.75\,\mathrm{kHZ}^{-1}$ (50%), α_{NLA}=1, $w = 62.0\,\mathrm{kHZ}^{-1}$

weight and the strength of adaptation in the receptor layer. For fixed receptor adaptation strength, the width decreases with increasing weight, and for fixed weight, stronger receptor adaptation will increase the width. Therefore, for a sufficiently wide distribution of receptor thresholds, the range across which adapted response curves can be shifted is limited by the receptor adaptation strength rather than the receptor threshold distribution.

The onset tuning curve can be tuned arbitrarily steep, which improves the ability to differentiate between nearby intensities. To realize optimal intensity discrimination across a large intensity range the onset response curve should be as steep as possible, while the width of the steady state response curve should ideally cover the full range of intensities represented in the receptor population, so that adapted response curves can be shifted to all relevant background intensities. In the NL-A-model, this combination requires very strong adaptation in the receptor layer.

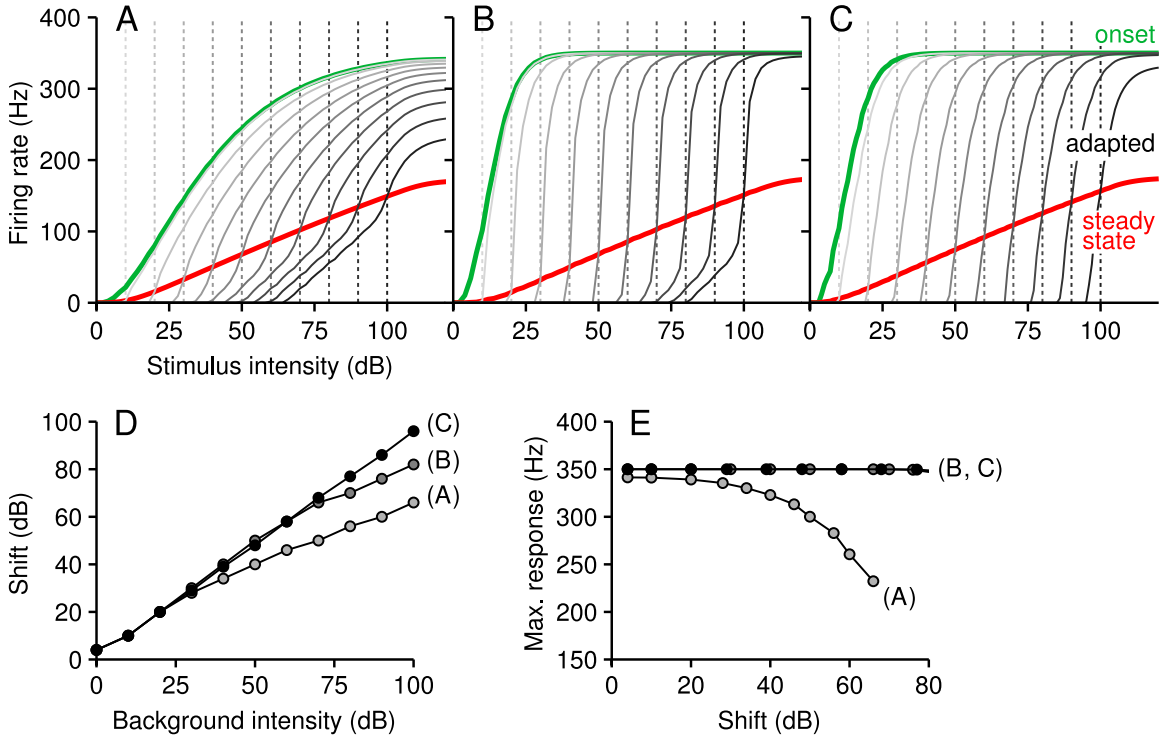

Figure 2.5: A-NL-model (adaptation precedes saturation). **A**–**C** response curves for different combinations of adaptation strengths and weight factor. The onset and steady state response curves are indicated in green and red, respectively, adapted response curves to several background intensities are indicated in grey, dotted vertical lines of respective color mark the corresponding background intensity. **D** Threshold shift of adapted response curves for the models in **A**–**C**. **E** Maximum responses of adapted response curves for the models in **A**–**C**. Parameters: **A** $\alpha_R = 3.75\,\mathrm{kHZ}^{-1}$ (50%), α_{ANL}=0.5, $w = 12.5\,\mathrm{kHZ}^{-1}$; **B** $\alpha_R = 23.75\,\mathrm{kHZ}^{-1}$ (90%), α_{ANL}=0.5, $w = 62.0\,\mathrm{kHZ}^{-1}$; **C** $\alpha_R = 0\,\mathrm{kHZ}^{-1}$, α_{ANL}=0.96, $w = 62.0\,\mathrm{kHZ}^{-1}$

Secondly, the case is considered in which the saturating non-linearity follows the adaptation in the output neuron (A-NL-model). For low receptor adaptation strengths and large width of onset response curves (small synaptic weight) the response curves of the A-NL-model do not differ much from those of the NL-A-model under the same parameter conditions (compare fig. 2.4 A vs fig. 2.5 A). Merely the thresholds of adapted response curves are shifted to slightly larger intensities in the A-NL-model than in the NL-A-model. If adaptation in the receptor layer is very strong and weights are large, a difference between the two models is revealed (fig. 2.4 B vs fig. 2.5 B): in contrast to the adapted response curves of the NL-A-model the adapted response curves of the A-NL-model show no reduction in their maximum firing rate as they shift to larger intensities. In the A-NL-model a reduction in the maximum firing rate of adapted response curves occurs only at intensities at which all receptors are fully saturated.

The most striking difference between the models is observed for the combination of low receptor adaptation strengths and large weight (fig. 2.4 C vs fig. 2.5 C). This combination results in steep onset and adapted response curves in both models. In the NL-A-model the steady state response curve has a narrow dynamic range and consequently adapted response curves can only shift for a small amount. In contrast, in the A-NL-model the width of the steady state response curve is wide and the adapted response curves can shift across the full intensity range. For the A-NL-model, this parameter combination yields high intensity resolution for the full relevant intensity range.

The differences between the NL-A-model and the A-NL-model can be understood by taking a step back, looking at the sum of receptor responses under different conditions. The input to the output neuron in both models is the sum of receptor responses with adaptation in the input layer (fig 2.6 A).

In the NL-A-model, the non-linearity acts on this input directly (fig 2.6 B1). Simplified, the saturating non-linearity clips the responses at a certain firing rate. This will naturally not only limit the response but also the dynamic range of response curves for an amount roughly proportional to the inverse of the slope of the response curve, the latter is determined by the synaptic weight. If adaptation in the receptor layer is weak, the slopes of onset and steady state response curve do not differ much and consequently, the dynamic range of the steady state response curve will be only slightly larger than that of the onset response curve. On the other hand, if receptor adaptation is strong, the steady state response curve might be hardly affected by the non-linearity and its dynamic range will be limited by the margins of the receptor population only. Adapted response curves can only be shifted to intensities within the dynamic range of the steady state response curve. This explains why the NL-A-model can only realize a combination of high intensity resolution (steep onset and adapted response curves) across a wide range of intensities with very strong adaptation in the receptor layer.

In the A-NL-model the situation is different, because the output neuron's adaptation mechanism acts on the linear sum (fig.2.6 C1), and the non-linearity acts on this twofold adapted input (fig.2.6 C2). The model works in principle without any adaptation in the receptor layer, the critical parameter to realize large shifts in both models is the amount of adaptation occurring before the saturation. For the fixed parameters of the non-linearity the dynamic range of the onset response curve depends on the synaptic weight, while the dynamic range of the steady state response curve depends on the total adaptation occurring before the non-linearity.

2.2.4 Invariance model

A different approach to the problem is taken based on the observation that at one specific average stimulus intensity only a fraction of the receptors in the population is able to encode changes in stimulus intensity, while most receptors are either fully saturated or not activated at all. The invariance model assigns the highest synaptic weight to those receptors that have their operating point at the current stimulus intensity and close to it.

In the following the weights follow a Gaussian function that peaks for the receptor centred at the current intensity (fig. 2.7 E). The weight distribution follows changes in stimulus intensity with a time constant of 40 ms, i.e. corresponding to the time constant of adaptation

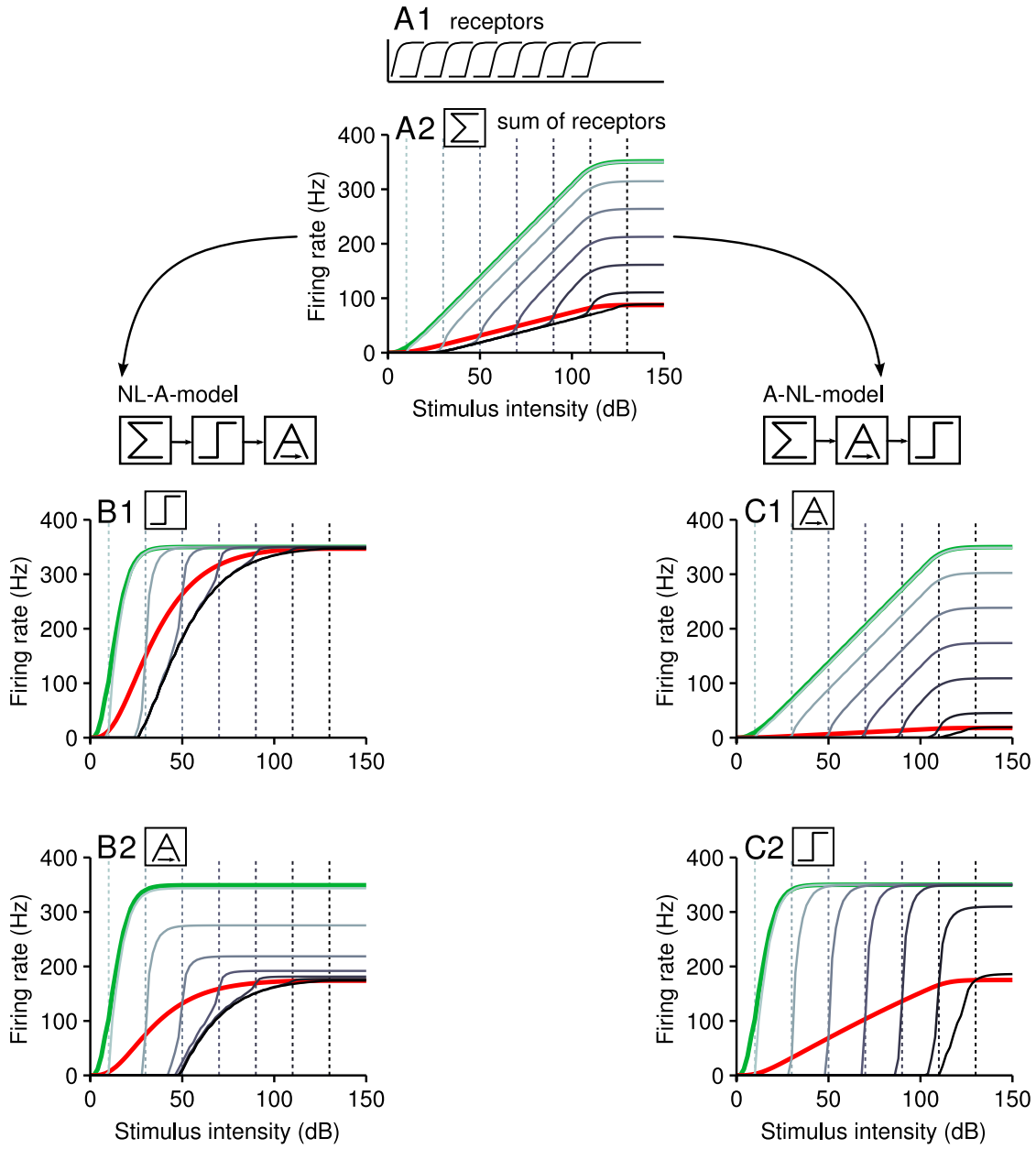

Figure 2.6: Scheme of the NL-A-model and the A-NL-model. Onset and steady state response curves are indicated in green and red, respectively, adapted response curves to several background intensities are indicated in grey, dotted vertical lines of respective color mark the corresponding background intensity. **A1** Symbolic of response curves of the receptor population. **A2** Sum of receptor responses with adaptation in receptors, the input to both models. **B** Following steps in the NL-A-model: saturation (**1**) and adaptation in the interneuron (**2**). **C** Following steps in the A-NL-model: adaptation in the interneuron (**1**) and saturation (**2**).

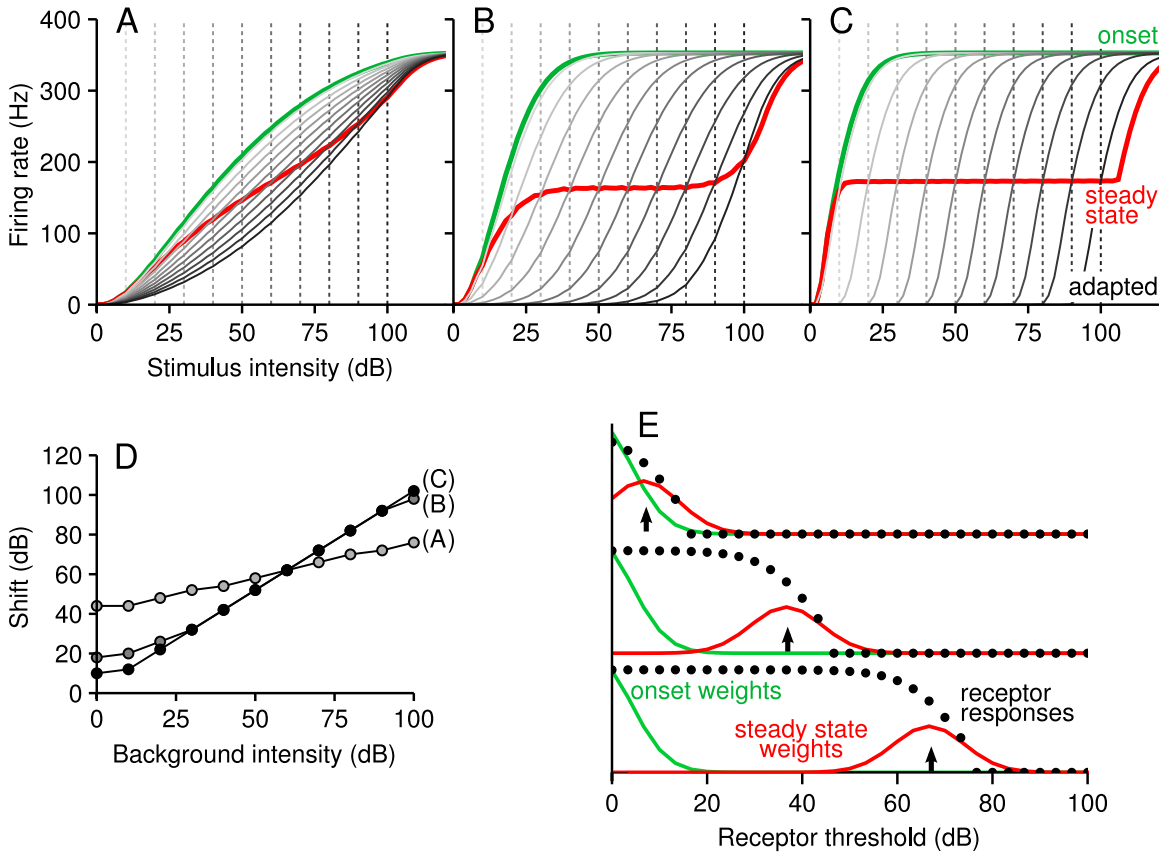

Figure 2.7: Invariannce model. **A** –**C** show the response curves of the invariant model for three different width of the distribution of synaptic weights. The onset and steady state response curves are indicated in green and red, respectively, adapted response curves to different background intensities are indicated in grey, dotted vertical lines of respective color mark the corresponding background intensity. **D** Shows the shift of adapted response curves with background intensity for the three model parameters above. **E** Schematic of the invariant model, black dots represent the responses of receptors as a function of their threshold for different stimulus intensities (indicated by arrows), *green* synaptic weights at stimulus onset, *red* the synaptic weights in steady state. Parameters: **A** σ_w=500; **B** σ_w=30; **C** σ_w=1

in the other models. The shift of the weight distribution is the only necessary adaptation mechanism in the model, receptors and the output neuron do not possess an intrinsic response driven adaptation mechanism.

The width of the response curves depends on the width of the distribution of weights, i.e. how many receptors are connected with non-zero weight. Figure 2.7 A to C show the response curves of the invariance model for three widths of the weight distribution.

The width of onset and steady state response curves are approximately identical, and the adapted response curves are parallel shifted versions of the onset response curve, each centred at the background intensity the neuron had been adapted to. True intensity invariance

is shown in a flat steady state response curve, which is reached by the invariant model, except for marginal intensities. The size of the margins depends on the width of the weight distribution. If the width of the weight distribution is not excessively large, the shift of adapted response curves as a function of the background intensity approaches identity (fig. 2.7 D).

In the invariance model the onset response curve can not have a narrower width than individual receptors, and the shift of adapted response curves is limited by the finiteness of receptors. Adapted response curves do not change their slope or maximum response for large background intensities.

2.3 Discussion

In this chapter different models were derived to gain insight into the question how adaptation to the signal mean arises in a convergent sensory network and how adaptive properties are transmitted over consecutive levels of such a network. Convergent feed forward networks represent a basic design common to many sensory systems A well accessible model system is the auditory system of the cricket, in which feed forward convergence of a receptor population with different response thresholds yields adaptation to background intensities in the ascending interneuron AN1.

2.3.1 Models

All models used a receptor population with uniformly distributed response thresholds that were distributed over a range of 100 dB and otherwise identical receptor response curves. The distribution of thresholds was chosen to differ in shape and width from that observed in crickets (which is roughly bell shaped and covers approximately 50 dB, see Imaizumi and Pollack 2001) because the distribution of receptor thresholds sets an ultimate limit to the adaptive shift in the output neuron. Using a wide distribution (relative to the width of the dynamic ranges of the model neurons) it is possible to identify additional parameters that limit the adaptive shift (see below).

Receptor model The mechano-electrical transduction in receptors was modelled by a Boltzmann function. The transduction non-linearity in combination with a response driven adaptation mechanism that acts subtractive on the input resulted in a pattern of adaptive shift similar to that found in auditory receptors of grasshoppers (Benda et al., 2001) and also auditory nerve fibres of cats (Wen et al., 2009): The onset and steady state response curves have a similar dynamic range. The shift of adapted response curves is roughly limited to the dynamic range of the onset and steady state response curve and is accompanied by a strong reduction in the maximum response.

In the auditory nerve of mammals various mechanisms may sum up to yield the observed adaptation properties: The transduction process in the cochlear hair cell shows adaptation to sustained displacement, which shifts the displacement-current relation along the displacement axis (Crawford et al., 1989). Further adaptive processes might occur at the synapses

between hair cell and auditory nerve fibre; and eventually there could be adaptation in the auditory nerve cell itself. Transducer adaptation and dynamic synapses have not been accounted for in the model, yet many characteristic features can be explained with spike driven adaptation in the auditory nerve fibre.

Unlike vertebrate hair cells, the auditory receptor cells of locusts and crickets send axons to higher order neurons and generate spikes themselves (Gray, 1960). It is known that there is input driven adaptation in locust receptors, but the adaptation observed in auditory receptors seems to be dominated by spike driven adaptation (Gollisch and Herz, 2004; Fisch et al., 2012).

Output neuron models Summation of the receptor responses expands the dynamic range of the output neuron to the intensity range covered by all receptors both in onset and steady state. The price is a reduction in the sensitivity. Adapted response curves differ depending on the site of adaptation. Adaptation in receptors will not shift the thresholds of adapted response curves except for the amount given by the shift of an individual receptor. Instead, adapted response curves show a characteristic transition from the slope of the steady state response curve to the slope of the onset response curve at the background intensity. Adaptation in the output neuron will produce adapted response curves that shift parallel to the onset response curve to the right. Independent of the site of adaptation the saturation of all response curves occurs at the same intensity, namely when the least sensitive receptor is recruited. The adapted response curves saturation level reduces with shift.

A static saturating non-linearity in the output neuron can be adjusted to affect the onset response stronger than the steady state response, if there is response adaptation before the saturation step. If adaptation precedes the non-linearity, the onset and steady state response curves will have different slopes and will consequently be clipped at different intensities by the saturation. The adaptation step preceding the saturation can occur in the receptor layer (NL-A-model), the output neuron or both (A-NL-model). In the NL-A-model the non-linearity is followed by an adaptation step in the output neuron, in the A-NL-model, the non-linearity is preceded by an adaptation driven by the sum of receptor responses. In both models, the adapted response curves shift their dynamic range to the background intensity if that lies within the dynamic range of the steady state response curves. For background intensities beyond the saturating point of the steady state response curve, the adapted response curves show a decrease in slope and no further shift.

The characteristic difference between the two models is, that in the NL-A-model the shift of adapted onset response curves is accompanied by a decrease in their maximum response for all shifts, while the adapted response curves of the A-NL-model maintain their maximum response constant until the shift exceeds the saturation point of the steady state response curve.

The dynamic range of the steady state response curve is a limiting factor for the range of adaptive shift in both models. That means that the parallel shift is restricted to the range of intensities for which the models are not intensity invariant. At background intensities where the steady state response curve is saturated, the models still encode intensity differences, but only below the current background. The ideal adjustment of the non-linearity would

be such, that the steady state response curve remains largely unaffected while the onset response curve is clipped so that it has a large slope when it uses its full response range, or rather a slope which corresponds to the accuracy of intensity discrimination needed by the respective system. How large the dynamic range ratio between steady state and onset can be depends on the amount of adaptation acting before the saturating non-linearity.

The invariance model uses a completely different approach. Instead of using response driven adaptation currents as in the models before, it adjusts the synaptic connections to the receptors in a way to focus on those receptors which their dynamic range centred close to the actual intensity. The adjustment is modelled to occur not instantaneously but on a time scale identical to the adaptation mechanisms used in the other models. Adapted response curves shift in parallel to the onset response curve, their dynamic range depends on the width of the distribution of synaptic weights, i.e. the size of the receptor subpopulation that is integrated with non-zero weight. In contrast to the NL-A-model and the A-NL-model, the steady state response curve has the same dynamic range as the onset response curve and the shift of adapted onset response curves is not limited by the dynamic range of the steady state response curve.

This is a strong argument to measure both, the onset and adapted response curves (representing the coding of fast fluctuations in the stimulus) as well as the steady state response curve (that represent the coding of slow stimulus components). If the steady state response curve is found to have a larger dynamic range than the onset/adapted response curves, and if the shift of adapted response curves is limited in relation to the steady state response curve, the underlying mechanism could include shifting adaptation and a static non-linearity.

Another difference between the NL-A-model and A-NL-model on one side and the invariance model on the other side is that in the latter the slope of the output neurons response curve is limited by the slope of the response curve of an individual receptor, while in the former models it is not. The response curves of the NL-A-model and A-NL-model can in principle become arbitrarily steep, and – more importantly – they can also be steep if the response curves of individual receptors were shallow. These models would also work with a population of receptors in which every receptor has the exact same response curve that spans the full relevant intensity range, or some intermediate organization pattern. This is of relevance for the auditory system of mammals, where range fractionation in the classical sense (i.e. as observed in the cricket) does not exist. Although intensity range fractionation could arise in there for pure tone stimuli by recruiting receptors with distant frequency tuning (*spread of excitation*), it does not seem to be essential for a constantly high discrimination across large intensity ranges (Viemeister and Bacon, 1988).

2.3.2 Impact of static saturating non-linearities

An important finding of this modelling study is that apparently complex characteristics of adapted response curves can emerge as a consequence of the combination of one adaptation mechanism that acts subtractive on the input with a *static* saturating non-linearity. Saturating non-linearities that map the input to a neuron to a limited range have characteristic effects on the shape of response curves when followed by a shifting adaptation. Because the input range ends at some intensity the range available to drive the neuron will decrease

as the response curve is shifted in parallel to larger intensities. This results in the break down of the maximum response with increasing shift of adapted response curves. In the receptor model, the non-linearity is given by the mechano-electrical transduction, in the NL-A-model it is included as a computational element. In the sum of receptor responses and in the A-NL-model the limitation of the input range is given by the finiteness of the receptor population. The decrease in maximum response of adapted response curves is therefore an emergent property of the models that involve a static saturating non-linearity. Interestingly, this feature has been observed in auditory receptors of grasshoppers (Benda et al., 2001), auditory nerve fibres of cats (Wen et al., 2009), the AN1 of the cricket *Teleogryllus oceanicus* (Benda and Hennig, 2008), and neurons in the IC of guinea pigs (Dean et al., 2005).

Auditory nerve fibres of the cat have similar adaptive properties as grasshopper auditory receptors, i.e. a very limited capacity to shift to larger intensities and a reduction in the maximum response. These fibres additionally show a reduction in the baseline activity with shift which was interpreted as an adaptation mechanisms that shifts the response curves down (Wen et al., 2009). This phenomenon can be reproduced by the here presented receptor model by adding an offset to the static non-linearity used to model the mechano-electrical coupling (eqn. 2.1). The drop in baseline activity would thus result from a static non-linearity, not from an additional adaptation mechanisms.

2.3.3 Biophysical realization

The connectivity of the cricket AN1 is very straight forward and allows for some contemplation of possible biophysical mechanisms underlying the saturation and response adaptation in the NL-A-model and A-NL-model.

Origin of the non-linearity in the AN1 The NL-A-model and A-NL-model require a sharply saturating static non-linearity to give the desired shape of response curves. The saturation could act either on the membrane potential or limit the maximal spike frequency. In the NL-A-model it clearly needs to be a mechanisms that limits the membrane potential, the adaptation mechanism could than be any spike driven adaptation current, while in the A-NL-model it could be both.

On the level of the membrane potential the saturation might be mediated by a third neuron type which imposes inhibitory input to the output neuron. In the cricket, there is a local interneuron in either hemisphere of the prothoracal ganglion (the omega neuron, ON1), which is driven by receptors. The ON1s mutually inhibit one another and the respective contralateral AN1s (Wohlers and Huber, 1982; Selverston et al., 1985). This contralateral inhibition is, however, an unlikely candidate for the non-linearity in the NL-A-model and the A-NL-model. Firstly, the response curves of the AN1 that inspired the models were recorded under ipsilateral stimulation, i.e. the ipsilateral ON1 would have inhibited the contralateral ON1 and therefore the inhibition to the recorded ipsilateral AN1. Secondly, the ON1's inhibitory input comes with a delay (Hennig, 1988), while it needed to be very quick and precisely timed to affect the onset response.

A possible mechanism is dendritic saturation (Bernander et al., 1994; Bush and Sejnowski, 1994; Mainen et al., 1996; Koch and Segev, 2000; Prescott and De Koninck, 2003). Although

the morphology (in particular the localization of the soma) of insect neurons differs from that of vertebrate neurons, synaptic saturation in dendrites has also been described for visual motion sensitive neurons in the blowfly (Haag et al., 1992; Egelhaaf et al., 1994; Borst et al., 1995). The projection field of receptors in the AN1 is distinctly branched (Wohlers and Huber, 1982) so that it is a plausible candidate for non-linear integration.

For the A-NL-model a spike frequency limiting mechanisms was possible, in particular spike refractoriness. Yet it is not likely that refractoriness actually has this computational effect on response curves. Integrate and fire models with relative refractoriness will show a soft decrease in slope rather than a sharp saturation, and only an absolute refractoriness can reproduce the sharp saturation needed by the model. In Hodgkin-Huxley like models the firing rate does not saturate in a sharp way – instead the model neuron undergoes a bifurcation back from the limit cycle oscillation to a stable steady state at large input currents. This so called depolarization block is observed in real neurons (e.g. Grace et al. 1997; Dovzhenok and Kuznetsov 2012). Spike refractoriness might therefore not be suited as a biophysical mechanism of sharp saturation.

Biophysical basis of adaptation The model of subtractive adaptation used throughout this study has been derived from detailed models of spike driven adaptation currents: Benda and Herz (2003) showed that the different spike driven adaptation currents all act subtractive to the input current and thus cause a shift in the current-response relation. Here, the adaptation dynamics was modelled in the simplest form, assuming the steady state adaptation to be proportional to the driving force of adaptation. This strictly holds only for linear stimulus response relations, but still will capture the essential features (Gollisch and Herz, 2004). In the receptor model and the NL-A-model, the adaptation is clearly output driven, and could well be based on spike driven adaptation currents.

In the A-NL-model adaptation is driven by the sum of receptor responses, a quantity which might be computed in the membrane potential of the output neuron, and this quantity drives the adaptation. This requires slow voltage dependent adaptation currents that are activated at subthreshold levels of the membrane potential (Brette and Gerstner, 2005; Prescott and Sejnowski, 2008).

Invariance model The invariance model was constructed as a reference model that implements strict intensity invariance and a strictly parallel shift of response curves with changes in the background intensity. A biophysical realization would require to adjust synaptic weights based on the firing frequency of receptors in response to the background intensity. The major challenge is to realize the sharpness of the bandpass filter necessary to selectively transmit the input from receptors within their dynamic range only.

2.3.4 Conclusions

In summary, the firing rate models of the individual receptor and the output neuron (the NL-A-model and A-NL-model) are surprisingly successful in reproducing the shift of response curves with changes in background intensity observed in the auditory system of crickets, and

also mammals. Three insights are particularly interesting: First, the interaction of static non-linearities with adaptation that results in complex characteristics of adapted response curves, namely the reduction in maximum firing rate with increasing shift, a decrease in the slope of adapted response curves for large background intensities, and also a reduction in the baseline response with increasing shift.

Second, the output neuron models that contain a static saturating non-linearity are not restricted to receptor populations intensity with range fractionation but would work with a population of identical receptors with shallow response curves, too. The exact organization of the receptor population with respect to e.g. thresholds, slopes, adaptation strengths would influence the shape of the response curves of the output neuron in detail, but not their overall adaptive behaviour.

Eventually, the model designed to generate strictly intensity invariant responses and parallel shifts of response curves with background intensities does not capture the two before mentioned points.

3 Coding Properties of the Models

The previous chapter was dedicated to the problem of how adjustments of a neuron's operating point to changing background intensities arise in a convergent feed forward circuitry. While the previous chapter focused on finding possible principles underlying the emergence of shifting adaptation, the following chapter addresses the question of how the derived models perform with respect to intensity discrimination and and the encoding of time varying stimuli.

The efficient coding hypothesis (Barlow, 1961, 2001; Simoncelli, 2003) claims that to ensure an efficient representation of the signal, a single neuron should make use of its full response range. To efficiently encode a given distribution of stimulus intensities under the constraint of a limited neuronal response range, the neuron should adjust its sensitivity and dynamic range such that typically encountered intensities arouse responses between threshold and saturation level. Basically, the mutual information between signal and response is maximized if the response-functions correspond to the cumulative probability distribution of the stimulus intensities if the noise in the neural response is additive and has a constant standard deviation (Laughlin, 1981; Nadal and Parga, 1994). These studies considered the problem of optimal response curves for static response curves. In the derived output neuron models, the response curves shift along the intensity axis with slow changing components of the stimulus (i.e. the mean), so that the full response range can be used to encode the fast fluctuations around the stimulus mean. But does this adaptive shift lead to best intensity discrimination around the background intensity? And do steep response curves that shift with changing background intensities result in a superior intensity discrimination than shallow response curves that cover the full intensity range? In order to answer these questions, the Fisher information was used to quantify the accuracy of intensity discrimination at different background intensities for the models derived in chapter 2.

Additionally, in this chapter, the models' responses to time varying stimuli are analysed by considering noise response curves and estimating the mutual information between stimuli and responses for different stimulus conditions. Noise stimuli with different means and standard deviations were used to find out if the models prefer stimuli with a standard deviation that matches their dynamic range and if the shift of response curves enables the neuron models to maintain maximal mutual information if the stimulus mean is varied.

3.1 Methods

3.1.1 Intensity discrimination

To quantify the neuron models' ability to discriminate between two similar intensities, the Fisher information was estimated from the neurons response curves. To this purpose, the

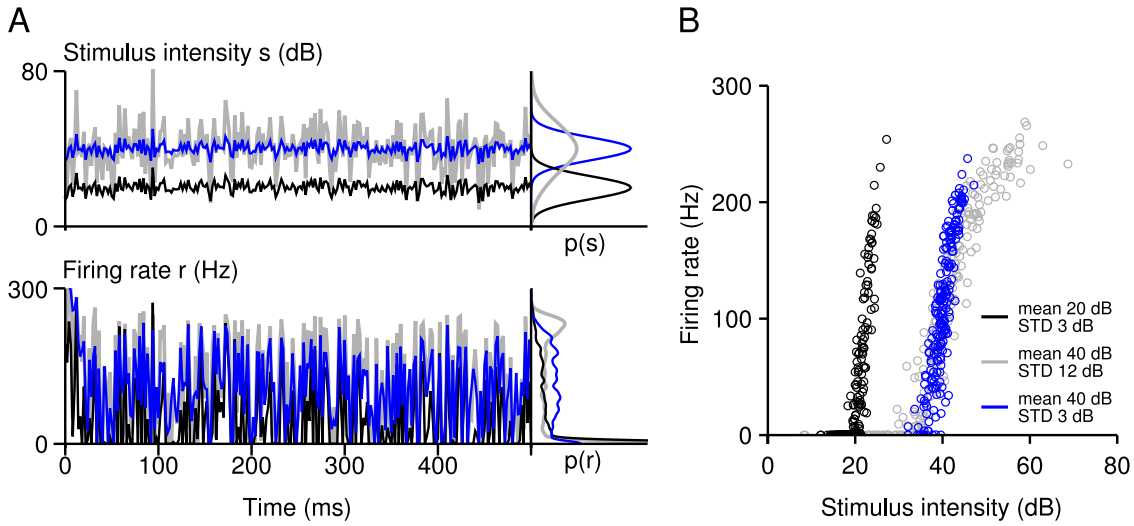

Figure 3.1: Noise stimuli and noise response curves. **A** Exemplary noise stimuli (*upper panel*) with different mean and standard deviation and corresponding firing rate responses (*lower panel*) with their probability distributions on the right. **B** Noise response curves constructed from the responses in A.

stimulus paradigm from chapter 2 was used to calculate the onset, steady state and adapted response curves (see fig. 2.1 for a schematic of the stimulation paradigm).

The models were driven for 400 ms by background intensity s_B, and the value of the firing rate and adaptation variables were stored and in a next step used as starting conditions when the models were stimulated by short test pulses (20 ms duration). The intensities of test pulses were 0 to 150 dB in steps of 1 dB. Background intensities of 20 to 100 dB in steps of 20 dB were used for output neurons, and background intensities from 15 to 50 dB in steps of 5 dB were used for the individual receptor. The mean $\langle r \rangle$ and standard deviation σ_r of the output neurons' responses across 1000 repetitions were calculated.

The Fisher information $J(s)$ at stimulus intensity s was estimated as (Brunel and Nadal, 1998)

$$J(s) = \frac{\left(\frac{d\langle r \rangle}{ds}\right)^2}{\sigma_r^2} \,. \tag{3.1}$$

3.1.2 Encoding of noise stimuli

Complementary to constant intensity stimulation, the models were driven by 20 s band pass filtered (20 to 1000 Hz) noise of several means and standard deviations (fig. 3.1). The signal mean was varied from 0 to 40 dB in steps of 5 dB and from 40 to 80 dB in steps of 10 dB, and standard deviations (STD) of 0, 3, 6, 12, 24, 36, and 96 dB were used.

Noise response curves were constructed from the last 19 s of the responses for every stimulus, i.e. for the stationary part of the response. To compare the noise response curves over

different stimulus conditions they were fitted with a nonparametric algorithm (Nadaraya, 1964; Watson, 1964), using $N_B = N/1000$ bins ($N = 199000$ being the number of data points), a bandwidth of $b = \frac{max(r)-min(r)}{1.8N_B}$, and 100 resampling cycles.

The mutual information $I_M(S, R)$ (Shannon et al., 1949) between the stimulus and the responses was estimated (for the last 19 s) to quantify how much information the neural responses carry about a respective stimulus. To compare the mutual information over different stimulus conditions, it was normalized by the stimulus entropy $H(S)$. The mutual information and stimulus entropy were estimated using the algorithm of Moddemeijer (1989).

3.1.3 Model equations

In this chapter the neuron models from chapter 2 were used with the parameter combinations given below and expanded by a noise term to model response variability.

Receptor Model In the receptor model the noise is added to the normalized receptor current I_j

$$I_j(t) = \frac{1}{1 + \exp\left(-c\left(s(t) - s_j^o\right)\right)} - I^o + \sigma_I \xi(t) \tag{3.2}$$

where ξ is a Gaussian random number and σ_I its standard deviation determining the noise level in the receptor. The firing rate response of individual receptors is given by

$$r_{R,j}(t) = \frac{r_R^{max}}{\sqrt{1 - I^o}} \sqrt{[I_j(t) - A_{R,j}(t)]_+} \tag{3.3}$$

where r_R^{max} is the maximum firing rate, $[\cdot]_+$ symbolizes rectification to positive values, and $A_{R,j}$ is the adaptation current following

$$\tau_R \frac{dA_{R,j}(t)}{dt} = -A_{R,j}(t) + \alpha_R \cdot r_{R,j}(t) \tag{3.4}$$

where τ_R is the adaptation time constant, and α_R the adaptation strength.

The following parameters were used for all receptors in the population: $c = 0.2\,\mathrm{dB}^{-1}$, $I^o = 0.16$, $\sigma_I = 0.05\,\mathrm{Hz}$, $r_R^{max} = 350\,\mathrm{Hz}$, and $\tau_R = 40\,\mathrm{ms}$. For the individual receptor, the adaptation strength α_R was $9\,\mathrm{kHz}^{-1}$ (corresponding to 75 % reduction in the firing rate between onset and steady state), or $0\,\mathrm{kHz}^{-1}$, and the operating point s^o was set at 25 dB.

Network The network consisted of $N = 30$ receptors converging to one output neuron. The receptor operating points s_j^o were uniformly distributed between 12 and 112 dB, or normally distributed with mean 62 dB and a standard deviation of 17 dB.

Sum-model The firing rate of the general sum-model is given by

$$r_{sum}(t) = \frac{1}{N} \sum_{i=1}^{N} r_{R,i}(t) + \sigma_r \xi t - A_{sum} \; . \tag{3.5}$$

Here and in the following models ξ is a Gaussian random number and σ_r its standard deviation determining the noise level in the output neuron, and N is the number of receptors. The adaptation variable A_{sum}, follows

$$\tau_A \frac{dA_{sum}(t)}{dt} = -A_{sum}(t) + \alpha_{sum} \cdot r_{sum}(t) \tag{3.6}$$

where τ_A is the time constant of adaptation in the output neuron.

Adaptation only in the receptor layer ($\alpha_R = 9\,\mathrm{kHz}^{-1}$, $\alpha_{sum} = 0$), and adaptation only in the output neuron ($\alpha_R = 0\,\mathrm{kHz}^{-1}$, $\alpha_{sum} = 0.76$) were considered. In all output neuron models the time constant of adaptation in the output neuron was 40 ms, and noise standard deviation σ_r wass 10 dB.

NL-A-Model and A-NL-model The NL-A-model and A-NL-model from chapter 2 feature a saturating non-linearity Θ (identical for both models)

$$\Theta(x) = 2 \cdot \left(\frac{1}{1 + \exp(-x)} - 0.5 \right) . \tag{3.7}$$

The models differ in the relative position of the saturation and the adaptation in the output neuron. The firing rate response of the NL-A-model (saturation precedes adaptation in the output neuron) is given by

$$r_{NLA}(t) = \left[r^{max} \Theta\left(w \cdot r_{\sum}(t) \right) - A_{NLA}(t) \right]_+ + \sigma_r \xi t \tag{3.8}$$

where $r_{\sum} = \frac{1}{N} \sum_{i=1}^{N} r_{R,i}(t)$ is the sum of receptor responses, r^{max} is the maximum firing rate of the output neuron, w weights the receptor input (all receptors are equally weighted), and A_{NLA} is the adaptation variable in the output neuron which, in the NL-A-model, follows:

$$\tau_A \frac{dA_{NLA}(t)}{dt} = -A_{NLA}(t) + \alpha_{NLA} \cdot r_{NLA}(t) \tag{3.9}$$

with the adaptation time constantτ_A, and the adaptation strength of the NL-A-model α_{NLA}.

The parameters of the NL-A-model were $r^{max} = 350\,\mathrm{Hz}$, $\alpha_R = 9\,\mathrm{kHz}^{-1}$, $\alpha_{NLA} = 1$, and $w = 62\,\mathrm{kHz}^{-1}$.

In the A-NL-model (saturation follows adaptation in the output neuron) the output neuron's response is given by

$$r_{ANL}(t) = r^{max} \Theta\left(\left[w \cdot r_{\sum}(t) - A_{ANL}(t) \right]_+ \right) + \sigma_r \xi t \tag{3.10}$$

where A_{ANL} is the adaptation current in the output neuron, which in this model follows:

$$\tau_A \frac{dA_{ANL}(t)}{dt} = -A_{ANL}(t) + \alpha_{ANL} \cdot w \cdot r_{\sum}(t) \tag{3.11}$$

with α_{ANL} being the adaptation strength of the A-NL-model.

The A-NL-model was analysed for two parameter combinations, i.e. either with adaptation in the receptors ($\alpha_R = 9\,\mathrm{kHz}^{-1}$, $\alpha_{NLA} = 0.8$) or without adaptation in receptors ($\alpha_R =$

$0\,\mathrm{kHz}^{-1}$, $\alpha_{NLA} = 0.96$). The maximum firing rate r^{max} was 350 Hz and the weight w $62\,\mathrm{kHz}^{-1}$ for both cases.

Invariance Model The output neuron's response according to the invariance model is given by a weighted sum of receptor responses:

$$r_I(t) = \sum_{i=1}^{N} w_i(t) r_{R,i}(t) + +\sigma_r \xi t \tag{3.12}$$

where $r_{R,i}$ is the response of the i^{th} receptor, and w_i is the weight factor for the connection between the i^{th} receptor and the output neuron, which is defined at any time as

$$w_i(t) = e^{\frac{(i-g(t))^2}{2\sigma_w^2}} \tag{3.13}$$

where $i = 1, 2, ...N$ refers to the receptor indices in order of increasing response threshold, and g is the center of the weight function on the receptor grid. It underlies a slow dynamics with time constant τ_g

$$\tau_g \frac{dg(t)}{dt} = -g(t) + \bar{g}(s(t)) \tag{3.14}$$

where $\bar{g} = \mathrm{cdf}^{-1}(s(t))$, $\mathrm{cdf}^{-1}(\cdot)$ denotes the inverse cumulative distribution function of receptor thresholds. The weights are normalized to the total weight $w_i \to \frac{w_i}{\sum_{j=1}^{N} w_j}$. The width of the weight distribution σ_w was fixed at 5, and the receptor adaptation strength was set to $\alpha_R = 0\,\mathrm{kHz}^{-1}$.

3.2 Results

3.2.1 Intensity discrimination

To compare the ability of the different models to discriminate nearby intensity differences at across different absolute intensity levels, the Fisher information functions were estimated from the response curves.

Individual receptor As shown in chapter 2 the dynamic range of the receptor covers about one fifth of the considered intensity range, its adapted response curves are shifted in parallel through the dynamic range of the onset and steady state response curve, and their maximum response decreases with shift.

The Fisher information functions of the onset and steady state response curves of the individual receptor peak at the center of its dynamic range and fall off symmetrically to both sides, approaching zero to the boundaries of the dynamic range (fig. 3.2, B1). The Fisher information of the steady state responses reaches overall lower values than that of the onset response not only because of the shallower slope but also because of a larger response variability in steady state. The Fisher information functions estimated from adapted

response curves peak where the respective adapted response curve rises most steeply. As the adapted response curves in the receptor are not shifted markedly beyond the dynamic range of the onset response curve, for background intensities larger than about 5 dB above absolute threshold, the peak Fisher information is no longer centred at the background intensity either and declines quickly with increasing shift (fig. 3.2, C1).

Sum of receptor responses As the next step, two variations of the sum of receptor responses are considered, i.e. adaptation acts either exclusively in the receptor layer or in the output neuron. The adaptation strengths of the output neurons was adjusted so that the same reduction in firing rate (i.e. the same total amount of adaptation) was reached as for adaptation in the receptors.

The onset and steady state response curves of both sum-models are essentially identical, rising linearly over the full range of intensities represented by the receptor population (fig. 3.2, A2 and A3). The Fisher information functions show a plateau, reaching approximately constant levels across the linearly rising range of the response curves (fig. 3.2 B2 and B3). Due to the shallower slope of response curves as compared of those of the receptor model, the Fisher information reaches only about one tenth of the peak value of the individual receptor.

If adaptation acts only in the receptors the adapted response curves initially rise with the slope of the steady state response curve and change their slope to that of the onset response curve at their respective background intensity. If adaptation acts only in the output neuron, the adapted response curves shift in parallel for an amount corresponding to the background intensity. The Fisher information functions of adapted response curves are basically similar for both variants of the sum-model (fig. 3.2 C2 and C3). The Fisher information rises sharply just below the background intensity and is flat for all intensities above the background intensity and drops to zero when the responses saturate. If adaptation occurs in the receptor layer, there are small peaks in the Fisher information at the background intensity which reflect a transient steep part of the adapted response curves where they change their slope at the background intensity.

NL-A-model, A-NL-model, and invariance model In the NL-A-model, A-NL-model and the invariance model the output neuron shifts its response curves along the intensity axis, adjusting their operating point to the background intensity. Does this adaptive shift also adjust the best intensity discrimination to the current background intensity?

The NL-A-model and A-NL-model with 75 % adaptation in receptors (i.e. firing rate decreases to 25 % of onset response) plus a version of the A-NL-model without adaptation in the receptor layer were considered. The model parameters were chosen such that the onset response curves resembled that of an individual receptor with respect to width and slope, and adaptation in the output neuron was adjusted to give the same total amount of adaptation.

In the NL-A-model, the onset response curve saturates at about 25 dB while the steady state response curve saturates at approximately 60 dB. The onset response curves of the A-NL-model variants are approximately identical to that of the NL-A-model, their steady state response curves rise linearly over the full range of intensities covered by the receptor popula-

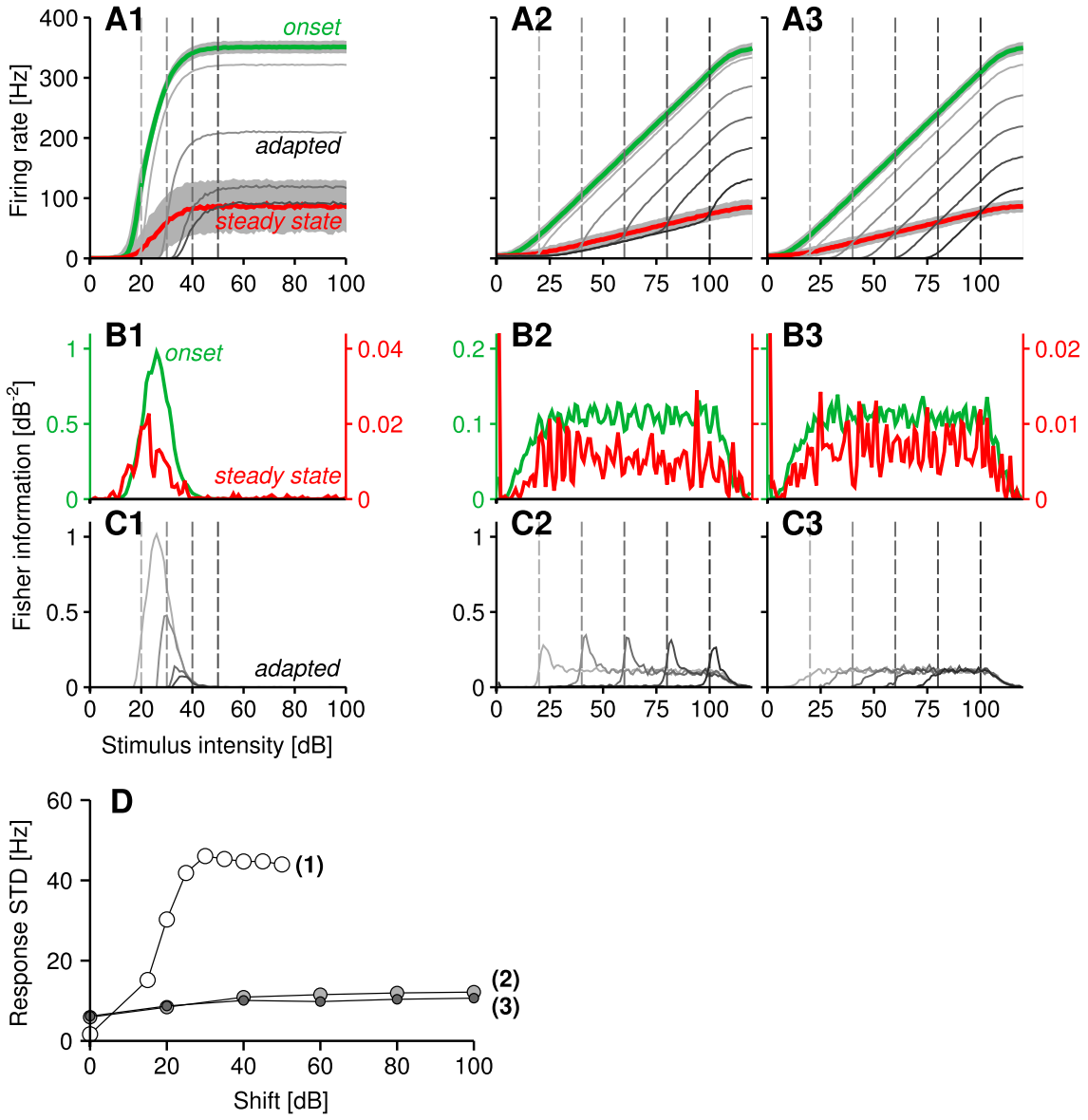

Figure 3.2: Fisher information functions for individual receptor and sum of receptor responses. **A** Intensity response curves for the individual receptor (**1**), the sum of receptor responses with adaptation in receptors (**2**), and the sum of receptor responses with adaptation in the output neuron (**3**). *green* onset response curve, *red* steady state response curve, *grey* adapted response curves, respective background intensities are indicated by dashed lines of respective color. **B** Fisher information functions for the models in **A** for onset and steady state response curve, and **C** for adapted response curves. **D** Response standard deviation of the individual receptor as a function of intensity for the onset (*green*) and adapted response curves (*grey*) in **A** Parameters: **1** $\alpha_R = 9\,\mathrm{kHz}^{-1}$ (75%); **2** $\alpha_R = 9\,\mathrm{kHz}^{-1}$ (75%), $\alpha_{sum} = 0$; **3** $\alpha_R = 0\,\mathrm{kHz}^{-1}$, $\alpha_{sum} = 0.76$

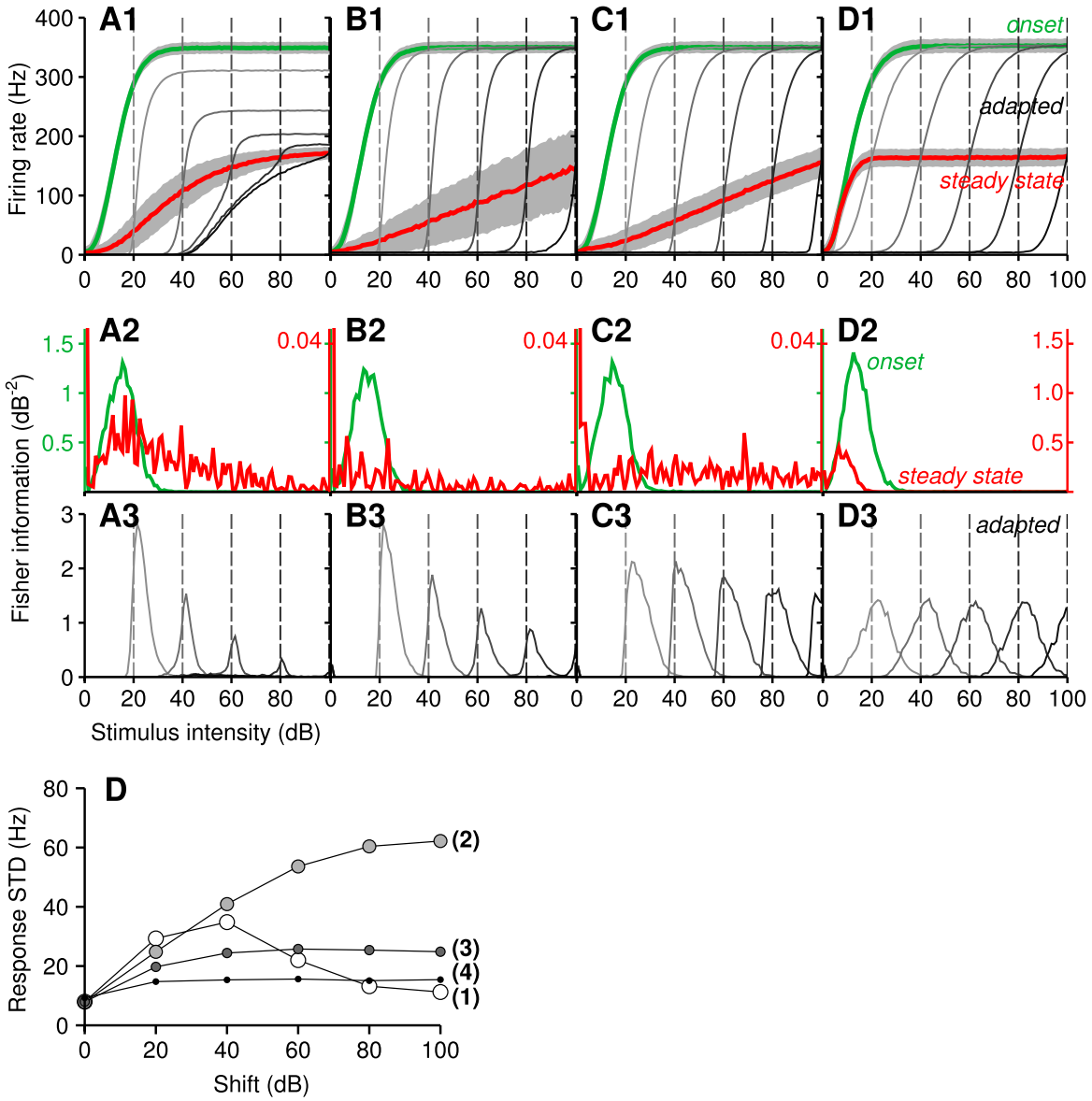

Figure 3.3: Fisher information functions for the NL-A-model, the A-NL-model, and the invariant model. **A** Intensity response curves for the NL-A-model (**1**), the A-NL-model with adaptation in receptors and the output neuron (**2**), the A-NL-model with adaptation only in the output neuron (**3**), and the invariance model (**4**). *green* onset response curve, *red* steady state response curve, *grey* adapted response curves, respective background intensities are indicated by dashed lines of respective color. **B** Fisher information functions for the models in **A** for onset and steady state response curve and **C** for adapted response curves. **D** Peak of the response standard deviation of adapted response curves as function of their shift for the 4 models.Parameters: **1** $\alpha_R = 9\,\mathrm{kHz}^{-1}$ (75%), $\alpha_{NLA} = 1.00$, $w = 62.0\,\mathrm{kHz}^{-1}$; **2** $\alpha_R = 9\,\mathrm{kHz}^{-1}$ (75%), $\alpha_{ANL} = 0.80$, $w = 62.0\,\mathrm{kHz}^{-1}$; **3** $\alpha_R = 0\,\mathrm{kHz}^{-1}$, $\alpha_{ANL} = 0.96$, $w = 62.0\,\mathrm{kHz}^{-1}$; **4** $\alpha_R = 0\,\mathrm{kHz}^{-1}$, $\alpha_{IV} = 0.76$, $\sigma_w = 5$

tion and saturate at approximately 120 dB. Consequently, the Fisher information functions of the onset response curves are similar for the three models peaking at the centre of the dynamic range of the onset response curve and falling off approximately symmetrical to the left and right (fig. 3.3 B1 – B3). For the steady state response curves the Fisher information differs between the models: In the NL-A-model the Fisher information of the steady state response curve peaks approximately at the same intensity as for the onset response curve, but it decreases softly towards larger intensities. In the A-NL-model the Fisher information of the steady state response curve is overall lower . While it stays approximately constant if adaptation occurs only in the output neuron, it decreases with intensity if adaptation occurs in the receptor layer, too (fig. 3.3 B2 – B3, respectively), although the trial averaged steady state response curves are identical in both cases. This difference in Fisher information is caused by differences in the response standard deviation (response STD) of the steady state response curve which increases with increasing mean response if there is adaptation in the receptor layer, while it stays constant if adaptation occurs in the output neuron only (fig. 3.3 A2 – A3).

However, the more interesting question is if the shift of adapted response curves realized by these models is able to also shift the region of maximal discrimination to the background intensity. Indeed, for all three models the Fisher information functions of adapted response curves peak at the background intensity, and they all reach similar peak values that are about 1.5 times larger than the peak Fisher information in the individual receptor (fig. 3.3 C1 – C3). The peak Fisher information decreases with increasing background intensity for all models, strongest for the NL-A-model and least for the A-NL-model without adaptation in the receptor layer. In the NL-A-model the decrease in peak Fisher information is primarily due to the decrease in slope of adapted response curves with increasing shift. Additionally, at medium shifts (background intensities around 40 dB) the response STD of adapted response curves is largest (fig. 3.3 D). In the A-NL-models, the adapted response curves hardly change slope with shift and the decrease in peak Fisher information primarily results from the increase in response STD with shift (3.3 D).

But why is the increase in response variability with increasing background intensity larger if there is adaptation in the receptors? In the individual receptor, the response variability of the steady state response curve is larger than that of the onset response curve. The reason is that adaptation contributes to the response variability of a neuron because the response does not only depend on the actual intensity but also on the adaptive state of the neuron. Because of the noise added to the neural responses, the exact time course of the response of a neuron model will vary even for constant stimuli and thus result in slightly different adaptation states which then contribute to the total response variability. In the A-NL-model with receptor adaptation an increase in background intensity leads to the integration of an increased number of receptors in their adapted and hence more variable state, which leads to an increase in the response variability of the output neuron with increasing background intensity (see steady state response curve in fig. 3.3 A2).

In the sum-model with receptor adaptation the effect is not obvious because the noise added to the output neuron dominates the response variability. In the A-NL-model with receptor adaptation the summed receptor responses are saturated and than rescaled and so

the noise of the receptor responses is amplified as compared to the sum-model, and dominates over the noise added to the output neuron.

The invariance model was designed to yield responses that are invariant with the mean stimulus intensity (reflected in a flat steady state response curve) and a perfectly parallel shift of adapted response curves with background intensity. The parameters of the model were chosen to give an onset response curves which corresponds to the onset response curves of the NL-A-model and A-NL-model with respect to width and slope, and consequently the Fisher information function for the onset response curve resembles that of the other models (fig. 3.3 D2). In contrast to the NL-A-model and A-NL-model, the steady state response curve of the invariance model saturates slightly before the onset response curve (fig. 3.3 D1), so that the Fisher information peaks at low intensities (ca 10 dB). As expected from this model, the peak and shape of Fisher information functions for adapted response curves is independent of the shift. It peaks at the respective background intensity and falls symmetrically to lower and higher intensities (fig. 3.3 D3). Somewhat surprisingly, the NL-A-model, A-NL-model and invariance model reach comparably high peak values of Fisher information. In particular the A-NL-model without adaptation in the receptor layer performs even slightly better than the invariance model and almost invariant over background intensities, although it is clearly not intensity invariant, as its steady state response curve rises linearly with intensity.

Influence of the distribution of receptor thresholds Figure 3.4 A shows the hight of the Fisher information of adapted response curves at the background intensity summarized for all models resulting with a uniform distribution of receptor thresholds.

To test the influence of the distribution of receptor thresholds, the NL-A-model, A-NL-model and invariance model were simulated using Gaussian distribution with a mean of receptor operating points of 62 dB and a standard deviation of 17 dB (fig. 3.4 B).

For the Gaussian distribution of receptor thresholds, all four models have the highest values of Fisher information for background intensities of 60 dB, i.e. where the distribution of receptor operating points is centred. The peak Fisher information is higher than for a uniform distribution of receptor thresholds, reflecting the locally larger density of receptor thresholds. For all models the discrimination ability decreases to background intensities lower and higher than 60 dB. While in the A-NL-model with and without receptor adaptation and the invariance model the decrease is approximately symmetric for larger and smaller background intensities, it decreases more steeply for larger than for smaller background intensities in the NL-A-model.

Already with a uniform distribution of receptor thresholds the performance with respect to intensity discrimination was surprisingly similar for the NL-A-model, A-NL-model and the invariance model. For the Gaussian distribution of receptor thresholds the differences between the models become even less pronounced. In particular, no intensity invariance as defined by a flat steady state response curve (that does not transmit any information about the slow components of the stimulus, i.e. the mean) is needed to realize almost invariant discrimination across different background intensities. Interestingly, it is the adaptation in the receptor layer and its influence on the response variability in the output neuron that deteriorates the discrimination ability for larger backgrounds in the A-NL-model.

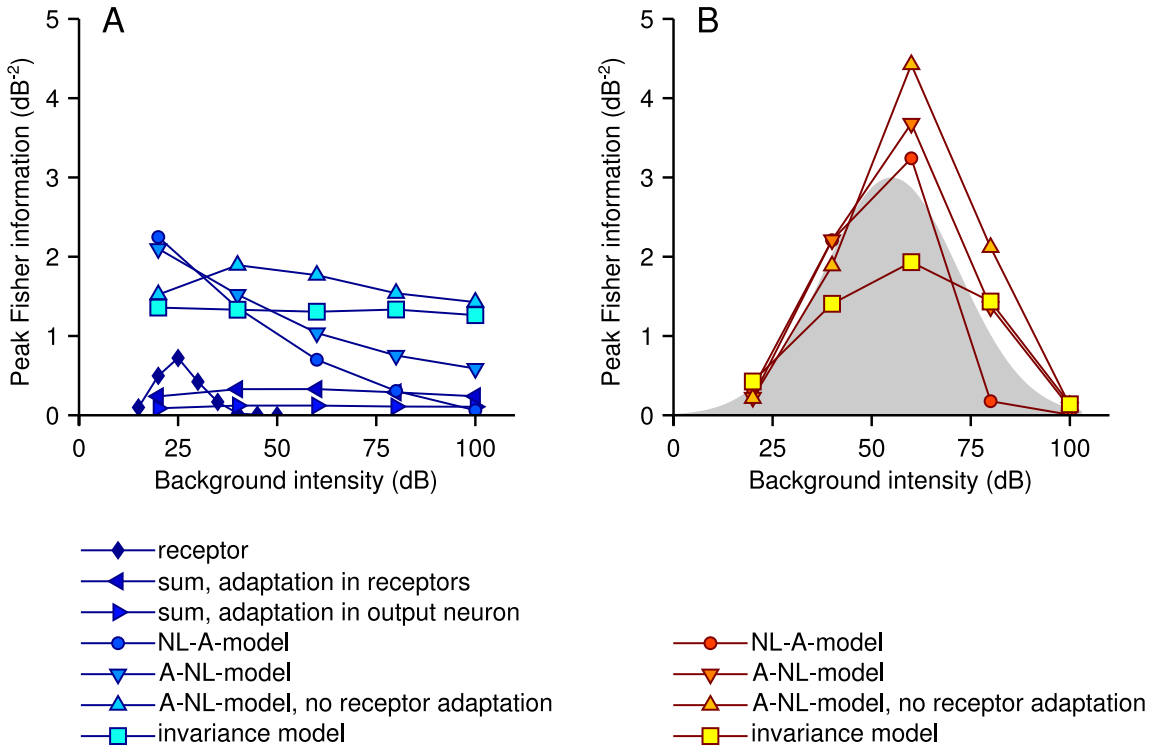

Figure 3.4: Peak Fisher information for different distributions of receptor thresholds. **A** Maximum values of Fisher information of adapted response curves plotted versus the background intensity for a uniform distribution of receptor thresholds for the individual receptor and different output neuron models. **B** Maximum values of Fisher information of adapted response curves plotted versus the background intensity for a Gaussian distribution of receptor thresholds for the NL-A-model, the A-NL-model, and the invariance model.

3.2.2 Encoding of noise stimuli

The encoding of time varying stimuli is a more realistic problem than encoding piecewise constant stimuli. The efficient coding hypothesis states that to maximize the mutual information between the neural response and the stimulus a neuron should set its input-output-relation so that all responses are used with equal probability. For a noise free system, this is realized by choosing the cumulative probability distribution of the stimulus as its intensity response curve (Laughlin, 1981). Optimal response curves derived for noisy responses will differ depending on the relation of the response variability on its mean McDonnell and Stocks (2008), but basically, the operating point and width of the optimal response curve is closely related to the mean and standard deviation of the stimulus.

In this study, the response curves of the models are not fixed but change due to adaptation – how does this effect their coding of time varying stimuli? In the following, the neuron models were driven with band pass filtered noise stimuli to explore how time dependent stimulus waveforms are transmitted as quantified by noise response curves and mutual information.

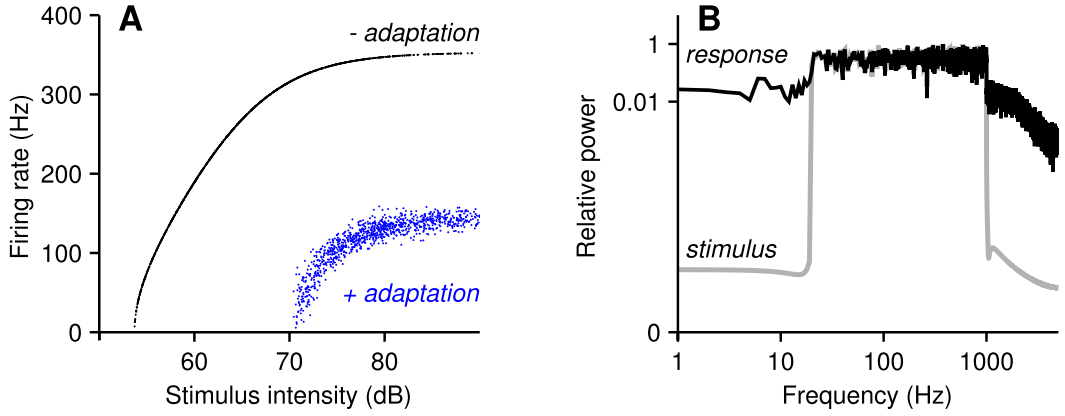

Figure 3.5: Adaptation introduces response variability. **A** Response curves generated from responses to a noise stimulus (receptor model), without (*black*) and with (*blue*) adaptation. The model was noise free, the variability of the response is solely caused by the response driven adaptation. **B** Although the stimulus (*gray*) was band pass filtered to exclude low frequencies to avoid driving adaptation. In spite of excluding low frequencies from the stimulus the response (*black*) is not free of these frequencies so that adaptation is driven anyway.

Noise response curves are generated from the stationary part of the response to a time varying stimulus (i.e. after the decay of the transient) by plotting the signal intensity versus the response at every time point, resulting in a scattered plot (see fig. 3.1).

Even without a noise term added to the receptor current or the output neuron responses, the noise response curve is scattered in a deterministic way that depends on the stimulus time course (fig. 3.5 A). The reason is that due to adaptation, the response to a particular intensity does not only depend on the actual intensity but also on the adaptive state of the neuron which is determined by the responses elicited by previously encountered intensities. In contrast, the response standard deviation to constant stimuli is only increased by adaptation if the neural response is actually noisy. The noise signal was band pass filtered with a lower cut off frequency of 20 dB to avoid the activation of adaptation by lower stimulus frequencies. However, due to the non-linearities of neural transduction the neural response contains low frequencies anyway, which drives the adaptation mechanisms.

Influence of signal variance on noise response curves The models were stimulated with bandpass filtered noise of different means and standard deviations, and noise response curves were constructed from the models' responses. Using a lower cut off frequency of 20 Hz for the noise stimuli, the noise response curves capture the models' coding scheme for fast fluctuating stimuli. For static stimuli, the coding of fast fluctuating stimuli is represented by the onset and adapted response curves. However, the noise response curves to stimuli with a particular mean intensity differ from the adapted response curves for the corresponding background intensity with some respect.

The noise response curves are (except in the invariance model) not invariant under changes of the signal standard deviation (signal STD), and only overlap with the adapted response curves from constant stimuli for small standard deviations. One effect of increasing the signal STD is a difference in the shift of the noise response curve the direction of which depends on the signal mean. For signal means in the lower half of the intensity range covered by receptors (i.e. below 50 dB for the output neuron models), the response curves of all models are shifted to increasingly higher intensities as the signal STD increases (fig. 3.6). For larger signal means (i.e. above 50 dB) an increase in the signal STD leads to increasingly smaller shifts. This is plausible, considering that adaptation is driven by the neurons' responses to the stimulus and not by the stimulus itself. Therefore, for large signal STDs the signal is clipped more strongly by a neuron's response threshold or saturation point, depending on the signal mean. So the response distribution that drives the adaptation has a higher or lower mean than the signal distribution. This effect is observed in all models except for the invariance model in which the neurons have no response driven adaptation mechanisms.

In the models that include adaptation in the receptor layer there is a second effect of increasing signal STD, namely a decrease in the slope of response curves. This is most prominent in the NL-A-model (fig. 3.6 B, D, E). As the signal STD increases the total adaptation in the receptor population increases because more receptors are activated and individual receptors are stronger activated. Consequently, the number of unadapted receptors that could contribute full maximum responses decreases reducing the slope of the summed responses.

A decrease in the slope of response curves with increasing signal STD is referred to as gain control. In the NL-A-model and the A-NL-model it emerges as an epiphenomenon from the interaction of shifting adaptation in a range fractionating receptor population with non-linearities in the output neuron.

Mutual information as a function of signal mean and standard deviation The Fisher information functions showed the models' ability to discriminate nearby intensities at different background intensities. From these results the different models are expected to also vary with respect to the encoding of time varying stimuli. The mutual information is estimated for the responses to a noise stimuli with different means and standard deviations to find the models' preferred combination of stimulus parameters.

To compare different stimulus conditions, the mutual information was normalized by the stimulus entropy. The maximal values of the so normalized mutual information increases from receptor to the output neuron models. The highest values are reached by the invariance model closely followed by the A-NL-model without adaptation in the receptor layer, while the A-NL-model's maximum mutual information is markedly lower. The same holds for the sum-model – it reaches larger maximum values of mutual information if adaptation exclusively occurs in the output neuron than if adaptation occurs in the receptors.

The models differ with respect to their tuning to combinations of signal mean and variance (where the tuning is defined by the mutual information between the model's response to various stimulus conditions). The individual receptor is relatively sharply tuned to a combination of signal mean and signal STD that corresponds to its operating point and dy-

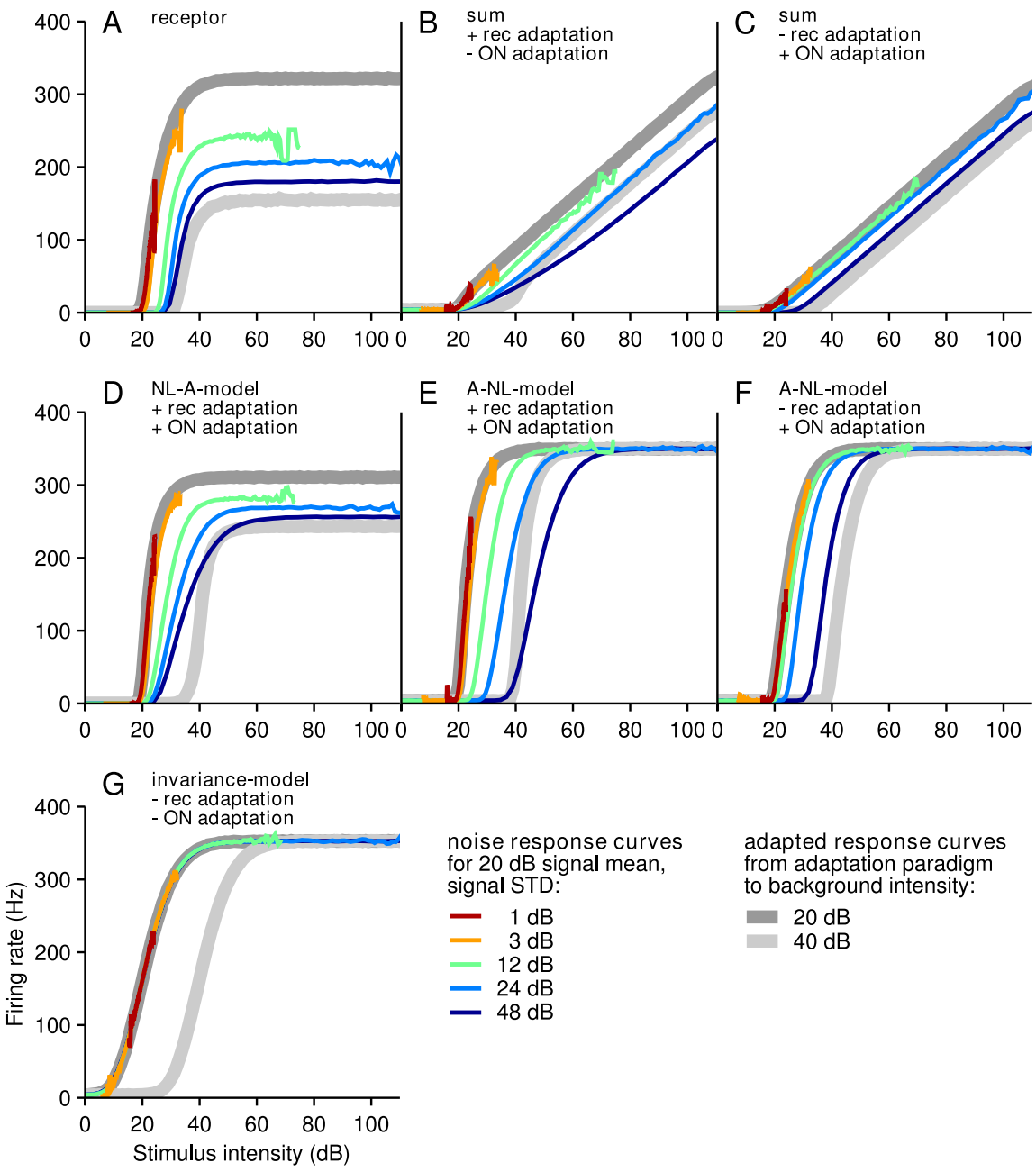

Figure 3.6: Noise response curves for different signal standard deviations for **A** the individual receptor, **B** the sum of receptor responses with adaptation in receptors, **C** the sum of receptor responses with adaptation in the output neuron, **D** the NL-A-model, **E** the A-NL-model with adaptation in receptors, **F** the A-NL-model without adaptation in receptors, **G** the invariance model. The colored lines show fits to the noise response curves for different standard deviations. The grey lines show adapted response curves to constant stimuli for two background intensities, one equal to the mean of the noise stimulus (*dark gray*) and one 20 dB larger (15 dB in **A**).

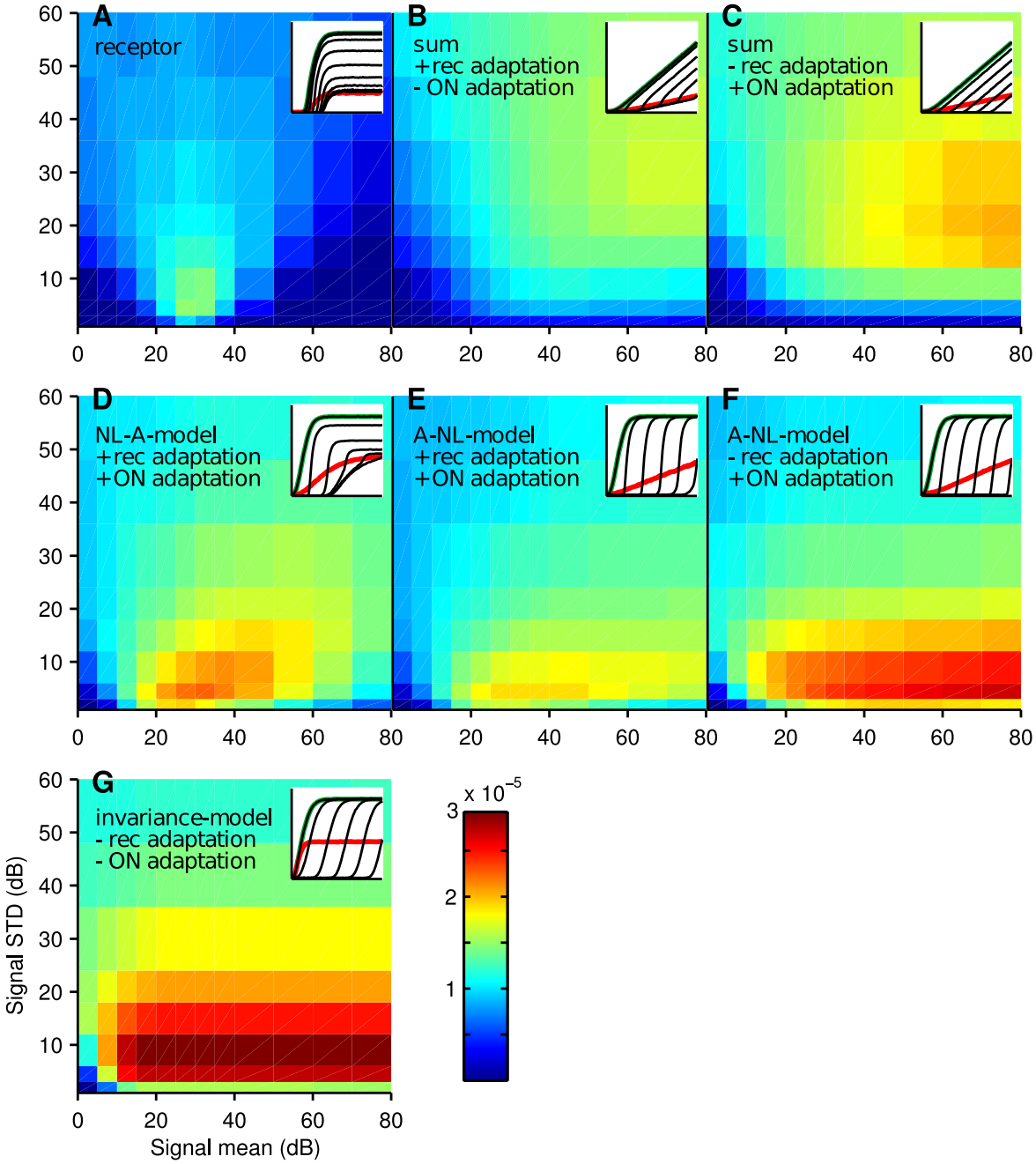

Figure 3.7: Mutual information normalized by the signal entropy as a function of stimulus mean and standard deviation for **A** the individual receptor, **B** the sum of receptor responses with adaptation in receptors, **C** the sum of receptor responses with adaptation in the output neuron, **D** the NL-A-model, **E** the A-NL-model with adaptation in receptors, **F** the A-NL-model without adaptation in receptors, **G** the invariance model. The normalized mutual information is shown in the color plots, insets show the response curves (for constant stimuli) of each respective model.

namic range width. As already observed for the Fisher information, this sharp tuning reflects the individual receptors inability to substantial adaptive adjustments to changing stimulus statistics. The sum-models reach relatively high values of mutual information over a wide range of signal means and signal STDs (fig. 3.7 B, C). In the NL-A-model, the tuning is again sharpened to smaller signal STDs matching width of the model's adapted response curves. Compared to the individual receptor, the NL-A-model maintains high mutual information over a wider range of signal means, corresponding to the width of its steady state response curve (fig. 3.7 D). The A-NL-model shows a relatively sharp tuning to signal STD matching the width of the adapted response curves, while the mutual Information is approximately constant over all tested signal means (fig. 3.7 E, F). The invariance model is tuned to signal STD in a similar way as the A-NL-model, and invariant across signal means (fig. 3.7 G).

Interestingly, the peak values of mutual information are markedly lower in the A-NL-model with adaptation in the receptor layer as compared to the A-NL-model with adaptation in the output neuron only. This is again caused by adaptation acting as a source of response variability, which had already been observed in the Fisher information (fig. 3.2 and 3.3) and noise response curves (fig. 3.6 A).

3.3 Discussion

Shifting adaptation potentially enables a neuron to stay sensitive to small intensity differences over a wide range absolute intensities in spite of its limited response range. In this chapter, the accuracy of intensity discrimination has been quantified for different models by estimating the Fisher information from response curves for different background intensities. Furthermore, the encoding of time varying stimuli was explored by estimating noise response curves and the mutual information for different stimulus conditions.

3.3.1 Intensity discrimination

Do models that shift their response curves to the actual background intensity also discriminate best between intensities around the background? And do these models have an advantage with respect to intensity discrimination above the pure sum of receptor responses?

Indeed, all three models that realize shifting adaptation in the output neuron (NL-A-model, A-NL-model, and invariance model) best discriminate intensities around the background intensity. In contrast, for the sum of receptor responses the Fisher information functions have roughly the shape of a step function rising from zero at the background intensity and staying constant thereafter, i.e. there is no adjustment of highest discrimination accuracy around the background intensity. Additionally, the peak values of Fisher information reached by the NL-A-model, A-NL-model, and invariance model were similar and markedly larger than the peak values reached by the sum-model.

While the Fisher information is centred symmetrically at the background intensity in the invariance model, it has a bias towards intensities larger than the background in the NL-A-model and A-NL-model. The bias of Fisher information towards intensities larger than the mean intensity found in the NL-A-model and A-NL-model has been observed in real

neurons (Dean et al., 2005). In the models it is a result of the shifting adaptation and can be introduced in the invariance model, too, if a response driven adaptation mechanism is included in the receptor layer or output neuron.

A surprising finding was that response driven adaptation could have a negative effect on the Fisher information. A decrease of peak Fisher information with increasing background intensity observed in the A-NL-model depended strongly on the adaptation in the receptor layer, as revealed by the comparison of the A-NL-model with and without adaptation in receptors. The decrease was markedly stronger if receptors adapted, because adaptation contributes to the response variability of a neuron. As the background intensity increases an increased number of adapted and hence more variable receptor responses is integrated.

The way in which the response variance varies within a response curve also influences the shape of the Fisher information functions, e.g. the location of the peak and before mentioned asymmetries. In this chapter, the noise in the response of an output neuron results from additive noise in the receptor current and additive noise on the output neuron's response. Therefore, although the noise sources and strengths are identical for all output neuron models, the way in which the receptor responses are integrated affects the way in which the response variance depends on the response mean and which noise source is dominating. The sum-models average over the responses of all receptors, reducing the noise in the receptor response according to the number of receptors. With the chosen model parameters, the noise term added to the output neuron is dominant over the noise in the receptor layer in these models. In contrast, in the NL-A-model and A-NL-model the scaling factor that determines the slope of the onset and adapted response curves also scales up the variability of the receptor response so that its contribution is obvious in the response variability of the output neuron. This holds for the explicitly added noise terms as well as for the response variability that is introduced by the response driven adaptation mechanism.

Changing the distribution of receptor thresholds from uniform to Gaussian reduced the differences between the NL-A-model, A-NL-model and invariance model even more. The peak Fisher information at a given background intensity reflects the density of receptors centred close to this background intensity.

3.3.2 Encoding of time varying stimuli

For noise stimuli that change faster than the time scale of the adaptation dynamics of the neuron, the noise response curves were expected to be similar to the adapted response curves measured with constant stimuli. However, only for very small signal STDs the noise response curves actually overlapped with the corresponding adapted response curve. An increase in signal STD resulted in a changed shift in all models except for the invariance model, because the adaptation in these models is driven by the response not the stimulus. Stimuli with the same mean will elicit subthreshold or saturated responses more often as their variance grows so that the mean response changes with the stimulus variance if e.g. subthreshold responses are evoked more often than saturated responses or vice versa.

Interestingly, in the NL-A-model and A-NL-model with receptor adaptation an increase in signal STD additionally leads to a decrease in slope (and increase in dynamic range) of the noise response curves. With increasing signal STD the adaptation in the receptor

layer increases further reducing the available response range of receptors, which results in a smaller slope in the output neuron. The change in response slope in the NL-A-model does not adjust the neurons width of the dynamic range to match the width of the stimulus probability distribution, e.g. the mutual information for the NL-A-model shows no invariance with respect to signal STD. Still this finding implies that shifting adaptation in the receptor layer might contribute to slope changes in higher order neurons. Furthermore it emphasizes how the stimulus paradigm chosen to characterize the adaptational effects on a neuron's input output relation can influence the results.

With respect to the mutual information, the individual receptor shows a strong preference for stimuli with a mean close to its operating point and standard deviations corresponding to the width of its response curve. The output neuron models with linear response curves that rise over the full range of relevant intensities (sum-models) show little preference for mean or standard deviations. In contrast, the models with shifting adaptation show a clear preference for a certain range of standard deviations (smaller or equal to their dynamic range) while they encode reliably over a relatively wide range of mean intensities. The invariance with respect to signal mean is largest in the A-NL-model without receptor adaptation and the invariance model, which also reach the largest peak and total values of mutual information.

3.3.3 Adaptation as a source response variability

In all parts of this chapter response driven adaptation was found to increase response variability. One explanation of this phenomenon is that due to adaptation the response to a given intensity does not only depend on the actual intensity but also on the adaptive state of the neuron which depends on the past responses (for response driven adaptation). For constant stimuli an effect of adaptation on response variability occurs only if the neural responses are intrinsically noisy and only if the adaptation is response driven. In contrast, however, for time varying stimuli adaptation can act as the only source of response variability. A reduction in spike-count reliability due to adaptation has been found in spiking neurons (Avissar et al., 2007).

3.3.4 Shifting response curves and intensity invariance

An interesting finding of this chapter was the similarity in performance of the A-NL-model without receptor adaptation and the invariance model. The invariance model is intensity invariant in the sense of transmitting no information about the mean intensity, as reflected in its flat steady state response curve. In contrast, the steady state response curve of the A-NL-model rise linearly over the full intensity range that is covered by receptors, so that the models always transmits information about the mean intensity, i.e. its responses are not intensity invariant.

Both models realize a parallel shift of adapted response curves to the actual background intensity without a change in slope or maximum response. The peak Fisher information stays constant over all background intensities in the invariance model and almost constant in the A-NL-model, similarly, both models keep high values of mutual information over the full intensity range. In this sense, the A-NL-model shows a high degree of invariance.

3.3.5 Conclusions

In terms of intensity discrimination the shifting of steep response curves is clearly superior to wide response curves, centring the highest discrimination accuracy around the current intensity background. On the other hand, shifting adaptation does not lead to much larger peak or total values of mutual information than shallow response curves (exception: invariance model and the A-NL-model without receptor adaptation). But the two strategies differ with respect to their tuning to stimulus mean and variance. While the models with shallow response curves encode a large range of stimulus means and standard deviations with similar reliability, the models with shifting response curves have a clear preference for a small range of standard deviations. In this thesis the distribution of receptor thresholds is implicitly used to reflect the distribution of biologically relevant stimulus intensities. Based on this full distribution of intensities the efficient coding hypothesis would predict a response curve that rises over all these intensities to be optimal. Shifting steep response curves with the slowly changing stimulus mean was plausible if the intensity distribution encountered on short time scales is narrower than that encountered over long time scales.

In the previous chapter, the interaction of non-linearities with adaptation mechanisms that shift response curves along the input axis has been found to be responsible for complex features of the adapted response curves (e.g. reduction in maximum response). The results of this chapter again showed surprising effects that arise from the interaction of shifting adaptation with static non-linearities.

4 Comparing Adaptation in Ascending Auditory Interneurons of Two Cricket Species

In the first part of this thesis, the auditory interneuron AN1 of the cricket had been chosen as a model system to derive models that explain the emergence of adaptive shifts of response curves in a convergent network. A static saturating non-linearity in the output neuron together with adaptation in both receptors and the output neuron sufficed to reproduce a shifting of response curves. Depending on the placement of the adaptation mechanism in the output neuron and the non-linearity, the pattern of response curves differed characteristically. If the non-linearity preceded adaptation in the output neuron (NL-A-model), the maximal responses of adapted response curves decreased with increasing shift, whereas they remained constant if the saturation follows the adaptation in the output neuron (A-NL-model).

In the cricket species *Teleogryllus oceanicus*, adapted response curves show characteristics similar to that of the NL-A-model, i.e. they show a marked decrease in maximum response with increasing shift (Benda and Hennig, 2008). In a repetition of these experiments with crickets of the species *Gryllus bimaculatus* (Beul, 2010) the response curves showed no reduction in the maximum response of adapted response curves, similar to those generated by the A-NL-model. In this chapter, the data of the two species were re-analysed in the light of the models, and both models were fitted to either species' data sets to investigate if the differences between the response curves require for different models, or if one model could explain the deviations when adjusting parameters accordingly.

While the AN1 integrates the responses of the LF receptors and is assumed to participate in recognition and localization of conspecific songs, the second ascending interneuron (AN2) gets input from LF and HF receptors with higher impact of the HF receptors (Nolen and Hoy, 1987) and is considered to mediate predator avoidance via detection and localization of bat echolocation calls. The response curves of the AN2 in *G. bimaculatus* are similar in general to those of the AN1 in this species in that they are shifted towards an intensity background. They differ, however, by having a higher absolute response threshold and the detailed shape of their response curves, which often show an increase in slope around their operating point. The population of ultrasound receptors also has differing response thresholds, i.e. is similarly organized as the low frequency receptor population. However, the small size of the ultrasound receptor population (which comprises only about 10 receptors, Imaizumi and Pollack 2001 provides the interesting aspect of a potentially irregular distribution of thresholds. In the last part of this chapter the AN2 data were fitted by the two models using a smaller population of receptor thresholds.

4.1 Methods

4.1.1 Preparation and recording

Preparation Data were recorded from adult crickets of the species *Teleogryllus oceanicus* and *Gryllus bimaculatus*. The preparation technique is described in Benda and Hennig (2008) (see also Hennig (1988)) for *T. oceanicus* (the recordings from *T. oceanicus* used in this study are the same as those published in Benda and Hennig (2008)). The same procedure was used for *G. bimaculatus*.

Recording and stimulation Responses of the AN1 and the AN2 were obtained from extracellular dual hook electrode recordings from the connective between the prothoracal and the subesophageal ganglion, which contains the axons of AN1 and AN2. The voltage traces were stored for offline spike detection.

AN1 and AN2 are separable by their action potential amplitude and by comparing their physiological properties. The ANs were stimulated acoustically by loudspeakers positioned on the side ipsilateral to the input side of the recorded AN1 or AN2, perpendicular to the crickets longitudinal axis as described in Benda and Hennig (2008).

For details on recording and stimulation technique see Benda and Hennig (2008), experiments with *G. bimaculatus* followed the same scheme.

Pure tones of 4.5 kHz (AN1) and 16 kHz (AN2) were presented for 500 ms at different intensities, 30-93 dB SPL in steps of 3 dB SPL for *T. oceanicus* (Benda and Hennig, 2008), and 42-96 dB SPL in steps of 6 dB SPL for *G. bimaculatus*. The constant amplitude pulses were interrupted by 1.5 s periods of silence.

Experimentalists Experiments on *T. oceanicus* were carried out by Matthias Hennig and results of these experiments have been published before in another context (Benda, 2002; Benda and Hennig, 2008). *G. bimaculatus* AN1 and AN2 responses were recorded by Sarah Beul and analysed by Sarah Beul and myself.

4.1.2 Data analysis

The time dependent spike frequency $r(t)$ at a time point t, was calculated from the spike trains as the inverse of the interspike interval that contains the respective time point (compare Benda and Herz (2003); Benda and Hennig (2008); Hildebrandt et al. (2011)). Mean and standard deviation were calculated across 25 repetitions of the same stimulus, and the trial-averaged spike frequency was smoothed by a running average (3 ms rectangular time window).

Response curves The onset response r_0 was defined as the maximal spike frequency in a time window of 100 and 20 ms (*T. oceanicus* and *G. bimculatus*, respectively) following the onset of a test pulse. The steady state response r_∞ was defined as the mean response across a time window of 150 (100) ms starting 300 (400) ms after stimulus onset in *T. oceanicus* (*G. bimaculatus*). The differences in the intervals have no substantial effect on properties of the response curves.

Adapted response curves r_a were measured using the paradigm described in Benda and Hennig (2008): A pure tone of constant background sound intensity S_b is played for 800 ms allowing the neurons response to settle to steady state. From this background intensity test pulses of different intensities were presented for 50 ms for test pulse intensities above the background intensity and 100 ms for test pulse intensities below background intensity. The adapted response curves are constructed from the onset responses to these test pulses.

To avoid overestimation of responses at low frequencies, the spike frequency responses were compared to the spontaneous response, i.e. the time averaged spike frequency 200 ms prior to stimulus onset. If the response before and after stimulus onset (or onset of a test pulse in the adaptation paradigm) did not differ significantly by means of a Wilcoxon ranksum test, the onset and stationary responses were set to the value of the spontaneous response.

For parametrization response curves were fitted by a Boltzmann function:

$$h(s) = \frac{R^{max} - R^{min}}{1 + \exp\left(-k\left(s - S^o\right)\right)} + R^{min} \ . \tag{4.1}$$

For the steady state response curves and adapted response curves, R^{min}, R^{max}, k and S_o were fitted (MATLAB built in function nlinfit). The minimum response R^{min} of the onset response curve was fixed to the minimum response obtained from the fit to the steady state response curve, and only the three remaining parameters, R^{max}, k and S^o were fitted.

The threshold and saturation point were defined as the intensity at the intersection point of the tangential g to the Boltzmann function at the point $[S^o, h(S^o)]$ with R^{min} and R^{max}, respectively (Benda and Hennig, 2008)

$$\begin{aligned} g(s) &= \left.\frac{dh}{ds}\right|_{s=S^o} \cdot (s - S^o) + h(S^o) & (4.2)\\ &= \frac{k(R^{max} - R^{min})}{4}(s - S^o) + \frac{R^{max} - R^{min}}{2} + R^{min} \ . & (4.3) \end{aligned}$$

From $g(s) = R^{min/max}$ follow the threshold $S^{thr} = S^o - \frac{2}{k}$ and saturation point $S^{sat} = S^o + \frac{2}{k}$, the dynamic range width $DR = \frac{4}{k}$, and the slope $\Delta s = (R^{max} - R^{min})\frac{k}{4}$.

The adaptation state of a neuron is quantified by the shift A along the intensity axis of the adapted response curve relative to the onset response curve (defined by the difference in response thresholds of the onset and adapted response curve). A reduction in the coding range (the difference between maximum and minimum response, $R^{max} - R^{min}$) of adapted response curves with increasing shift A is quantified by normalizing the coding range of the adapted response curve to that of the onset response curve:

$$\gamma = \frac{R_a^{max} - R_a^{min}}{R_0^{max} - R_0^{min}} \tag{4.4}$$

where γ is the relative coding range of an adapted response curve, superscripts a and 0 refer to adapted and onset response curves, respectively. In general we evaluate the relative coding range γ as a function of the shift A of the respective response curve.

Data selection Recordings of 12 AN1s of *T. oceanicus*, 7 AN1s, and 9 AN2s of *G. bimaculatus* (from 12, 7, and 9 animals, respectively) were selected for fitting. Selected data sets had a spontaneous activity of less than 55, 75, and 55 Hz for *T. oceanicus* AN1, *G. bimaculatus* AN1, and *G. bimaculatus* AN2, respectively, and an absolute response threshold below 55 and 65 dB SPL (AN1 and AN2, respectively). The threshold of onset response curves measured in the beginning and end of each experiment must not differ more than 8 dB.

4.1.3 Models of the ascending interneurons AN1 and AN2

As the response curves of the two cricket species shared features of the response curves of the NL-A-model and A-NL-model but not the other output neuron models derived in chapter 2, these two models were used to mimic the network of the AN1 and AN2. The AN1's responses to low frequency pure tone stimulation corresponding to the carrier frequency of calling songs, and the AN2's response to ultrasound stimulation were simulated.

Receptor model Based on Imaizumi and Pollack (2001), $N_{LF} = 40$ low frequency receptors were used as input to the AN1, and $N_{HF} = 11$ high frequency receptors as input to the AN2 at ultrasound stimulation. The response characteristics of low and high frequency receptors was assumed to be identical, except for their adaptation strength α_R which was a parameter in the fitting process. Individual model receptors in a population differed only by their operating points s^o.

In the first step, the sound pressure level s is translated into a receptor current I, which is modelled by a Boltzmann function. For a receptor centred at s^o_j the normalized receptor current I_j is given by

$$I_j(t) = \frac{1}{1 + \exp\left(-c\left(s(t) - s^o_j\right)\right)} - I^o \tag{4.5}$$

where subscript j indicates the j$^{\text{th}}$ receptor in the population, s^o_j its operating point, c determines the slope and I^o an offset, $c = 0.2\,\text{dB}^{-1}$ and $I^o = 0.16$ were used for all receptors. The receptor current is then translated into the firing rate response of the receptor:

$$r_{R,j}(t) = \frac{r^{max}_R}{\sqrt{1 - I^o}} \sqrt{[I_j(t) - A_{R,j}(t)]_+} \tag{4.6}$$

where r^{max}_R is the maximum response identical for all receptors, and $[\cdot]_+$ symbolizes rectification to positive values. r^{max}_R was set to 350 Hz. The adaptation current $A_{R,j}$ follows

$$\tau_R \frac{dA_{R,j}(t)}{dt} = -A_{R,j}(t) + \alpha_R \cdot r_{R,j}(t) \tag{4.7}$$

with fixed time constant $\tau_R = 40$ ms (Benda and Herz, 2003). The adaptation strength α_R is a free parameter in the following fitting process, identical for all receptors in a population.

Models of the ascending interneurons The response curves of the AN1 and AN2 were fitted by the NL-A-model and the A-NL-model from chapter 2. The output neuron's response

according to the NL-A-model is given by

$$r_{NLA}(t) = \left[r^{max}\Theta\left(w \cdot r_{\sum}(t)\right) - A_{NLA}(t)\right]_+ \tag{4.8}$$

where $r_{\sum} = \sum_{i=1}^{N} r_{R,i}$ is the sum of receptor responses, w weights the receptor input, r^{max} scales the output firing rate, Θ denotes the saturating non-linearity (see below 4.12), and A_{NLA} is the adaptation current in the AN1 or AN2 which, in the NL-A-model, follows

$$\tau_{AN}\frac{dA_{NLA}(t)}{dt} = -A_{NLA}(t) + \alpha_{NLA} \cdot r_{NLA}(t) \tag{4.9}$$

with time constant τ_{AN}, and α_{NLA} the adaptation strength of the NL-A-model.

In contrast, in the the A-NL-model, the adaptation precedes the non-linearity and is driven by the summed input:

$$r_{ANL}(t) = r^{max}\Theta\left(\left[w \cdot r_{\sum}(t) - A_{ANL}(t)\right]_+\right) \tag{4.10}$$

where A_{ANL} is the dimensionless adaptation current in the AN1 or AN2, which, in this model, follows

$$\tau_{AN}\frac{dA_{ANL}(t)}{dt} = -A_{ANL}(t) + \alpha_{ANL} \cdot w \cdot r_{\sum}(t) \tag{4.11}$$

with time constant τ_{AN}, and the dimensionless adaptation strength of the A-NL-model α_{ANL}.

The saturating non-linearity Θ for both models is given by the sigmoid function

$$\Theta(x) = 2 \cdot \left(\frac{1}{1 + \exp(-x)} - 0.5\right) . \tag{4.12}$$

The non-linear function was fixed for all simulations. The offset of the non-linearity does influence the shape of the intensity response curves but effects can be compensated by adjustment of other parameters (in particular the weight w and receptor adaptation strength α_R) and with a sharp threshold of the non-linearity ($h_0 = 0.5$) the fitted receptor adaptation strengths α_R tended to be in a more plausible range. The adaptation time constants of receptors and ANs were set to 40 ms.

Model parameters In chapter 2 the model parameters with the strongest influence on the shape of response curves had been identified:

The maximum firing rate of an AN1 (AN2) r_{AN}^{max} and the synaptic weight w determine the scale and slope of response curves. An important factor is the adaptation strength of receptors α_R and the AN1 (AN2) α_{NLA} and α_{ANL} that influence the maximum response of the stationary response curve and the shift of adapted response curves. The receptor adaptation strength has also an effect in shaping the threshold region of adapted response curves. A large impact is imposed by the distribution of response thresholds (for simplicity called 'receptor distribution' from now on). The local density of receptor thresholds on the intensity axis is reflected in the slope of the there localised adapted onset response curves and the local slope of the stationary response curve. The receptor distribution has been found

to be roughly bell-shaped for low frequency receptors (i.e. the input to the AN1) while ultrasound receptors (input to the AN2) are somewhat bimodally distributed (Imaizumi and Pollack, 2001).

Based on these experimental findings, the AN1 data were first fitted with a Gaussian receptor distribution, the mean μ and standard deviation σ of which were fitted by the algorithm. The operating points of receptors s_i^o were calculated from the inverse cumulative normal distribution function F^{-1}

$$s_i^o = \mathrm{F}^{-1}(p_i; \mu, \sigma) \tag{4.13}$$

where $p_i = \frac{i-0.5}{N}$, $i \in [1, N]$, and

$$p_i = \frac{1}{\sqrt{2\pi\sigma^2}} \int_{-\infty}^{s_i^o} \exp^{-\frac{1}{2}\left(\frac{u-\mu}{\sigma}\right)^2} du \tag{4.14}$$

The number of receptors used in simulations was 40 for the AN1 models and 11 for the AN2.

Secondly, the models were fitted to the data using every receptor operating point s_i^o as an individual model parameter (AN2 data were only fitted with individual receptor thresholds, because at small numbers of receptors the exact position of individual receptors might play a role in shaping response curves). The probability density functions of the fitted receptor distributions were estimated from histograms using a kernel smoothing algorithm (MATLAB (c) function ksdensity) with a kernel width of 5 dB.

Eventually, 6 free parameters remain to be fitted in the case of a Gaussian receptor population, and 44 (AN1) and 15 (AN2) for individually fitted receptor thresholds.

Simulations Onset and steady state response curves were constructed from onset and steady state responses to stimulus intensity s (dB SPL). Since the firing rate models have no response latencies, the onset response was defined as the first data point of the response after stimulus onset, and the steady state response was defined as the last data point of the response to a 400 ms constant input. Adapted response curves were constructed from the onset responses to short test pulses after the model was adapted to a constant background intensity for 400 ms. The model was adapted to a background intensity only once and the steady state firing rate and adaptation current were used as initial values for test pulses of different intensities.

The response curves of experiments and simulations were evaluated identically.

Fitting procedure Prior to fitting the models to the data sets, the lowest spike frequency across all response curves was subtracted from all response curves to avoid the necessity to fit an overall offset. The models were fitted to the data using a MATLAB(c) built in fitting algorithm (fminsearch, 1500 iterations). The initial values were set individually by hand for each set of response curves to minimize the number of iterations required by the algorithm.

During the fitting process the total mean squared error between the modelled and measured response curves was minimised ($RMSE = rmse(r_0)+rmse(r_\infty)+\sum_{i=1}^{M} rmse(r_{a,i})$, $rmse(r_0)$, $rmse(r_\infty)$, and $rmse(r_{a,i})$ referring to the mean squared error for the onset response curve,

steady state response curve, and i$^{\text{th}}$ adapted response curve, respectively). The $rmse$ for any response curve $r(s)$ is defined as:

$$rmse(r(s)) = \sqrt{\frac{1}{N}\sum_{i=1}^{N}\left(r^{exp}\left(s_i\right) - r^{mod}\left(s_i\right)\right)^2} \tag{4.15}$$

where N is the number of data points in a response curve, superscripts exp and mod indicate the experimentally measured and modelled response curve, respectively. In this case, each response curve contributes the same weight to the fitting process.

To explore the models' ability to predict adapted responses from onset and steady state, the models were also fitted to the onset and steady state response curves alone ($RMSE = mse(r_0) + mse(r_\infty)$) and adapted response curves were simulated with the so obtained parameters (this will be referred to as the prediction paradigm in the following).

To compare the $RMSE$ across data sets with different numbers of adapted response curves, the total $RMSE$ across all response curves was calculated after termination of the fitting process normalised for the number of adapted response curves $RMSE = rmse(r_0)+rmse(r_\infty)+\frac{1}{M}\sum_{i=1}^{M} rmse(r_{a,i})$, M is the number of measured response curves.

4.2 Results

4.2.1 Differences in the response curves of T. oceanicus and G. bimaculatus

In principle, the response curves of *T. oceanicus* and *G. bimaculatus* follow a common scheme: in both species the AN1's adapted onset response curves are shifted towards the sound intensity they had been adapted to. However, the two species seem to show a qualitative difference with respect to their adapted response curves: while the maximum response of adapted response curves is reduced with increasing shift in *T. oceanicus* (Benda and Hennig, 2008) it seems rather constant in *G. bimaculatus* (Beul, 2010). In order to quantify possible differences between the two species' response curves, the response thresholds, dynamic ranges, coding ranges, slopes, and adaptive shifts are estimated from the response curves of 12 AN1s of *T. oceanicus* and 7 AN1s of *G. bimaculatus*.

Onset and steady state response curves The absolute response thresholds are on average around 40 dB in *T. oceanicus* and about 7 dB larger in *G.bimaculatus*. The average dynamic range of the onset response curve is almost identical in the two species, 16 and 15 dB (*T. oceanicus* and *G.bimaculatus*, respectively). In both species, the dynamic range of the steady state response curve is wider than that of the onset response curve, 29 dB (a factor 1.8) in *T. oceanicus* and 36 dB (factor 2.2) in *G. bimaculatus*. The coding range, i.e. the difference between minimum and maximum response, of onset response curves is 181 and 255 Hz in *T. oceanicus* and *G. bimaculatus*, respectively. The strength of adaptation estimated from the reduction in the coding range from onset to steady state is 55 % in *T. oceanicus* and 63 % in *G. bimaculatus*.

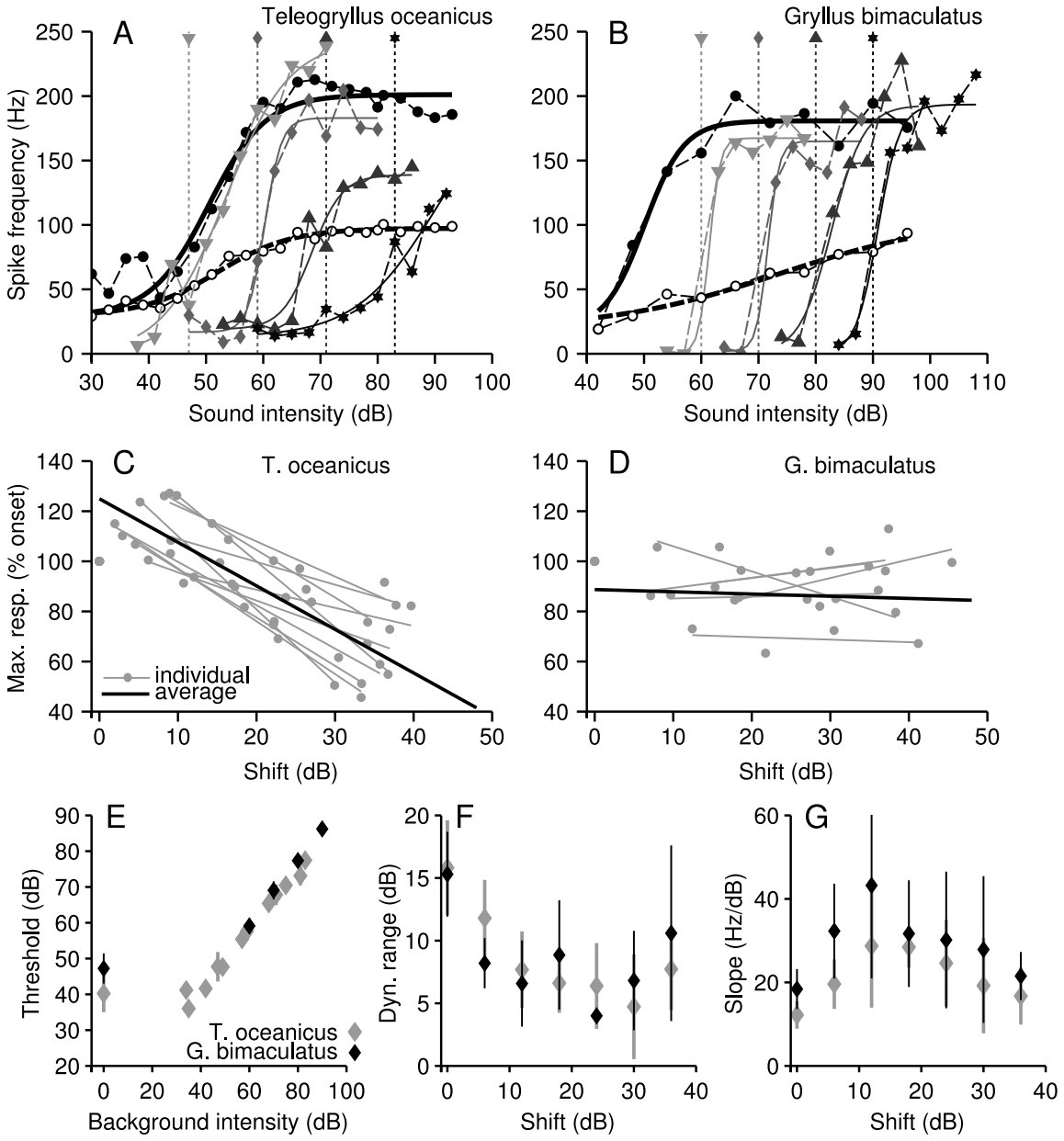

Figure 4.1: Differences between the response curves of *T. oceanicus* and *G. bimaculatus*. **A** and **B** Onset, steady state and adapted response curves of *T. oceanicus* and *G. bimaculatus*, respectively. Symbols connected by dashed lines represent measured data (black filled and open circles: onset and steady state response curves; grey: adapted response curves, the corresponding background intensities are indicated by vertical dotted lines). Solid lines are fits of Boltzman functions to the data. **C** and **D** Maximum response of adapted response curves relative to the maximum of the onset response curve as a function of their shift relative to the onset response threshold for *T. oceanicus* and *G. bimaculatus*. *solid grey lines* linear regression to the maximum responses of individual cells, solid black line: average regression line. **E** Response thresholds of onset and adapted response curves as a function of background intensity. **F, G** The dynamic range and slope of onset and adapted response curves as a function of their shift.

Adapted response curves The prominent difference between the two species is the decrease of maximum response of adapted response curves with increasing shift observed in *T. oceanicus* but not *G. bimaculatus*.

In figure 4.1 C and D) the maximum responses of adapted response curves (in percent of the maximum onset response) are shown a a function of their shift for all recordings of *T. oceanicus* and *G. bimaculatus*. The average regression line through the data points is -1.7 % per dB shift in *T. oceanicus* (significanly different from 0, signtest) but only 0.09 % per dB shift in *G.bimaculatus* (not significantly different from 0). Therefore, the decrease of maximum responses with shift is a consistent feature of the response curves of *T. oceanicus* but not *G. bimaculatus*.

Except for the reduction in maximum response the adapted response curves of both species behave largely similar. For *T. oceanicus* adapted response curves were measured to background intensities up to 83 dB, i.e. a range roughly 45 dB above response threshold. In the range between 40 and 83 dB, the adapted response curves shift approximately linearly with the background intensity with a slope of 0.86 (figure 4.1 C). The AN1 of *T. oceanicus* can therefore follow changes in background intensity over at least 43 dB, a range almost 3 times larger than the dynamic range of the onset response curve, and approximately 1.5 times larger than the dynamic range of the stationary response curve. In a similar way, the AN1s of *G. bimaculatus* shift their threshold linearly with background intensity across the range of background intensities tested (between 60 an 90 dB) with a slope of 0.9 (figure 4.1,C). Although lower and higher background intensities were not tested, it is possible to estimate a range of shift of at least 40 dB. The slopes of adapted response curves have maximum values at shifts between 12 and 18 dB in both species. Accordingly, the dynamic ranges of adapted response curves take very similar values in both species, ranging between a minimum of 4 to 5 dB at shifts between 12 and 30 dB and a maximum of 15 to 16 dB a small shifts (figure 4.1,E).

4.2.2 What causes the differences between the two species?

The population analysis of the response curves of *T. oceanicus* and *G. bimaculatus* confirmed that qualitative differences exist between the two species. The maximum responses of adapted response curves are indeed approximately constant in *G. bimaculatus* and decrease markedly in *T. oceanicus*. Furthermore, while the dynamic range of the onset responses is identical in both species, the dynamic range of the steady state response curve is larger in *G. bimaculatus*. These differences are interesting because they are very similar to the differences between the response curves generated by the NL-A-model and that of the A-NL-model (compare fig 2.6 in chapter 2). While the response curves of *T. oceanicus* resemble those of the NL-A-model, the response curves of *G. bimaculatus* resemble more those of the A-NL-model.

Consequently, each species response curves might be modelled best by one of the models. In order to test this assumption, both species response curves were fitted by both models.

Fits to the AN1 of T. oceanicus The decrease in the maximum response of adapted response curves characteristic of *T. oceanicus* is an inherent feature of the response curves

generated by the NL-A-model, whereas the maximum responses of adapted response curves generated by the A-NL-model stay constant up to background intensities that lay within the dynamic range of the steady state response curve (compare chapter 2). The NL-A-model is expected to yield good fits to the data of *T. oceanicus*, however, the A-NL-model might also yield good fit results if the distribution of receptor thresholds is relatively narrow. Indeed with respect to the root mean squared error (RMSE), the two models do not differ significantly (RMSE, 39 vs 38 Hz for the NL-A-model and the A-NL-model with Gaussian distribution of receptor thresholds, respectively; p¿0.05, Wilcoxon ranksum test).

Figure 4.2 A and B shows typical fits of the NL-A-model and the A-NL-model to the response curves of *T. oceanicus* with a Gaussian distribution of receptor thresholds. The fits of the NL-A-model and the A-NL-model are almost indistinguishable. Both models fairly reproduce the shapes of onset and adapted response curves, including the decrease in maximum response. The dynamic ranges and coding ranges of onset and steady state response curve in the example do not differ for the two models. Both models fit a steady state response curve which is shifted to larger intensities with respect to the experimentally measured one, a systematic error which is found in the majority of fits for this species. Notably, the fitted distributions of receptor thresholds (figure 4.2 A and B, lower panels) are almost identical for the two models, with a mean of 62 and 63 dB (NL-A-model and A-NL-model) and a standard deviation of 9 dB, respectively.

In the case of *T. oceanicus* the threshold part of onset response curves and adapted response curves to background intensities near absolute threshold often have a small shoulder. This shoulder is not reproduced by the models when the distribution of receptor thresholds is Gaussian. If response curves deviate from the strict sigmoid, this might be explained by the local densities of receptor thresholds. Therefore, the fitting was repeated with every receptor threshold being a parameter of the model assuming this would improve the fit (4.2 C and D). With such individually fitted receptor thresholds, the shoulder in the onset response curve is approached by the models. The resulting distributions of receptor thresholds (figure 4.2 C and D, lower panels) have heavier tails than the corresponding Gaussian distributions. However, the individually fitted thresholds of the two different models are very similar (mean 63 and 65 dB and standard deviation 16 and 14 dB for the NL-A-model and A-NL-model). In the example, the individual fitting of receptor thresholds did not result in a better fit. Across al 12 data sets, the individual fitting of receptor thresholds slightly improved the fit of both models, reducing the RMSE to 34 and 35 Hz (p¡0.05 for the A-NL-model, Wilcoxon ranksum test).

The thresholds, dynamic ranges, coding ranges an slopes of modelled response curves were estimated in the same way as for the experimental data to reveal whether the models fail to reproduce particular aspects of the data systematically. For the adapted response curves the fits yield very good matches of these response curve parameters with those estimated from experiments (fig. 4.3). In particular, the linear relation between adaptive shift and background intensity and the nonmonotone dependence of slope and dynamic range on the adaptive shift are well fit. The relative coding range of adapted response curves (figure 4.3, C) decreases almost linearly with the shift for shifts larger than zero. All models follow this decrease but underestimate the coding range for shifts between 6 and 12 dB.

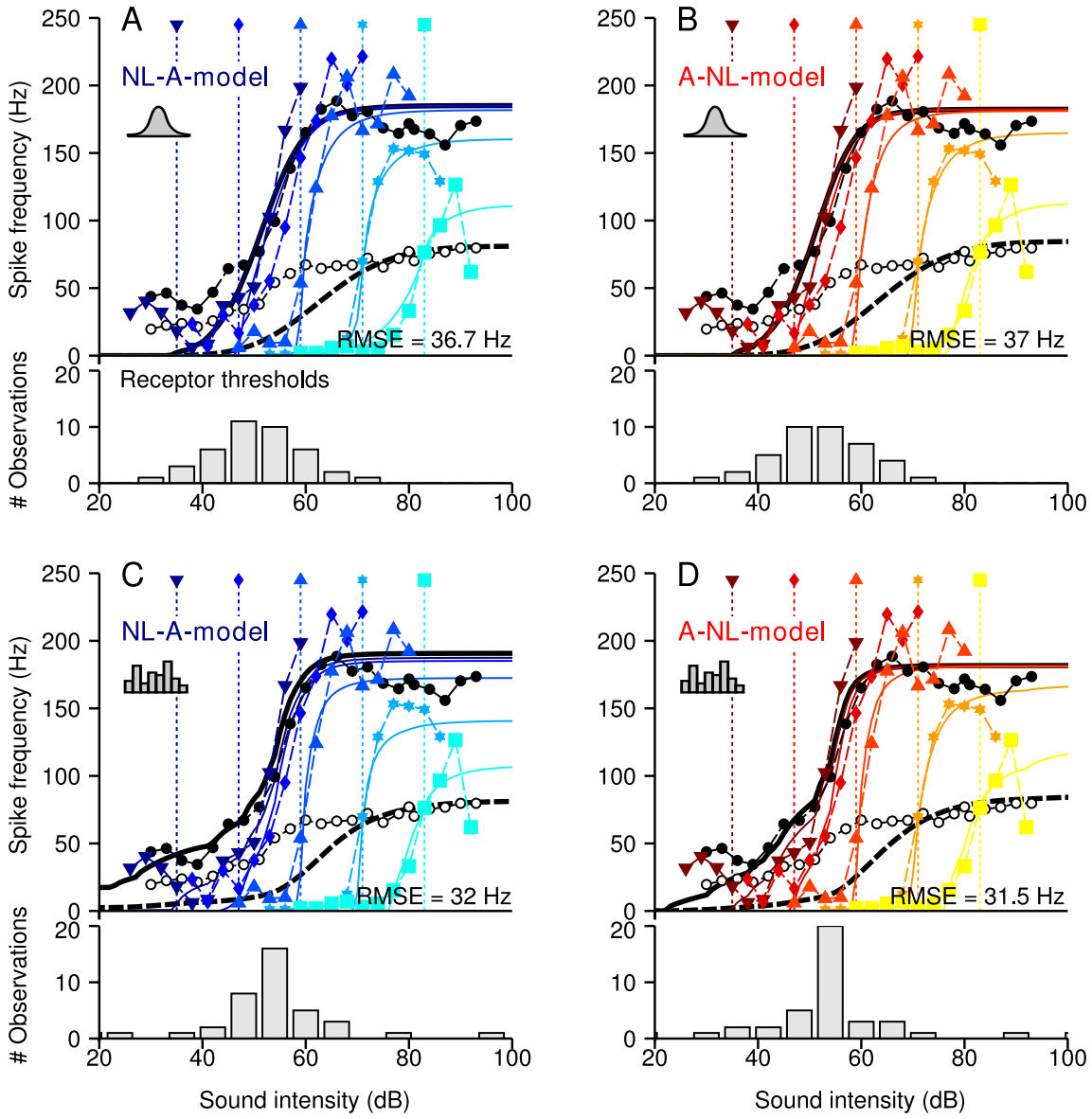

Figure 4.2: Model fits to intensity-response curves of *Teleogryllus oceanicus* AN1. Respective upper panels show intensity response curves, lower panels show the distribution of receptor response thresholds as resulting from the fitting procedures. Modelled responses are represented by solid lines, experimental data by markers connected by dashed lines. Onset and stationary responses (open and filled circles, respectively) are plotted in black, adapted responses color coded in blue (NL-A-model) and red (A-NL-model), respectively. The background intensities to adapted response curves are indicated by dashed lines in respective color. The mean squared error between data and fit is printed in every panel. **A** and **C** NL-A-model with Gaussian and individually fitted receptor thresholds, respectively. **B** and **D** A-NL-model with Gaussian and individually fitted receptor thresholds, respectively.

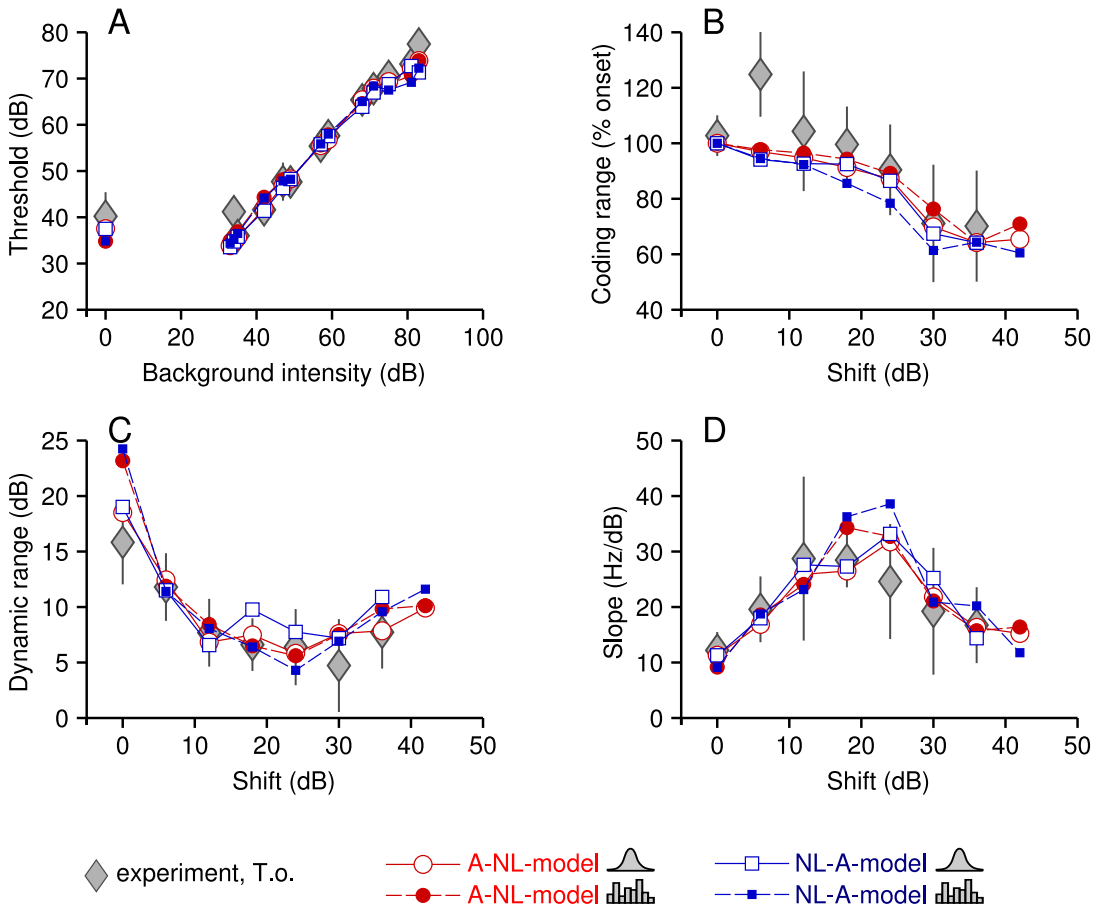

Figure 4.3: Parameters of adapted response curves for *T. oceanicus*. **A** Response thresholds as a function of background intensity, **B**–**D** relative coding range, dynamic range, and slope of adapted response curves as a function of their shift.

Larger deviations are found for the onset and steady state response curves with little differences between model (listed in tab. 4.1). The thresholds of fitted onset response curves tend to be slightly lower than those of the experimental data, while the thresholds of the steady state response curves tend to be larger for the fits. The dynamic range of onset responses is overestimated by all models, while the dynamic range of the steady state response curve is well reproduced. In summary the modelled onset response curves tend to be extended to lower intensities while the modelled steady state response curves are rather shifted to larger intensities. Consequently, the large ratio of dynamic ranges of steady state and onset response curves cannot be reached by any of the models. With respect to this ratio, the fits with Gaussian receptor thresholds were better than the fits with individually fitted receptor thresholds for both models.

The coding range of modelled onset and steady state response curves was significantly

Table 4.1: Summary of central features of the onset and steady state response curves of *T. oceanicus*, estimated from experiments and models. Asterisks denote significant deviations between model and experiment (p¡0.05, Wilcoxon ranksum test)

	I_{thr} [Hz]	Dynamic range [Hz]	Coding range [Hz]	Slope [Hz/dB]
T. oceanicus	*experiment*			
onset	40 ± 5	16 ± 4	181 ± 19	12 ± 3
steady state	37 ± 7	29 ± 9	83 ± 19	3 ± 0.8
stst/onset		1.8 ± 0.7	0.46 ± 0.09	
NL-A-model	*Gaussian*			
onset	37 ± 6	19 ± 4	208 ± 14 *	11 ± 2
steady state	46 ± 5 *	29 ± 4	109 ± 18 *	3.8 ± 0.7 *
stst/onset		1.53 ± 0.11	0.52 ± 0.08	
NL-A-model	*individual*			
onset	35 ± 4 *	24 ± 6 *	210 ± 14 *	9.2 ± 1.9
steady state	47 ± 5 *	26 ± 5	103 ± 17 *	4.1 ± 0.8 *
stst/onset		1.11 ± 0.37 *	0.49 ± 0.08	
A-NL-model	*Gaussian*			
onset	38 ± 5	19 ± 3	204 ± 15 *	11 ± 1
steady state	46 ± 5 *	29 ± 3	109 ± 19 *	3.7 ± 0.5 *
stst/onset		1.56 ± 0.12	0.53 ± 0.09	
A-NL-model	*individual*			
onset	35 ± 4 *	23 ± 5 *	204 ± 15 *	9.3 ± 1.7 *
steady state	46 ± 6 *	27 ± 4	101 ± 16 *	3.9 ± 0.6 *
stst/onset		1.18 ± 0.35 *	0.5 ± 0.09	

larger (between 20 and 30 dB) than found in experimental data for both models and both distributions of receptor thresholds (p¡0.05, Wilcoxon ranksum test). The main reason is an offset of onset and steady state response curves but not adapted response curves observed in the data. Furthermore, the maximum response rate of onset response curves is overestimated by the models if one or several adapted response curves had larger maximum responses. The maximum response curve of steady state response curves might be overestimated by a model if matching the adapted response curves maximum responses is inconsistent with the interneuron adaptation strength necessary to fit the maximum response of the steady state response curve.

Fits to the AN1 of Gryllus bimaculatus While is is plausible that both models are able to reproduce the response curves of *T. oceanicus* comparably well, the case is different for *G. bimaculatus*. The response curves of *G. bimaculatus* show no decrease in coding range of adapted response curves, and it is impossible for the NL-A-model to reproduce this. Therefore, for this species the A-NL-model is expected to be clearly superior to the NL-A-model. Surprisingly, across all 7 fitted AN1s of *G. bimaculatus* there was no significant

difference between the two models with a Gaussian distribution of receptor thresholds (RMSE 46 Hz for the NL-A-model and the A-NL-model).

Figure 4.4 shows a typical set of response curves of *G. bimculatus* fitted by the NL-A-model and the A-NL-model with Gaussian receptor thresholds and individually fitted receptor thresholds. As expected, the NL-A-model fails to reproduce constant maximum responses of adapted response curves (fig. 4.4 A, C). Surprisingly, the A-NL-model shows a slight decrease of the maximum response at the two largest background intensities, too (fig. 4.4 B, D), although it has the capacity to shift adapted response curves to high background intensities without a loss in coding range by using a wider distribution of receptor thresholds. The phenomenon is seen across all data sets. The reason that the A-NL-model is fitted in this way might be the particular shape of the *G. bimaculatus* response curves in the saturation region. In particular the adapted response curves to large background intensities often show only a decrease in slope than a saturation. The model cannot reproduce this change in slope or adapted response curves that have larger maximum response than the onset response curve. Modelled adapted response curves that reach maximum firing rates as high as that of the onset response curve would deviate strongly from the measured adapted response curves in the region of changed slope, causing a large error.

The fitted Gaussian distributions of receptor thresholds are identical for both models (mean 74 and 73 dB and standard deviation 15 and 14 dB, NL-A-model and A-NL-model). In the example, individual fitting of receptor thresholds slightly improves the quality of the fit for the NL-A-model but not in the case of the A-NL-model. The resulting receptor threshold distributions vary with respect to mean (79 and 69 dB) and standard deviation (22 and 16 dB, NL-A-model vs A-NL-model), but both distributions are slightly bimodal with one peak around 50 dB and another peak around 80 dB. Across all 7 data sets, the individual fitting of receptor thresholds did not significantly enhance the quality of fits.

The estimation of thresholds, dynamic ranges, coding ranges and slopes from the experimental and modelled response curves was more difficult than for *T. oceanicus* due to a smaller number of data points measured per response curves and a smaller sample of recordings (fig. 4.5). Nevertheless, the match of thresholds, dynamic ranges and slopes estimated from simulated response curves with that estimated from the experimental response curves is good (fig. 4.5 A, C, D). The plot of the relative coding range confirms the impression from the example, namely that both models fail to reproduce the constant coding for all shifts. Especially for the largest shift of 36 dB the relative coding range drops strongly for all models, but not the data. Notably, an individual fitting of receptor thresholds did not yield a better match of relative coding ranges.

As for *T. oceanicus* the onset and steady state response curves are less well matched than the adapted response curve (tab. 4.2). The fitting error of onset and steady state response curves are qualitatively similar to those in *T. oceanicus*, i.e. the fitted onset response curves are wider and have lower threshold than experimental ones and fitted steady state response curves are shifted towards larger intensities with respect to the experimental ones. The absolute coding range of onset and steady state response curves is strongly overestimated by 9 to 35 and 24 to 30 dB (onset and steady state) by both models and independent on the distribution of receptor thresholds, but the A-NL-model's fits produce smaller deviations.

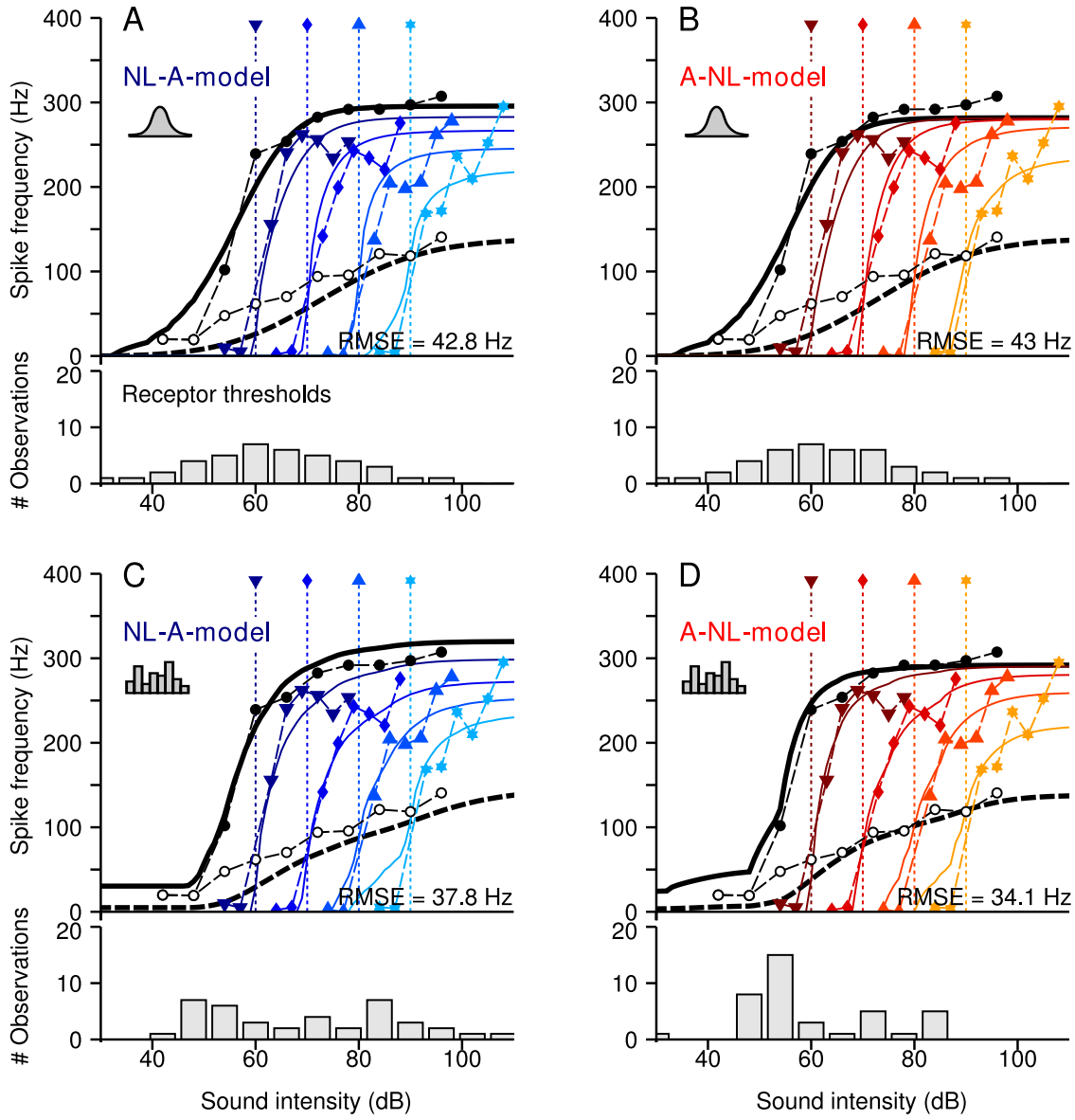

Figure 4.4: Model fits to intensity-response curves of *Gryllus bimaculatus* AN1. Respective upper panels show intensity response curves, lower panels show the distribution of receptor response thresholds as resulting from the fitting procedures. Modelled responses are represented by solid lines, experimental data by markers connected by dashed lines. Onset and stationary responses (open and filled circles, respectively) are plotted in black, adapted responses color coded in blue (NL-A-model) and red (A-NL-model), respectively. The background intensities to adapted response curves are indicated by dashed lines in respective color. The mean squared error between data and fit is printed in every panel. **A** and **C** NL-A-model with Gaussian and individually fitted receptor thresholds, respectively. **B** and **D** A-NL-model with Gaussian and individually fitted receptor thresholds, respectively.

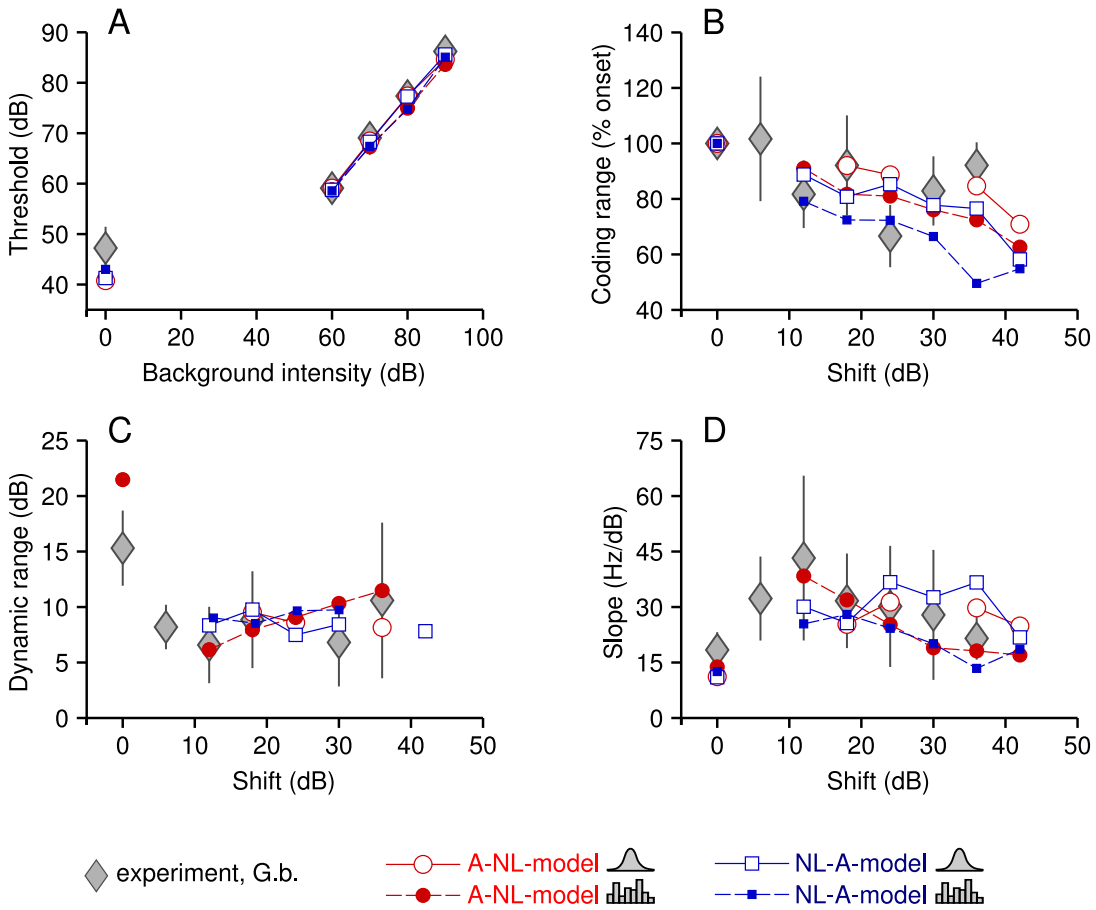

Figure 4.5: Parameters of adapted response curves for *G. bimaculatus*. **A** Response thresholds as a function of background intensity, **B**–**D** relative coding range, dynamic range, and slope of adapted response curves as a function of their shift.

Also, because the variability of this value is large across the population, the deviations from the experimental data are not significant for onset response curves. As in *T. oceanicus* this is caused by an offset in the data which is only apparent in onset and steady state, but not in adapted response curves and some data sets in which the adapted response curves reach higher maximum responses than the onset response curve.

4.2.3 The role of model parameters

For both cricket species the fits of the NL-A-model and the A-NL-model do not differ with respect to the RMSE. However, the two models fitted the model parameters differently, which is analysed in the following.

While maximum firing rate r_{max} and the weight factor w were not significantly different for the NL-A-model and the A-NL-model, a systematic difference was found for the receptor

Table 4.2: Summary of central features of the onset and steady state response curves of *G. bimaculatus*, estimated from experiments and models. Asterisks denote significant deviations between model and experiment (p¡0.05, Wilcoxon ranksum test)

	I_{thr} [Hz]	Dynamic range [Hz]	Coding range [Hz]	slope [Hz/dB]
G. bimaculatus	*experiment*			
onset	47 ± 4	15 ± 3	255 ± 70	17 ± 5
steady state	35 ± 11	36 ± 13	101 ± 13	3.1 ± 1
stst/onset		2.2 ± 0.73	0.37 ± 0.05	
NL-A-model	*Gaussian*			
onset	41 ± 4 *	27 ± 5 *	270 ± 74	10 ± 2 *
steady state	53 ± 4 *	39 ± 6	131 ± 18 *	3.5 ± 0.7
stst/onset		1.41 ± 0.09 *	0.45 ± 0.08	
NL-A-model	*individual*			
onset	43 ± 5	26 ± 6 *	290 ± 68	12 ± 3 *
steady state	51 ± 4 *	39 ± 6	130 ± 26	3.5 ± 0.5
stst/onset		1.45 ± 0.11 *	0.42 ± 0.09	
A-NL-model	*Gaussian*			
onset	41 ± 5 *	26 ± 5 *	264 ± 72	11 ± 2 *
steady state	52 ± 5 *	40 ± 6	131 ± 20 *	3.5 ± 0.7
stst/onset		1.5 ± 0.12	0.46 ± 0.09	
A-NL-model	*individual*			
onset	42 ± 4 *	21 ± 4 *	265 ± 71	13 ± 3
steady state	50 ± 4 *	36 ± 5	125 ± 23	3.7 ± 0.6
stst/onset		1.6 ± 0.12	0.44 ± 0.1	

adaptation strength α_R (fig. 4.6 A1 and A2).

Adaptation strengths While the A-NL-model fitted α_R values corresponding to roughly 50 % reduction in the firing rate for both cricket species – a value which is in a plausible range for cricket auditory receptors (Farris et al., 2004). The NL-A-model fitted significantly larger receptor adaptation strength, corresponding to 76 % reduction in *T. oceanicus* and 80 % reduction in *G. bimaculatus* (p¡0.05, Wilcoxon rank sum test) when receptor thresholds were from a Gaussian distribution. Interestingly, the individual fitting of receptor thresholds did not affect the receptor adaptation strengths of the A-NL-model, but led to a reduction in the receptor adaptation strengths fitted by the NL-A-model (to 69 % reduction for *T. oceanicus* and 68 % in *G. bimaculatus*).

The strength of adaptation in the AN1 itself cannot be compared between models, because it is not driven by the same force. However, in the NL-A-model the AN1 adaptation strength tends to be larger for individually fitted receptor thresholds than for a Gaussian distribution in both species (fig. 4.6 B1 and B2, p¡0.05, Wilcoxon rank sum test). This is comprehensible, because the receptor adaptation strengths are lower for individually fitted thresholds and

consequently more AN1 adaptation is needed to fit the steady state maximum response. The AN1 adaptation strengths resulting from fits with the A-NL-model do not differ significantly between the different distributions of receptor thresholds in both species.

Receptor thresholds In addition to the receptor adaptation strength, the distribution of receptor thresholds has a large impact on the shape of response curves.

Notably, for any particular AN1, the distributions of receptor thresholds fitted by the two models were usually similar. In *T. oceanicus* only in 2 of 12 cells the Gaussian distributions fitted by the NL-A-model differed significantly from the one fitted by the A-NL-model (p¡0.05, Kolmogorov-Smirnov test), the distributions of individually fitted receptor thresholds never differed significantly for the two models. In *G. bimcaulatus*, the Gaussian distributions of receptor thresholds fitted by the NL-A-model and the A-NL-model never differed significantly, the distributions of individually fitted receptor thresholds by the two models differed significantly in 2 of 7 cells.

The distributions of individually fitted receptor thresholds tend to share some features: In *T. oceanicus* the distributions tend to have slightly heavier tails than a Gaussian. In *G. bimaculatus* they often have a broad plateau (NL-A-model) or are slightly bimodal (A-NL-model).

Pooling all Gaussian distributions fitted to the cells of one cricket species, the pooled distribution resulting from the NL-A-model is very similar to that of resulting from the A-NL-model (fig. 4.6 C1 and C2). For *T. oceanicus* they peak at 53 to 55 dB, have a standard deviation of 12 to 13 dB, and are almost symmetrical . For *G. bimaculatus* the distributions are significantly wider (p¡0.05, Levene test) with standard deviations of around 17 dB and peak at significantly larger intensities between 65 and 68 dB.

The distributions of pooled individual thresholds differ a little more for the two models, but are similar in general features (fig. 4.6 D1 and D2): For *T. oceanicus* they have a large peak at 52-55 dB approximately identical to the mean of the respective distribution of Gaussian receptors, and they have a heavy tail towards larger intensities, or a small second peak around 90 dB in the case of the A-NL-model. For *G. bimaculatus* the distribution of individually fitted receptor thresholds of the A-NL-model has a major peak at 55 dB and second smaller peak between 75 and 90 dB, while for the NL-A-model the distribution is almost flat between 55 and 90 dB having more receptors at larger intensities. Note that this broader, more uniform like distribution of receptor thresholds of the NL-A-model comes along with a significantly smaller receptor adaptation strength.

The distribution of individually fitted receptor thresholds differs significantly from the distribution of Gaussian receptor thresholds for the A-NL-model in *T. ocanicus*, and for both models in *G. bimcaulatus* (p¡0.05, Kolmogorov-Smirnov-test).

For *T. oceanicus* the response thresholds of auditory receptors have been measured experimentally by Imaizumi and Pollack (2001) and show large similarity to the distributions resulting from the fits to this species data in this study. For *G. bimaculatus* the receptor thresholds seem to extend to larger values, which fits the larger dynamic range of the steady state response curve in this species and presumably a larger capacity to adjust the operating point of the AN1 across a larger range of background intensities without so much loss in

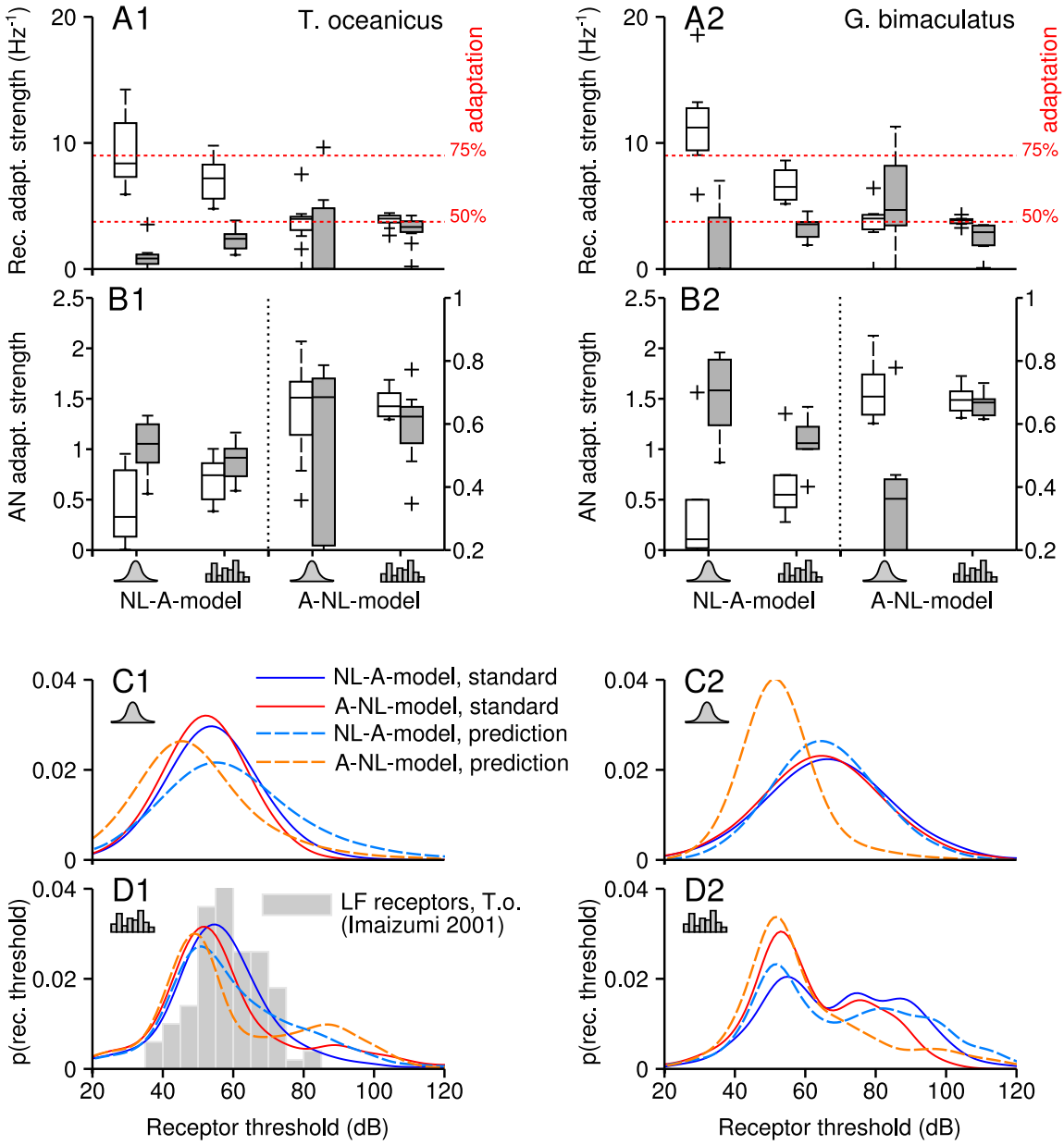

Figure 4.6: Fitted model parameters. **A** Receptor adaptation strengths fitted by the NL-A-model and A-NL-model to the response curves of *T. oceanicus* (**1**) and *G. bimaculatus* (**2**). **B** Interneuron adaptation strengths fitted by the NL-A-model and A-NL-model to the response curves of *T. oceanicus* (**1**) and *G. bimaculatus* (**2**). **C** Gaussian distributions of receptor thresholds fitted to *T. oceanicus* (**1**) and *G. bimaculatus* (**2**) (kernel estimate). **D** Distributions of individually fitted receptor thresholds for *T. oceanicus* (**1**) and *G. bimaculatus* (**2**) (kernel estimate). Histogram shows the distribution of receptor thresholds found for *T. oceanicus* in experiments, redrawn from Imaizumi and Pollack (2001).

coding range.

4.2.4 Can the models predict adapted response curves from onset and steady state responses?

In the models, once the onset and steady state response curve are fixed the adapted response curves are unambiguously determined. If the models perfectly described the data, the adapted response curves should be predictable from fitting the models only to the onset and steady state response curve. This will be referred to as the prediction paradigm in contrast to the standard fitting paradigm in which the models were fitted to all response curves.

Response curves Under the prediction paradigm, the onset and steady state response curves are usually better reproduced than under the standard paradigm. For both cricket species, the steady state response curve is significantly better fit under the prediction paradigm (p¡0.05, Wilcoxon rank sum test) (fig. 4.7 and 4.8 A1 and A2).

On the other hand, the prediction of adapted response curves from fits to onset and steady state response curve is not very convincing. Figures 4.7 and 4.8 B1 and B2 show the RMSE of individual response curves resulting under the prediction paradigm, showing the smaller RMSE for onset and steady state response curves and the strongly increased RMSE for adapted response curves which tends to grow with increasing shift.

Generally, for both species, all models fail to reproduce the shift or adapted response curves and the relative coding range (fig. 4.7 C and D). I.e. the adapted response curve are not shifted far enough and their maximum response declines to strongly. The best predictions are obtained from the A-NL-model with individually fitted receptor thresholds.

For *T.oceanicus* the NL-A-model predicts shifts correctly up to a background intensity of approximately 60 dB, for larger backgrounds no further shift is predicted. The A-NL-model fits the shift much better (fig. 4.8 C). For *G.bimaculatus*, both models fail completely to reproduce the shift of adapted response curves no matter what distribution of receptor thresholds was used (fig. 4.8 C). The relative coding range of predicted adapted response curves is underestimated by all models in both species.

Which model parameters cause the differences? Typically the NL-A-model fitted significantly (p¡0.05, Wilcoxon rank sum test) smaller values of the receptor adaptation strength under the prediction paradigm (fig. 4.6 A, B). The difference between the standard and prediction paradigm is stronger in *T. oceanicus* than in *G. bimaculatus* which reflects the differences in the dynamic range of the steady state response curves of the two species. With fixed nonlinearity, the receptor adaptation strengths determines where the steady state response curve is hit by the saturation and consequently how wide it will be — and the steady state response curve is wider in *G. bimaculatus* than in *T. oceanicus*.

On the other hand, the interneuron's adaptation strength is typically larger under the prediction paradigm (p¡0.001, Wilcoxon rank sum test for the Gaussian distribution of receptor

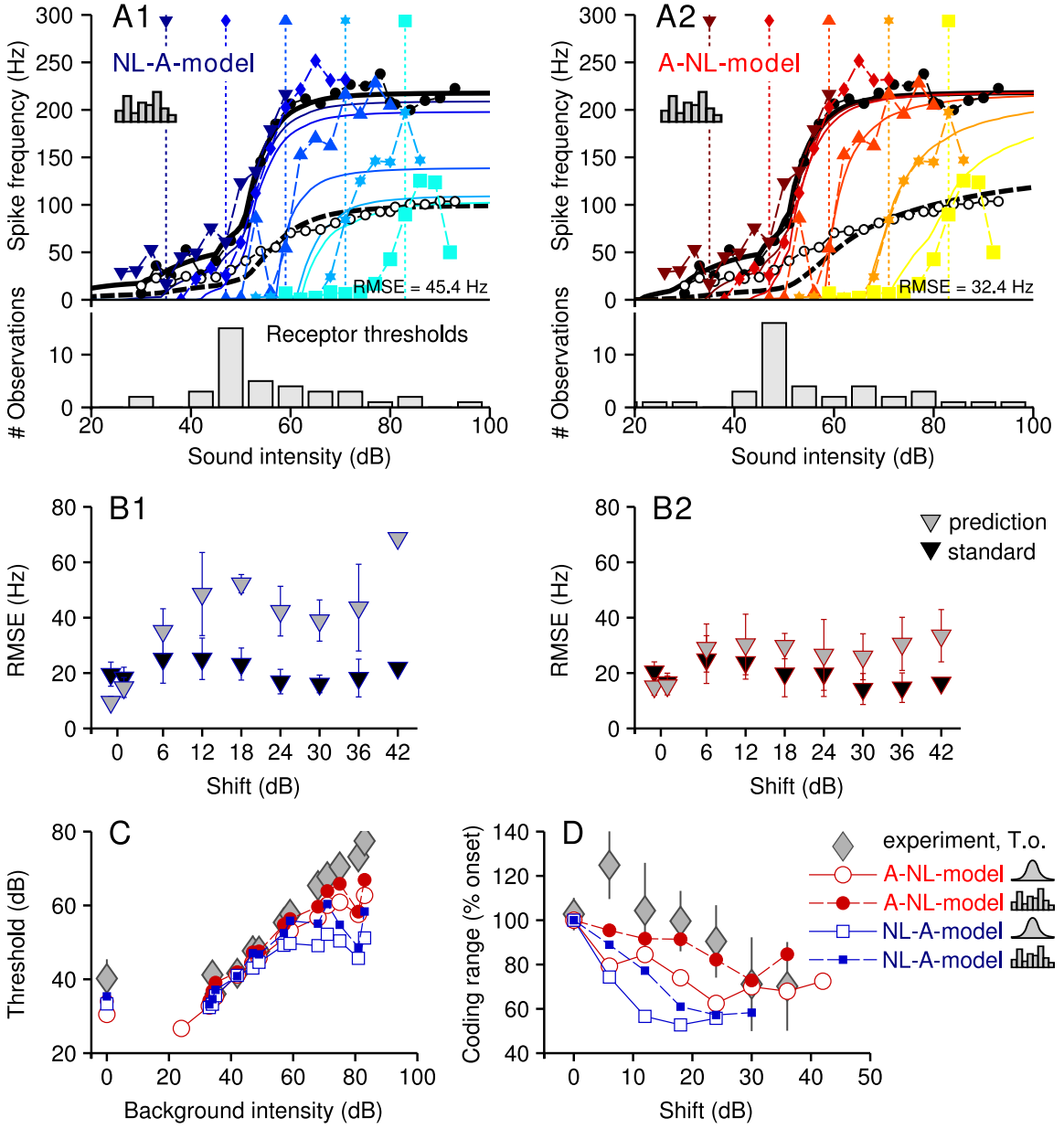

Figure 4.7: Fitted response curves for one set of AN1 response curves of *Teleogryllus oceanicus* under the prediction paradigm. **A** Response curves resulting from a fit (*solid lines*) to the onset and steady state response curves by the NL-A-model (**1**) and the A-NL-model (**2**) with individually fitted receptor thresholds together with experimental data (*markers and dashed lines*). *lower panel* Histograms of the fitted receptor thresholds. **B** Root mean squared error of the adapted response curves above as a function of background intensity under the standard paradigm (all response curves fitted) and the prediction paradigm (only onset and steady state response curve fitted) for the models in A. **C** Thresholds of adapted response curves plotted versus background intensity for experiments and different models. **D** Relative coding range of adapted response curves plotted versus their shift for experiments and different models.

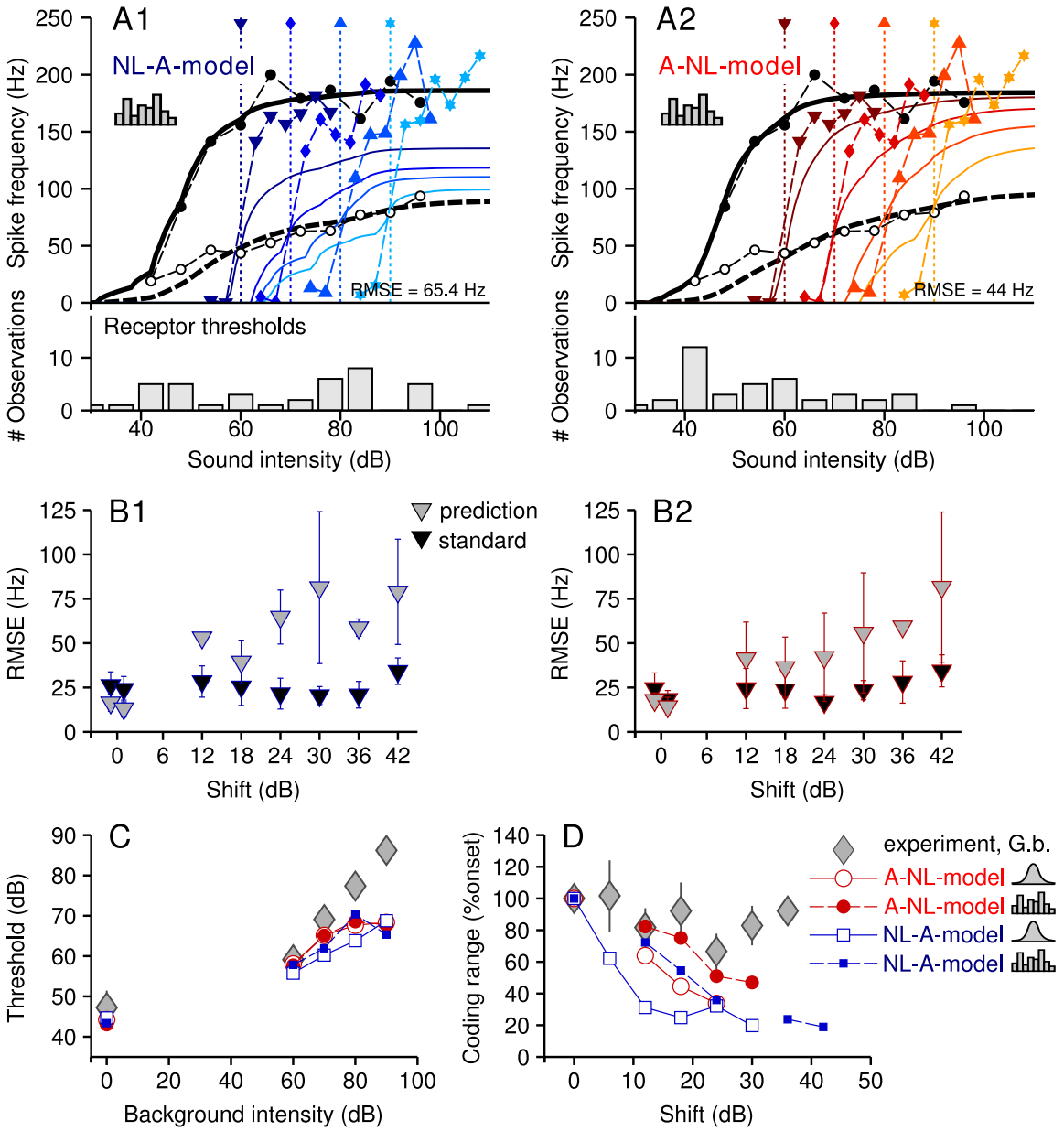

Figure 4.8: Fitted response curves for one set of AN1 response curves of *G. bimaculatus* under the prediction paradigm. **A** Response curves resulting from a fit (*solid lines*) to the onset and steady state response curves by the NL-A-model (**1**) and the A-NL-model (**2**) with individually fitted receptor thresholds together with experimental data (*markers and dashed lines*). *lower panel* Histograms of the fitted receptor thresholds. **B** Root mean squared error of the adapted response curves above as a function of background intensity under the standard paradigm (all response curves fitted) and the prediction paradigm (only onset and steady state response curve fitted) for the models in A. **C** Thresholds of adapted response curves plotted versus background intensity for experiments and different models. **D** Relative coding range of adapted response curves plotted versus their shift for experiments and different models.

thresholds, not significant for individually fitted receptor thresholds), compensating for the reduced receptor adaptation strength (fig. 4.6 C, D).

In contrast to the NL-A-model, the A-NL-model shows typically no large differences in the adaptation strength resulting under the prediction paradigm and those resulting from fits to all response curves 4.6 A-D).

Receptor thresholds Compared for individual recordings, the Gaussian distributions of receptor thresholds fitted under the prediction paradigm, often varied significantly from that fitted under the standard paradigm (p¡0.05, Kruskal-Wallis-test), while the individually fitted thresholds rarely did.

Pooled across all recordings, the largest differences between the prediction paradigm and the standard paradigm were found for the Gaussian distributions fitted by the A-NL-model, which for both species were narrower and peaked at a slightly lower intensity (fig. 4.6 E, F). Also the distributions of individually fitted receptor thresholds show a slight bias towards lower intensities under the prediction paradigm for the A-NL-model (fig. 4.6 G, H). The differences between distributions fitted by the NL-A-model under the prediction and standard paradigm differ only weakly (fig. 4.6 E-H).

4.2.5 Can the models reproduce response curves of the AN2?

Finally, we consider the second ascending interneuron AN2 of *G: bimaculatus* which gets input from ultrasound receptors and low frequency receptors and mediates the avoidance response to high intensity ultrasound stimuli. Stimuli were presented at 16 kHz, activating primarily the ultrasound receptors.

AN2 Data The response curves of the AN2 of *G. bimaculatus* at 16 kHz stimulation are roughly sigmoid with adapted response curves that shift their thresholds towards higher intensities with increasing background intensities. A typical example is shown in fig. 4.9 A and B. The relation between the threshold of adapted response curves and background intensity is in good approximation linear (see fig. 4.9, C) within the tested range of background intensities of 60 and 90 dB. The absolute response thresholds of the AN2 are on average about 10 dB larger than those of the AN1. The absolute coding range is on average 339 Hz in onset and 98 Hz in steady state, i.e. 72 % reduction of the firing rate, implicating a stronger overall adaptation in the AN2 than in the AN1. The maximum responses of adapted response curves do not decrease with shift, but their slope increases with shift (fig. 4.9 D and F). The dynamic range of the onset response curves is relatively large, on average 25 dB, i.e. 10 dB larger than that of the AN1. In contrast to the AN1 the steady state response curve is not much wider than the onset response curve (32 dB). The response curves of the AN2 often show irregularities in shape, typical are **'bumps'** in the onset response curve and different slopes in the steady state response curve.

Models of the AN2 The input to the AN1 at ultrasound stimulation was modeled to be solely from ultrasound receptors, potential contribution of low frequency receptors to

ultrasound at large intensities was ignored. The population of ultrasound receptors was found to be approximately a quarter as large as that of low frequency receptors, i.e. in the order of 10. The model was set up with 11 receptors. With such a small number of receptors the exact position of the thresholds of individual receptors can have a large impact on the shape of response curves. Therefore only individually fitted receptor thresholds were considered for the AN2.

Modelled response curves Figure 4.9 A and B show the results of fitting the NL-A-model (left, blue color code) and the A-NL-model (right, red color code) to one data set of AN2 response curves.

The models are able to reproduce the different slopes and even bumps to a certain degree. The response curves fitted by the NL-A-model and th A-NL-model are almost indistinguishable for many of the fitted cells. Across all fitted cells the RMSEs do not differ for the two models (61 vs 60 Hz for the NL-A-model and the A-NL-model).

The key features of the response curves are very well and almost identically reproduced by both models(fig. 4.9 C – F) : they follow the linear shift of thresholds with background intensity, the monotone decrease of the dynamic range and the increase of the slope of adapted response curves with their shift, with a slight bias to fit shallower and wider response curves. The relative coding ranges of adapted response curves are slightly underestimated. This is probably because the maximum responses of the adapted response curves in the AN2 often exceed the maximum response of the onset response curve which is not reproducible for the models. In order to fit to all response curves, the maximum responses of the onset response curves are overestimated.

Model parameters As for the AN1, the receptor adaptation strengths fitted by the NL-A-model are significantly larger than the ones fitted by the A-NL-model (63 % vs 50 %, fig. 4.10 A). However, in the AN2 the receptor adaptation strength fitted by the NL-A-model are low compared to the ones fitted to the AN1. The other model parameters are similar for both models.

Receptor threshold distribution On the level of individual cells, the impact of the position of individual receptor thresholds becomes particularly important. The fitted thresholds of only 11 high frequency receptors that converge to an individual AN2 usually stretch across a range of around 50 dB. Often, most of the receptor thresholds cluster around 80 dB, and very few or even single around 40 to 50 dB. Given the small number of receptors, the distribution has gaps of up to 10 or more dB. This particular pattern of allocation in the models causes the large width of the onset response curve and even to some extend its often irregular shape, the slopes of adapted response curves depending on where they are centred, and the change in the slope of the steady state response curve.

In the majority of recorded cells the onset response curve shows bumps in its rising part, indicating that they may be features of the AN2 not artefacts of the measurement. The fits follow these to a certain degree supporting the hypothesis that the irregularities mirror the underlying receptor threshold distribution.

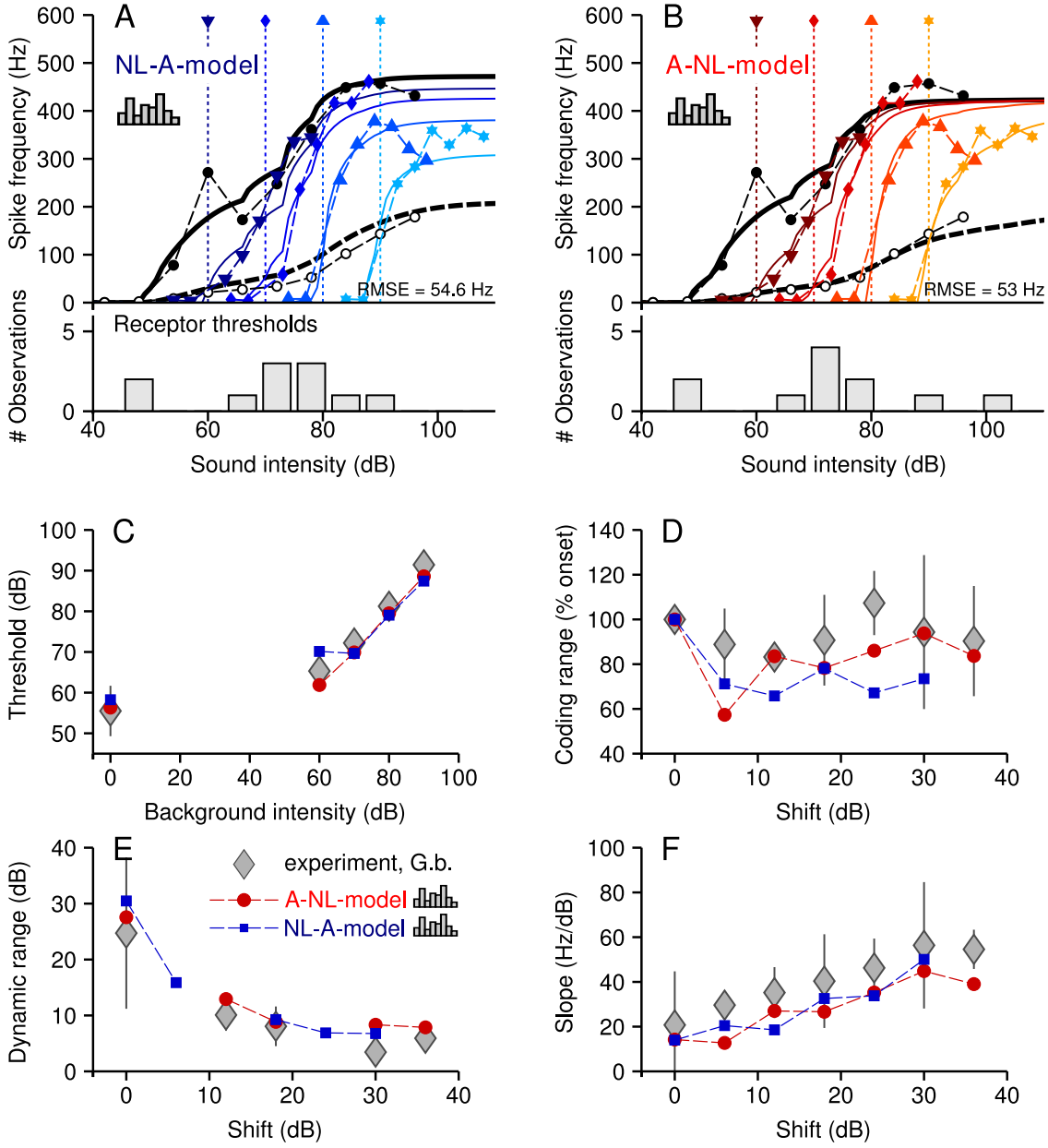

Figure 4.9: Model fits to AN2 intensity-response curves of *G. bimaculatus*. **A** and **B** NL-A-model (blue color code) and A-NL-model (red color code), individually fitted receptor thresholds. *lower panels* Distribution of receptor response thresholds as resulting from the fitting procedures. Modelled responses are represented by solid lines, experimental data by markers connected by dashed lines. Onset and stationary responses (open and filled circles, respectively) are plotted in black, adapted responses color coded in blue and red respectively). The background intensities to adapted response curves are indicated by dashed lines in respective color. **C** Response thresholds of adapted response curves plotted versus background intensity for experiments and the two models. **D**–**F** Relative coding range, dynamic range and slope of response curves plotted versus their shift for experiments and the two models.

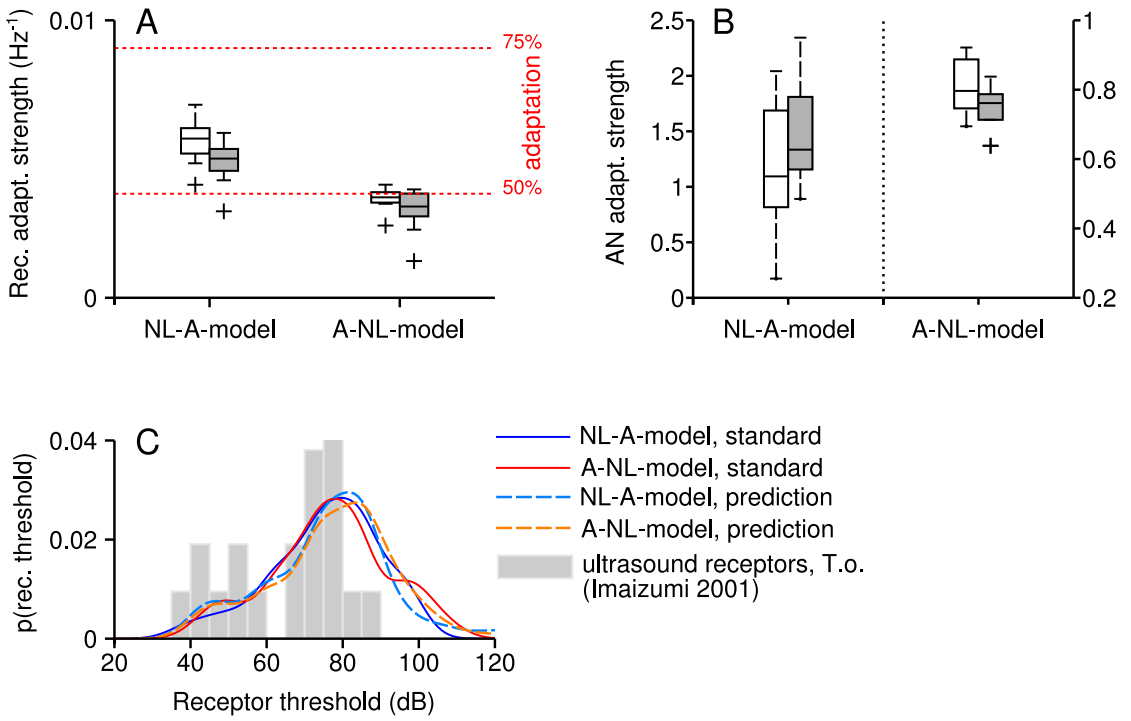

Figure 4.10: Fitted model parameters for the AN2 of *G. bimaculatus*. **A** Receptor adaptation strengths resulting from the NL-A-model and the A-NL-model under the standard and prediction paradigm. **B** AN2 adaptation strengths resulting from the NL-A-model and the A-NL-model under the standard and prediction paradigm. **C** Distribution of receptor thresholds fitted to the AN2 by the NL-A-model and the A-NL-model under the standard and prediction paradigm together with a histogram of the response thresholds of ultrasound receptors found in experiments, redrawn from Imaizumi and Pollack (2001).

The receptor thresholds fitted to the same AN2 recording never differed significantly for the two models (Kolmogorov-Smirnov-test).

Figure 4.10 C shows the probability density functions estimated from histograms of the fitted receptor thresholds pooled across all 8 data sets. There is no significant difference between the A-NL-model and the NL-A-model. The distribution has the major peak between 75 and 85 dB and a shoulder around 45 to 50 dB. The fitted distributions resemble that of ultrasound receptor thresholds determined from experiments by Imaizumi and Pollack (2001) (histogram in fig. 4.10 C) which is also bimodal with the major peak around 80 dB and a minor peak around 50 dB.

Prediction of adapted response curves from onset and steady state In contrast to the AN1, the adapted response curves of the AN2 could be predicted relatively good from models that were only fitted to the onset and steady state response curve (RMSE 79 and 73 Hz, NL-A-model and A-NL-model). Model parameters including the fitted receptor thresholds were not different from the ones obtained under the standard paradigm (see fig. 4.10) The

reason for the good prediction of AN2 adapted response curves is probably, that the range of background intensities tested was not large compared to the dynamic range of the onset and steady state response curve, in contrast to the experiments with on the AN1. This is also reflected in the comparably low receptor adaptation strengths fitted to the AN2 by the NL-A-model.

4.3 Discussion

In this chapter the output neuron models with shifting response curves were applied to fit the experimentally measured response curves of the ascending interneurons AN1 and AN2 of the cricket species *T. oceanicus* and *G. bimaculatus*.

4.3.1 Properties of the ascending interneurons AN1 and AN2

The response curves of the AN1 of *T. oceanicus* and *G. bimaculatus* were analysed to quantify apparent differences between the species. The onset response curves of both species were found to have the same dynamic range, while the steady state response curves of *G. bimaculatus* were significantly wider than those of *T. oceanicus*. The most obvious difference is a marked decrease of maximum responses of the adapted response curves with shift of *T. oceanicus* which is absent in *G. bimaculatus*. The response threshold of the AN1 is similar in both species.

Compared to the AN1, the AN2 has an about 15–20 dB larger threshold, larger firing rates, and a wider onset response curve when tested at 16 kHz. The onset and steady state response have a similar width, whereas adapted response curves become steeper with increasing shift. The onset response curve often shows irregularities like bumps, while the steady state response curves often show a change in slope around the center of its dynamic range.

4.3.2 Model performance

In spite of their simplicity, both models reproduce the three qualitatively different sets of response curves surprisingly well. They explain several features of the response curves of the different neurons: A decrease in the maximum responses of adapted response curves associated with their shift (compare chapter 2), and changes in slope within response curves as well as between adapted response curves to different background intensities.

The expectation was that the NL-A-model would generate good fits to the AN1 response curves of *T. oceanicus* but fail in reproducing the adapted response curves of *G. bimaculatus*, because it cannot produce constant maximum responses of adapted response curves. The A-NL-model on the other hand should be able to reproduce AN1 response curves of both cricket species. While it can produce constant maximum response of adapted response curves, it can also reproduce a decrease by fitting a narrower distribution of receptor thresholds.

Indeed both models were able to fit the data of *T. oceanicus* equally well, and they fitted almost the same distribution of receptor thresholds. Surprisingly, the NL-A-model did not generate significantly worse fits to the data of *G. bimaculatus* than the A-NL-model. The

adapted response curves to larger background intensities often decrease in slope instead of saturating sharply which could not be reproduced by either of the two models. This problem could perhaps be solved by choosing a different non-linearity to better fit the shape of adapted response curves. In this case, the A-NL-model would likely yield better fits than the NL-A-model. Both models yielded almost identical fits to the data of the AN2.

Model parameters The NL-A-model realized its good performance by fitting unreasonably large receptor adaptation strengths (i.e. larger than 75 % reduction in the firing rate by adaptation). Interestingly, the receptor adaptation strengths fitted by the NL-A-model were significantly smaller if receptor thresholds were fitted individually. In contrast, the A-NL-model fitted receptor adaptation strengths of ca. 50 % reduction independent of the distribution of receptor thresholds.

Next to the receptor adaptation strengths, the receptor thresholds had a strong influence in fitting the models to different data sets. Notably, the response thresholds, Gaussian or individual, that were fitted to an individual recording were typically very similar. The distributions of receptor thresholds fitted to *G. bimaculatus* were on average wider than those fitted to *T. oceanicus*, which For *T. oceanicus* experimental data on the response thresholds of the low frequency receptor population exist (Imaizumi and Pollack, 2001). The distribution fitted by both models to the data of this species matched the experimentally measured distribution well with respect to width and peak location.

The impact of the receptor thresholds became especially conspicuous in the AN2, were the population of receptors was very small. The receptor thresholds fitted to individual AN2s never differed for the two models. Often, single or few low thresholds were fitted, separated from a cluster of higher thresholds by a gap of several dB. The large dynamic range of the onset response curve, the increasing slope and decreasing dynamic range of adapted response curves, and the change in slope of the the steady state response curve could be reproduced due to the local densities of receptor thresholds. Even the bumps often observed in the onset response curves are to some extend reproduced by the models due to the gaps between receptor thresholds.

Overall, the A-NL-model was more robust in the fits of qualitatively different sets of response curves, and under various conditions. I.e. the fitted parameters were less sensitive to changes of the receptor distribution, it yielded better predictions of adapted response curves from fits to onset and steady state response curve, and its receptor adaptation strengths were in a rather plausible range.

Limitations of the models Both models were found to make systematic errors in fitting the onset and steady state response curve when they were fitted to all response curves. The dynamic range of onset response curves was overestimated and the steady state response curve was slightly shifted to the right compared to the curves measured in the experiments. Shortly: from the model's point of view, the adapted response curves of both cricket species shift over a range which is larger than expected from the steady state and onset response curve.

This hints on a process missed by the models. There might by an inhibition which acts at

large intensities, reducing the maximum firing rate of the steady state response curve, while it is not fast enough to affect the onset and adapted onset responses. For *G. bimaculatus* the soft saturation of adapted response curves to large background intensities, while the onset response saturates rather sharply, is puzzling. This might be captured in a change of the non-linearity depending on the background intensity.

4.3.3 Conclusions

In summary, both models can explain a number of features of the response curves of the AN1 and AN2. Under the assumption that the ascending interneurons indeed implement the elements suggested by the NL-A-model and A-NL-model – which of the models was to favour? The direct comparison showed no significant differences in the models ability to fit either of the data sets as quantified by the RMSE. However, if the shape of adapted response curves of the AN1 of *G. bimaculatus* had been better fit by the models, the A-NL-model would have probably yielded a better fit quality than the NL-A-model. Furthermore, the A-NL-model resulted in more robust parameter values and more likely receptor adaptation strengths. Both models could be considered the extreme cases of one general model, in which one adaptation mechanism acts on the level of the membrane potential before the saturation step and another one is driven by the saturated response. The two cricket species could then use different weighting of the individual adaptation steps.

Naturally, completely different mechanisms could underlie the performance of the crickets ascending interneurons. However, response driven adaptation clearly exists in the AN1 and AN2 (Hildebrandt et al., 2011), and most likely in the receptors. Using these known mechanisms and assuming only one further element – a saturating non-linearity – the models in this study could not only reproduce the adaptive shift but also more complex features like decreasing maximum responses, and changes in slope within and between response curves. However, the fits to the AN1 show a systematic conflict between the width of the steady state response curve and the range over which adapted response curves are shifted. This indicates the existence of mechanisms not captured by the here derived models.

That other adaptation mechanisms exist in other cricket species was shown for the AN2. In the AN2 of *Teleogryllus leo* adaptation to a stimulus background affects the response curves in different ways depending on the stimulus frequency used (Hildebrandt et al., 2011): At low frequencies, the response curves qualitatively resemble those of the AN1 in *T. oceanicus*, i.e. adapted response curves shift their operating point in parallel towards the background intensity. The response curves at ultrasound stimulation are steeper and adapted response curves display a marked reduction in slope together with a slight shift. This divisive adaptation is probably caused by presynaptic inhibition (Hildebrandt et al., 2011). In the AN2 of *G. bimaculatus* the response curves do not reduce their slope with increasing background for low and high frequency stimulation (Beul, 2010). Thus it seems likely that no presynaptic inhibition exists in the latter species.

5 Summary and Conclusions

Adaptive shifts of response curves are observed in many sensory systems, on diverse processing levels and in different species but often little is known about the underlying circuitry and mechanisms. The auditory system of the cricket provides an excellent model system as it shows adaptive shifts of response curves in low level interneurons and the underlying circuitry is well described and particularly simple: a population of receptors that differ with respect to their response thresholds (intensity range fractionation) converges onto an ascending interneuron (the AN1). While intensity range fractionation is generally assumed to serve the increase of the dynamic range of the full system, little is known how such populations of neurons are integrated by upstream neurons. The central topic of this thesis is how intensity range fractionation in low level sensory neuron populations could contribute to an integrating neuron's ability to adjust its operating point to slow components of the signal intensity.

A feed forward network of range fractioning receptors that converge to one output neuron was set up as the basic model framework. Neural responses were modelled by firing rate models including a response driven mechanism of spike frequency adaptation that acts subtractive on the input current to the neuron (subtractive SFA). The major finding was that the interaction of subtractive SFA and a static saturating non-linearity can not only realize the shift of response curves over a substantial intensity range but also reproduces other properties of shifting response curves observed experimentally. Furthermore, the models using a combination of adaptation and saturation shifting yield shifting response curves in the output neuron also for receptor populations with identical thresholds.

The Fisher information functions for intensity response curves showed that the shift of intensity response curves enables the model neurons to center their region of best intensity discrimination around the current mean intensity. The slope of intensity response curves constructed from responses to noise stimuli decreased with increasing stimulus variance if spike frequency adaptation was present in the receptor layer. This effect is restricted to receptor populations with differing response thresholds.

Fitting the models to the AN1 of two cricket species revealed that the distribution of receptor thresholds plays an important role in shaping the response curves of the output neuron in detail. The receptor thresholds fitted to the response curves of the cricket species *Teleogryllus oceanicus* matched well with those measured experimentally. Additionally the fits showed that a large amount of spike frequency adaptation needs to occur before the saturation step. The required amount of adaptation seems to be larger than that observed in receptors experimentally (this should be verified in further experiments as elaborate data on the adaptation strength in cricket auditory receptors are missing).

5.1 Shifting response curves

Shifts of response curves in response to changes in an intensity background or mean intensity have been described in many sensory systems (e.g. Laughlin and Hardie 1978; Albrecht et al. 1984; Shapley and Enroth-Cugell 1984; Ohzawa et al. 1982; Barlow and Földiák 1989; Benda et al. 2005; Benda and Hennig 2008; Beul 2010; Hildebrandt et al. 2011) and are generally thought to adjust the limited dynamic range of the neuron to match the current most probable intensities.

The models that produced shifting response curves (NL-A-model, A-NL-model, invariance model) were all able to shift their operating points to match the actual background intensity over a considerable range of different background intensities. The shift of response curves enabled the model neurons to center the region of best intensity discrimination – as quantified by the Fisher information – at that particular background intensity. Similarly, the encoding of time varying stimuli by these models was good over the range of mean intensities across which the response curves were shifted.

The NL-A-model and A-NL-model realize shifting response curves by a combination of subtractive adaptation in receptors and the output neuron and a saturating non-linearity. In these models, the steady state response curve is not flat but transmits information about the absolute stimulus intensity, i.e. the responses are not intensity invariant, consistent with findings in the inferior colliculus (IC) in mammals (Dean et al., 2005). The accuracy of intensity discrimination and the mutual information decrease with increasing mean intensity. The degree of reduction in peak Fisher information and mutual information was influenced by the strength of response driven adaptation in the network, as adaptation increases the response variability in the model neurons. A contribution of adaptation to response variability has been found experimentally (Avissar et al., 2007), and is plausible as by adaptation the response to a particular stimulus intensity does not only depend on the actual intensity but also on the adaptive state of the neuron.

5.2 Inherent properties of the derived models

In experimental studies, the shift of response curves is often associated with additional changes in the shape of response curves, e.g. a decrease in maximum response (Dean et al., 2005; Benda and Hennig, 2008; Wen et al., 2009), a limited range of shift (Dean et al., 2005), a reduction in baseline response (Wen et al., 2009), and different widths of the dynamic ranges of onset and steady state response curves (see chapter 4). Here it was found that all these effects can, in principle, result from the interaction of static saturation and subtractive adaptation, as implemented for example in the receptor model, and the output neuron models with static non-linearity.

5.2.1 Interaction of static saturation and subtractive adaptation

The difference in the width of the onset and steady state response curves is a consequence of saturation that follows an adaptation step. Due to the adaptation the steady state response

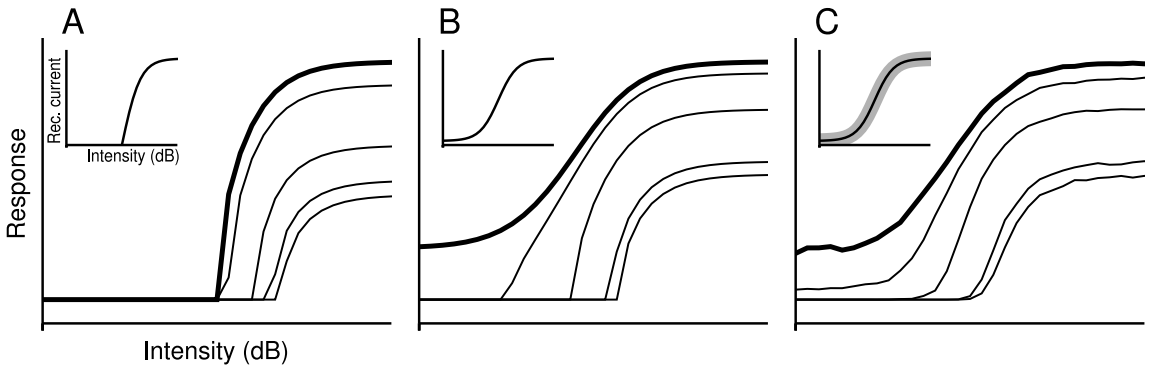

Figure 5.1: Interaction of a saturating non-linearity with subtractive adaptation causing reduction in maximum and baseline response in the receptor for three different conditions. The model consists of one non-linearity modelling the mechano-electrical coupling and an adaptation mechanism driven by the receptors response (i.e. following the non-linearity). **A** Non-linearity with sharp threshold and no offset, **B** Non-linearity with soft threshold and non-zero offset, **C** same as in **B** but with additive noise on the receptor current.

is in general lower than the onset response so it is affected by the saturation mechanism at higher intensities.

The key to understanding the remaining effects is that while the neural response is plotted versus the stimulus intensity (a quantity that is not limited from above), the neural response is determined by a saturating function of the intensity, e.g. the receptor current or the (saturated) sum of receptor responses (referred to as input in the following). This limited input range determines the neural firing rate which in turn drives the adaptation. Plotting the neuron's firing rate as a function of its input, the adaptation mechanism used here causes a purely parallel shift of the input-output relation (see fig. 2.2), but since the input can only take limited values, so does the response, which limits the adaptive shift to the dynamic range of the steady state response curve in these models. As adaptation shifts the response threshold on the input axis, the input range left to drive the neural response decreases with increasing adaptation, resulting in the decrease in maximum response of adapted response curves. A limitation of the input range occurs at different sites in the model network: The receptor model uses a sigmoid non-linearity to model the transduction of sound pressure into a receptor current, similarly a sigmoid non-linearity was used by the NL-A-model and A-NL-model. But a limitation of the input range also results from the finiteness of the intensity range that is covered by the receptor population. A decrease in baseline firing rate observed in auditory nerve fibres of mammals (Wen et al., 2009) can be reproduced by the receptor model by using a non-linearity with non-zero offset to model the transduction process (see fig. 5.1).

In principle, these 'side-effects' accompanying the shift of response curves might be explained differently. E.g. Wen et al. (2009) propose the existence of two qualitatively different adaptation mechanisms, one shifting response curves along the intensity axis (referred to as

dynamic range adaptation), and one shifting response curves down (referred to as firing rate adaptation). However, a collective emergence of these effects by a a combination of a static non-linearity and qualitatively identical adaptation mechanisms is a strong argument that these mechanisms contribute to the adaptive behaviour of the output neuron.

Noise response curves may differ from response curves to constant stimuli. In this work the terms onset, steady-state and adapted response curves were used for response curves constructed from responses to constant stimuli under different conditions. The onset and adapted responses represent the onset responses to intensity pulses presented after the neuron's response to a period of silence (onset response curve) or constant background intensity (adapted response curves) had settled to steady state. The steady-state response is the response .

The differentiation between onset/adapted and steady-state means a separation of time scales determined by the time constant of adaptation. The onset response curve represents the input-output relation for stimulus components that change on a time scale which is fast with respect to the adaptation dynamics, while the steady-state response curves represents the input-output relation for stimulus components that change on a slower time scale.

For the case of response curves constructed from responses to time varying stimuli the term steady-state is often used for the state in which the adaptation has reached a constant mean level and the response is stationary in the sense that its mean does not change over time (see fig. 3.1, e.g. Dean et al. 2005). If the stimulus changes on a time scale faster than the time scale of adaptation, the response curves constructed from the stationary part of the response are similar to the (adapted) onset response curves. If the stimulus changes on a slower time scale than that defined by the adaptation the resulting response curve rather corresponds to the steady state response curve.

However, the response curves resulting from different stimulation paradigms might show additional differences. In all models that included response driven adaptation, the shift of response curves did not only depend on the stimulus mean but also on the stimulus variance. Surprisingly, the noise response curves of the NL-A-model showed a marked decrease in slope with increasing signal variance.

The dependence of the shift on the stimulus variance is a consequence of an adaptation mechanism that is driven by the response and not the intensity itself (output driven). For large stimulus variances the response is . The slope change results from adaptation in the range fractionating input population in which a larger number of receptors are driven into adaptation as the signal variance increases. Varying the mean and standard deviation of a stimulus could therefore yield hints on the organization of the input neurons.

Overall, the study indicates that different stimulus paradigms to quantify response curves complement one another and could help to roughly identify underlying mechanisms.

5.2.2 The influence of the receptor organization

The organization of the receptor population was found to play a major role in shaping response curves. The adapted response curves are steep for background intensities at which the

density of receptor thresholds is high and shallower where the density is low, irregularly distributed receptor thresholds are reflected in changing slopes of the output neuron's response curves. Not surprisingly, the accuracy of intensity discrimination at a given background intensity was found to be large where the density of receptor thresholds is large.

5.3 The dynamic range problem

Cricket auditory receptors are indeed organized in a classical range fractionating manner, i.e. having relatively similar response curves that differ predominantly with respect to their response thresholds. The auditory nerve fibres of mammals do not follow this organization. While the range of processed intensities in healthy human subjects is at least 120 to 130 dB, and accurate intensity discrimination with a resolution of about 1 dB is maintained at least up to 110 dB (Plack, 2005; Rosenblith and Miller, 1949), most auditory fibres are saturated by 60 dB (the high spontaneous rate fibres). Only few fibres (the low spontaneous rate fibres) have a dynamic range that extends to high intensities - for the price of a shallow response curve, that does not seem to support the high accuracy of intensity discrimination observed behaviourally (Viemeister, 1983; Viemeister and Bacon, 1988). A popular idea was that the underlying frequency tuning could account for intensity range fractionation via a spread of excitation. At higher intensities, the auditory fibres with their best frequency at the stimulation frequency will be saturated, but fibres tuned to remote frequencies are unsaturated and could be recruited, effectively representing a population of fibres with different response thresholds. It turned out, that spread of excitation was not necessary to explain the performance of the auditory system of mammals (Viemeister and Bacon, 1988).

Notably, in the NL-A-model and A-NL-model the slope of the output neuron's response curves does not depend on the slope of receptor response curves, and the models would also work with receptor populations not featuring intensity range fractionation. They only require that the receptors somehow represent the relevant intensity range, in particular they would work with an organization as it is found in the auditory nerve fibres of mammals. Assuming the spontaneous activity to reflect the intrinsic response variability of auditory nerve fibres also for superthreshold intensities, the lower spontaneous activity might thus make up for the smaller number of auditory nerve fibres that encode for high intensities.

An interesting question is which of the two possible scenarios – a population with range fractionation or a homogeneous population with shallow response curves – was preferable depending on where and in what way intrinsic noise enters the network and the nature of the stimulus.

5.4 Onset versus steady state response curves

The findings from this thesis imply that the onset and steady state response curve of the higher order neuron that integrates a range fractionating receptor population may differ considerably with respect to their dynamic range. This dynamic range difference was found for the NL-A-model and A-NL-model, but also in the response curves of the AN1 of *T. oceanicus* and *G. bimaculatus*.

Such a difference in dynamic ranges enables a neuron to encode the slowly varying intensity components over the full intensity range covered by receptors with a limited accuracy, while high accuracy is saved for fast changing components in a limited range around the actual stimulus mean. On any time scale defined by adaptation time constants, the dynamic range of the respective response curve could reflect the width of the typical intensity distribution encountered on this specific time scale. On very short time scales the intensity will probably not make extreme excursions from its mean all that often, but on long time scales signals will cover larger intensity ranges.

Hildebrandt (2010) suggested a separation of tasks in time by adaptation: in the initial phase of the response the difference between signal means is large, but as adaptation acts the responses get more and more similar encoding the signal pattern independently of the absolute intensity. Thus, the responses of the AN1s in each hemisphere of a crickets prothoracic ganglion would encode interaural intensity differences only within the first few milliseconds, limiting localization to the initial part of the response, while the pattern would be encoded identically by both neurons if adaptation has reached a steady state. If the cricket or the sound source moved on a slower time scale than the communication signal and the neural adaptation, there would again be a difference between the responses of the neurons, reflecting the changed localization.

5.5 Outlook

In this thesis it was found that a shift of intensity response curves that adjust the neurons' operating point to changing background or mean intensities can be realized in a simple feed forward network with few computational elements. Saturating non-linearities together with response driven adaptation reproduces not only an adaptive shift but also several apparently complex properties of shifting response curves observed in some experimental studies.

An interesting finding was that range fractionation in the input population is not required by the models that use a saturation and adaptation. However, the influence of adaptation in the input layer on the response variability of the output neuron would be different if the input layer was organized differently.

An important open question remains whether there is a biophysical realization of the proposed models. While the subtractive adaptation mechanisms were derived from detailed biophysical models of diverse adaptation currents (Benda and Herz, 2003) the nature of the proposed sharp saturation in the output neuron is more challenging. For the cricket's AN1 a most promising candidate might be the morphology of the neuron at the projection site of auditory receptors (see e.g. Schildberger et al. 1986) which separates the site of synaptic integration sufficiently from the spike generator to allow for saturation (e.g. Hendrickson et al. 2011).

This study should be understood as a first approach to understand the integration of neurons with sigmoid response functions on the cellular level. While intensity range fractionation is generally thought to serve the extension of the dynamic range a sensory system, how such populations could contribute to the adaptation in higher order neurons. The results of this work highlight how measuring response curves for different conditions (onset, adapted onset,

steady-state, constant or time varying stimuli) might help to uncover underlying mechanisms. For example, reductions in the maximum response of response curves with increasing shift is a strong hint for the existence of a saturating non-linearity in combination with subtractive adaptation. Changes in slope of noise response curves for changes in the stimulus standard deviation could be a sign of intensity range fractionation in the input population. Irregularities in the shape of roughly sigmoid response curves might reflect the underlying distribution of response thresholds of the input neuron population. Furthermore, the results show which parameters should be accessed experimentally, namely: Where and how could the saturating non-linearity be realized? How strong is adaptation in input and output neurons? Against this background, experimental studies could now explore the integration of input populations in detail.

Appendix A

A1 Model equations

In the chapers 2 to 4 different scenarios of the integration of a receptor population were modelled, the general form of the models are given below.

A1.1 Receptor model

The transduction of stimulus intensity to receptor current was modelled by a Boltzman-function

$$I(t) = \frac{1}{1 + \exp\left(-c\left(s(t) - s^o\right)\right)} - I^o \tag{A1.1}$$

I is the (dimensionless) receptor current, s the stimulus intensity (in dB), s^o the operating point of the receptor, c determines the slope and I^o is an offset.

The firing rate response of the receptor is given by

$$r_R(t) = \frac{r_R^{max}}{\sqrt{1 - I_o}} \sqrt{\left[I(t) - A_R(t)\right]_+} \tag{A1.2}$$

r_R^{max} is the maximum firing rate, A_R the adaptation current, and $[\cdot]_+$ symbolises rectification to positive values. A_R has units of the receptor current and follows

$$\tau_R \frac{dA_R(t)}{dt} = -A_R(t) + \alpha_R \cdot r_R(t) \tag{A1.3}$$

with adaptation time constant τ_R, and adaptation strengths α_R.

Table A1.1: Parameters of the receptor model.

Parameter		Value*	Meaning
s^o	[dB]		receptor operating point
c	[dB^{-1}]	0.2	slope parameter of receptor transduction NL
I^o	n.u.	0.16	offset of transduction NL
r_R^{max}	[Hz]	350	maximum receptor response
τ_R	[ms]	40	receptor adaptation time constant
α_R	Hz^{-1}		receptor adaptation strength

*of parameters that were fixed throughout stimulations.

A1.2 Sum of receptor responses (sum-model)

The firing rate of the sum-model is given by

$$r_{sum}(t) = \frac{1}{N}\sum_{i=1}^{N} r_{R,i}(t) - A_{sum} \tag{A1.4}$$

$r_{R,i}$ is the firing rate the i^th receptor, N the number of receptors, and A_{sum} (has units of Hz) is the adaptation variable following

$$\tau_A \frac{dA_{sum}(t)}{dt} = -A_{sum}(t) + \alpha_{sum} \cdot \frac{1}{N}\sum_{i=1}^{N} r_{R,i}(t)(t) \tag{A1.5}$$

where τ_A (here as in the following models) is the time constant of adaptation in the output neuron, and α_{sum} the adaptation strength of the output neuron.

A1.3 NL-A-Model: non-linearity followed by adaptation

The output neuron's response according to the NL-A-model is given by

$$r_{NLA}(t) = \left[r^{max}\Theta\left(w \cdot r_{\sum}(t)\right) - A_{NLA}(t)\right]_+ \tag{A1.6}$$

$r_{\sum} = \frac{1}{N}\sum_{i-1}^{N} r_{R,i}$ is the sum of receptor responses, r_{NLA}^{max} is the maximum response of the output neuron, w weights the receptor input, Θ is the saturating non-linearity, and A_{NLA} is the adaptation variable (has units of Hz) in the output neuron, following

$$\tau_A \frac{dA_{NLA}(t)}{dt} = -A_{NLA}(t) + \alpha_{NLA} \cdot r_{NLA}(t) \tag{A1.7}$$

where α_{NLA} is the adaptation strength and τ_A is the adaptation time constant of the output neuron.

Θ denotes the saturating non-linearity given by the sigmoid function

$$\Theta(x) = 2 \cdot \left(\frac{1}{1+\exp\left(-x\right)} - 0.5\right) \ . \tag{A1.8}$$

A1.4 A-NL-Model: adaptation followed by non-linearity

The output neuron's response in the A-NL-model is given by

$$r_{ANL}(t) = r^{max}\Theta\left(\left[w \cdot r_{\sum}(t) - A_{ANL}(t)\right]_+\right) \tag{A1.9}$$

$r_{\sum}$ is the sum of receptor response rates (as in eq. A1.6), r^{max} is the maximum response of the output neuron, w weights the receptor input, Θ is the saturating nonlinearity given by eq. A1.8, and A_{ANL} is the adaptation variable in the output neuron. A_{ANL} is dimensionless and follows

$$\tau_{ANL}\frac{dA_{ANL}(t)}{dt} = -A_{ANL}(t) + \alpha_{ANL} \cdot w \cdot r_{\sum}(t) \tag{A1.10}$$

where α_{ANL} is the adaptation strength and τ_A is the adaptation time constant of the output neuron.

Table A1.2: Model parameters of the sum-model, the NL-A-model, and the A-NL-model

Parameter		Value*	Meaning
w	[Hz^{-1}]		synaptic weight in the NL-A model and A-NL-model
r^{max}	[Hz]		maximum response of the output neuron
α_x	n.u.		adaptation strength of a respective output neuron
τ_A	[ms]	40	adaptation time constant of output neurons

*of parameters that were fixed throughout stimulations.

A1.5 Invariance model

The output neuron's response in the invariance model is

$$r_I(t) = \sum_{i=1}^{N} w_i(t) r_{R,i}(t) - A_{IV} \tag{A1.11}$$

$r_{R,i}$ is the response of the i^{th} receptor, w_i the synaptic weight between the i^{th} receptor and the output neuron, and A_{IV} the response driven adaptation variable. w_i is defined as

$$w_i = e^{\frac{(i-g)^2}{2\sigma_w^2}} \tag{A1.12}$$

where $i = 1, 2, ...N$ refers to the receptor indices in order of increasing response threshold. The weights are normalised to the total weight $w_i \to \frac{w_i}{\sum_{j=1}^{N} w_j}$. g is the center of the weight function defined on the receptor grid which follows slow stimulus components

$$\tau_g \frac{dg(t)}{dt} = -g(t) + \bar{g}(s(t)) \tag{A1.13}$$

with time constant tau_g and stationary solution $\bar{g}$, given by the current stimulus intensity $s(t)$ mapped to the receptor index

$$\bar{g} = \mathrm{cdf}^{-1}(s(t)) \tag{A1.14}$$

$\mathrm{cdf}^{-1}(\cdot)$ denotes the inverse cumulative distribution function of receptor thresholds.

A_{IV} is the adaptation variable (units of Hz) driven by the neurons response

$$\tau_A \frac{dA_{IV}(t)}{dt} = -A_{IV}(t) + \alpha_{IV} \cdot r_I(t) \tag{A1.15}$$

with the adaptation time constant τ_A, and the adaptation strength of the invariance model α_{IV}.

Table A1.3: Parameters of the invariance model

Parameter		Value*	Meaning
w_i	[Hz]		synaptic weight for i^{th} receptor
σ_w	n.u.		width of the weight function
τ_g	[ms]	40	time constant of weight change
α_{IV}	n.u.		adaptation strength
τ_A	[ms]	40	adaptation time constant of output neurons

*of parameters that were fixed throughout stimulations.

A1.6 Neural noise

In chapter 3, noise is introduced in the neuron models. In the receptor model, Gaussian white noise is added to the receptor current (eq. A1.1)

$$I(t) = \bar{I}(t) + \sigma_R \zeta(t) \tag{A1.16}$$

$\bar{I}$ is the noise-free receptor current as in eq. A1.1, and $\zeta(t)$ a random variable from a zero-mean, unit-variance Gaussian distribution, and σ_R the standard deviation of the noise in the receptor.

In the output neuron models, the noise term is added to the firing rate response of any respective neuron model

$$r_{AN}(t) = \bar{r}_{AN}(t) + \sigma_{AN} \zeta(t) \tag{A1.17}$$

r_{AN} is the firing rate of one of the output neuron models and σ_{AN} the standard deviation of the noise in the output neuron. In all simulations in chapter 3, $\sigma_R = 0.05$ and $\sigma_{AN} = 10\,\text{Hz}$, otherwise, the noise was zero.

A2 Model parameters used in chapters 2 and 3

In chapters 2 and 3 the model parameters varied were the adaptation strengths of receptors α_R and the output neuron α_{AN}, the synaptic weight between receptors and output neuron w, and the width of the weight function of the invariance model σ_w. The receptor population had a size of $N = 30$, with operating points uniformly distributed between 12 and 112 dB. In chapter 3 additionally a Gaussian distribution of the operating points was used (mean $\mu_{s^o} = 62$, standard deviation $\sigma_{s^o} = 17$). Tables A2.1 and A2.2 list the parameter values used to generate the figures in chapters 2 2.

Table A2.1: Parameter values used to generate the figures in chapter 2. α_R: adaptation strength of receptors, α_{AN}: adaptation strength of the output neuron, w: synaptic weight, σ_w: width of the weight function.

Figure	Model	α_R [kHz^{-1}]	α_{AN}	w [kHz^{-1}]	σ_w
2.2 A	receptor-model	3.75			
2.2 B	receptor-model	23.75			
2.2 C	receptor-model	9.0			
2.3 A	sum-model	3.75	0		
2.3 B	sum-model	0	1.01		
2.3 C	sum-model	3.75	1		
2.4 A	NL-A-model	3.75	0.62	12.5	
2.4 B	NL-A-model	23.75	0.59	62.0	
2.4 C	NL-A-model	3.75	1.00	62.0	
2.5 A	A-NL-model	3.75	0.50	12.5	
2.5 B	A-NL-model	23.75	0.50	62.0	
2.5 C	A-NL-model	0	0.96	62.0	
2.6 A2	sum-model	9	0		
2.6 B1	NL-A-model	9	0	62.0	
2.6 B2	NL-A-model	9	1.00	62.0	
2.6 C1	sum-model	9	0.80		
2.6 C2	A-NL-model	9	0.80	62.0	
2.7 A	invariance-model	0	0		500
2.7 B	invariance-model	0	0		30
2.7 C	invariance-model	0	0		1

Fixed parameters were the maximum firing rate r^{max} (350 Hz), the adaptation time constants τ_R, τ_{AN}, τ_i (40 ms) of receptors and output neurons, and the sigmoid non-linearity in the NL-A-model and A-NL-model.

Table A2.2: Parameter values used in chapter 3. α_R: adaptation strength of receptors, α_{AN}: adaptation strength of the output neuron, w: synaptic weight, σ_w: width of the weight function.

Figure	Model	α_R [kHz^{-1}]	α_{AN}	w [kHz^{-1}]	σ_w
3.2 A, 3.4, 3.6 & 3.7 A	receptor-model	9			
3.2 B, 3.4, 3.6 & 3.7B	sum-model	9	0		
3.2 C, 3.4, 3.6 & 3.7C	sum-model	0	0.76		
3.3 A, 3.4, 3.6 & 3.7D	NL-A-model	9	1.00	62.0	
3.3 B, 3.4, 3.6 & 3.7E	A-NL-model	9	0.80	62.0	
3.3 C, 3.4, 3.6 & 3.7F	A-NL-model	0	0.96	62.0	
3.3 D, 3.4, 3.6 & 3.7G	invariance-model	0	0		5

A3 Model parameters fitted in chapter 4

In chapter 4 the NL-A-model and the A-NL-model were fitted to the response curves of the AN1 of *T. oceanicus* and the AN1 and AN2 of *G. bimaculatus*. Free parameters of the fits were the adaptation strengths of receptors and the output neuron α_R and α_{AN}, the synaptic weight between receptors and output neuron w, the maximum firing rate of the output neuron r^{max} and the parameters of the distribution of receptor operating points (mean μ and standard deviation σ of a Gaussian, or individual receptor operating points). Tables A3.1, A3.2, and A3.3 list the model parameters fitted under the standard paradigm (models were fitted to all response curves) and the root mean squared error (RMSE) of the fits averaged across all data sets of a respective AN and species. For fits with individual receptor operating points, the mean and standard deviation of the resulting distribution are given.

Table A3.1: Table of model parameters fitted to the response curves of the AN1 for *T. oceanicus* by the NL-A-model and the A-NL-model under the standard paradigm.

	NL-A-model				A-NL-model			
	Gaussian		individual		Gaussian		individual	
α_R [kHz^{-1}]	9.37	± 2.75	7.02	± 1.67	3.65	± 1.79	3.87	± 0.51
α_{AN}	439.08	± 362.26	698.82	± 206.92	648.59	± 146.08	664.44	± 45.2
w [kHz^{-1}]	23.95	± 7.98	24.95	± 4.48	20.53	± 4.26	23.46	± 3.58
r_{max} [Hz]	210.4	± 14	214	± 12.5	207.8	± 14.4	206.9	± 13.8
μ [dB]	62.5	± 5.6	63.7	± 1.2	60.1	± 4.5	65.4	± 0.4
σ [dB]	11.8	± 2.7	16.6	± 3.6	10.8	± 1.6	21.4	± 4.4
RMSE [Hz]	38.7	± 5.8	35.2	± 4.1	38.2	± 5.6	34.1	± 3.6

Table A3.2: Table of model parameters fitted to the response curves of the AN1 for *G. bimculatus* by the NL-A-model and the A-NL-model under the standard paradigm.

	NL-A-model				A-NL-model			
	Gaussian		individual		Gaussian		individual	
α_R [kHz^{-1}]	11.41	± 3.9	6.72	± 1.33	3.66	± 1.93	3.81	± 0.33
α_{AN}	391.19	± 559.53	652.89	± 351.17	705.24	± 96.26	677.53	± 44.75
w [kHz^{-1}]	24.25	± 11.84	18.84	± 2.14	22.84	± 6.46	19.92	± 3.87
r_{max} [Hz]	278.6	± 57.7	304.5	± 55	273.3	± 59.3	274.9	± 58.7
μ [dB]	74.8	± 4.1	76.8	± 2.9	73	± 4.3	68.8	± 1.5
σ [dB]	17.1	± 2.7	20.7	± 3	16.4	± 2.8	17.7	± 3.5
RMSE [Hz]	46.1	± 7.3	45.6	± 8.6	45.5	± 8	40.6	± 8.2

Table A3.3: Table of model parameters fitted to the response curves of the AN2 for *G. bimculatus* by the NL-A-model and the A-NL-model under the standard paradigm.

	NL-A-model		A-NL-model	
α_R [kHz^{-1}]	5.63	± 0.85	3.56	± 0.42
α_{AN}	1188.8	± 608.29	812.92	± 83.62
w [kHz^{-1}]	14.38	± 2.78	18.75	± 3.33
r_{max} [Hz]	421.6	± 100.6	367.1	± 77.9
μ [dB]	84.1	± 4.4	84.5	± 5.5
σ [dB]	15.2	± 4.2	15	± 2.2
RMSE [Hz]	60.9	± 10.8	59.9	± 10.8

Appendix B

B1 Estimation of the Fisher information

In chapter 3 the Fisher information was estimated from intensity response curves $r(s)$. Defining the response $r(s)$ to stimulus intensity s as

$$r(s) = f(s) + z \cdot \sqrt{g(s)} \tag{B1.1}$$

where $f(s)$ and $g(s)$ are deterministic functions of the stimulus intensity, and z is a random number from an arbitrary distribution Q, then in the limit of small σ the Fisher information can be written as (Brunel and Nadal, 1998)

$$J(s) = \frac{\left(\frac{df}{ds}\right)^2}{g(s)} \int \frac{\left(\frac{dQ}{dz}\right)^2}{Q} dz \tag{B1.2}$$

. If $f(s) = \mu_r(s)$ and $g(s) = \sigma_r(s)$ are the mean and standard deviation of the response across repetitions of the stimulus, and $Q(z) = \mathcal{N}(0,1)$ the normal distribution, the integral is equal to 1 (Brunel and Nadal, 1998), and consequently

$$J(s) = \frac{\left(\frac{d\mu_r(s)}{ds}\right)^2}{\sigma_r^2(s)} \tag{B1.3}$$

The Fisher information was approximated by this equation, although the response variability was not strictly Gaussian.

The mean and standard deviation of the response curve were estimated from 1000 repetitions of the stimulus, and slightly smoothed with a rectangular window over 2 successive data points. The derivative of the mean response with respect to the stimulus intensity was approximated numerically by the central difference

$$\frac{dr(s)}{ds} \approx \frac{r(s_{i+1}) - r(s_{i-1})}{s_{i+1} - s_{i-1}} \tag{B1.4}$$

$i = 1, ..., N$ referring to subsequent data points.

B2 Estimation of the mutual information

In chapter 3 the mutual information between stimulus and response $I_M(s,r)$ was used to compare how the different neuron models encode time varying stimuli of differing mean and standard deviation. To compare the mutual information between the responses of one model

to stimuli with different standard deviations, the mutual information was normalized by the stimulus entropy H_s.

The mutual information between stimulus and response is defined as (Shannon et al., 1949):

$$I_M(r,s) = \int_{-\infty}^{\infty}\int_{-\infty}^{\infty} f_{s,r}(s,r)\log\frac{f_{s,r}(s,r)}{f_s(s)f_r(r)}dsdr \tag{B2.1}$$

$f_{r,s}$ being the joint probability density function (joint pdf) of stimulus and response, or

$$I_M(r,s) = H_r + H_s - H_{rs} \tag{B2.2}$$

where H_s and H_r are the entropies of the stimulus and response, respectively, and H_{sr} is the joint entropy with

$$H_s = -\int_{-\infty}^{\infty} f_s(s)\log(f_s(s))ds \tag{B2.3}$$

$f_s(s)$ being the pdf of the stimulus (H_r equivalently), and

$$H_{s,r} = -\int_{-\infty}^{\infty}\int_{-\infty}^{\infty} f_{s,r}(s,r)\log(f_{s,r}(s,r))dsdr \tag{B2.4}$$

In this thesis, the estimators of the entropies and mutual information derived by Moddemeijer (1989) which are based on histograms representing the respective pdfs. The stimulus response plane is separated into into equally sized cells ($\Delta s \times \Delta r$). The number of samples observed in the $(i,j)^{th}$ cell is k_{ij}, the total number of samples N, and column sums are denoted as $k_{i\cdot} = \sum_{j=1}^{J} k_{ij}$ and $k_{\cdot j} = \sum_{i=1}^{I} k_{ij}$. The entropy and information is estimated as

$$\hat{H}_s = -\sum_i \left(\frac{k_{i\cdot}}{N}\log\frac{k_{i\cdot}}{N}\right) + \log\Delta s \tag{B2.5}$$

$$\hat{H}_{sr} = -\sum_{i,j} \left(\frac{k_{ij}}{N}\log\frac{k_{ij}}{N}\right) + \log(\Delta s\Delta r) \tag{B2.6}$$

$$\hat{I}_{sr} = \sum_{i,j} \left(\frac{k_{ij}}{N}\log\frac{k_{ij}N}{k_{i\cdot}k_{\cdot j}}\right) \tag{B2.7}$$

The estimates of the mutual information and entropy ignore temporal correlations in the data that result from band pass filtering of the Gaussian noise signal and from the adaptation dynamics. However, the same band pass filtered noise stimulus was scaled and shifted to generate stimuli with different means and standard deviations. The temporal correlation in the stimuli is therefore identical for all stimuli and can thus be ignored when comparing the mutual information for different means and standard deviations.

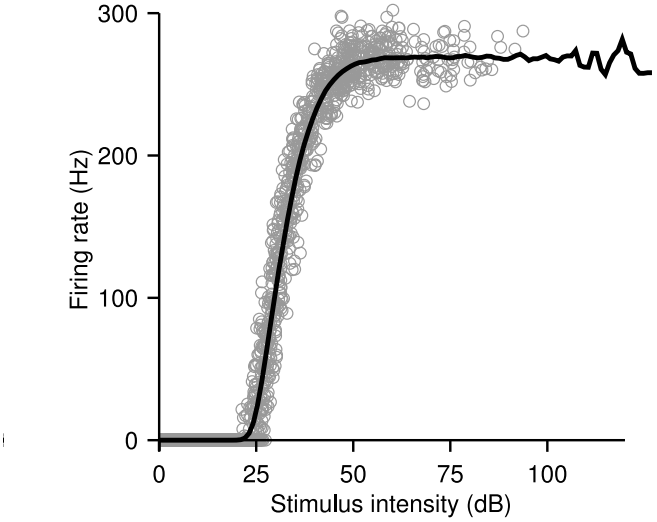

Figure B3.1: Example of the non-parametric regression (solid line) fitted to a noise response curve (*grey circles*).

B3 Non-parametric fit of noise response curves

In chapter 3 the neuron models' responses to noise stimuli of 20 s duration were computed and the noise response curves were constructed from the last 19 s, i.e. after the decay of the transient. To compare the noise response curves resulting from stimuli with different standard deviations they were fitted using non-parametric Nadaraya-Watson kernel regression (Nadaraya, 1964; Watson, 1964). Good fits to the steeply rising part of the response curves were obtained by calculating the number of bins as $N_B = N/1000$ ($N = 199000$ being the number of data points), and the bandwidth as $b = \frac{max_r - min_r}{1.8 N_B}$, and using 100 resampling cycles (an example of the fit is shown in fig. B3.1). Increasing the number of resampling cycles to 500 did not change the results.

Deutsche Zusammenfassung

C1 Einleitung

Die Kodierung der Reizintensitt in der Antwort von Nervenzellen ist eine der fundamentalen Aufgaben sensorischer Systeme. Die Intensitt ist hufig in der Antwortstrke eines Neurons kodiert, der Amplitude des Membranpotentials oder der Feuerrate, die Abhngigkeit der neuronalen Antwort von der Reizintensitt kann in Intensitts-Kennlinien (die Antwort des Neurons als Funktion der Reizintensitt) dargestellt werden. Der Intensittsbereich, der von sensorischen Systemen bei gleichbleibend hoher Intensittsauflsung verarbeitet werden kann, umfasst oftmals mehrere Grenordnungen. Gleichzeitig ist der Bereich begrenzt, ber den die neuronale Antwort variieren kann. Auerhalb diese 'dynamischen Bereichs' ist die Antwort unterschwellig bzw. gesttigt und kodiert keine nderungen der Intensitt.

Eine hohe Auflsung von Reizintensitten ist gegeben, wenn sich die Antworten des Neurons auf zwei hnliche Intensitten deutlich unterscheidet, d.h. wenn seine Kennlinie verhltnismig steil ist. Will ein Neuron dagegen einen groen Intensittsbereich erfassen, wird die Steigung der Kennlinie gering sein, dementsprechend werden nderungen der Reizintensitt nur verhltnismig kleine nderungen der neuronalen Antwort auslsen – die Intensittsauflsung ist gering. Verschiedene Phnomene scheinen der Entschrfung dieses Konflikts zu dienen, darunter die dynamische Anpassung von Kennlinien an langsam variierende Komponenten der Reizintensitt. In vielen Sinnessystemen wurden beispielsweise Verschiebungen der Kennlinien als Anpassung an eine vernderte Hintergrundintensitt oder einen vernderten Mittelwert beobachtet. Ein zugrunde liegender Mechanismus solcher Anpassungsleistungen ist Spikefrequenz-Adaptation, die Abnahme der Antwortstrke eines Neurons auf einen anhaltenden Reiz gleichbleibender Intensitt, die die meisten Neurone zeigen.

Im auditorischen System der Grille wird eine adaptive Kennlinienverschiebung bereits im aufsteigenden Interneuron AN1des Prothorakalganglions beobachtet. Das AN1erhlt direkten Eingang von einer Population ipsilateraler Rezeptoren, deren Antworteigenschaften sich in erster Linie durch ihre Antwortschwellen unterscheiden. Einzelne Rezeptoren der Population antworten nur ber einen kleinen Intensittsbereich dynamisch, whrend sie in ihrer Gesamtheit einen wesentlich greren Intensittsbereich abbilden. Es ist relativ wenig bekannt, wie solche Populationen von nachgeschalteten Neuronen integriert werden. In dieser Arbeit wurde die Entstehung adaptiver Kennlinienverschiebung in einem konvergenten neuronalen Netzwerk nach dem Vorbild des AN1 der Grille modelliert. Besonderes Interesse galt dabei dem Zusammenspiel von Nichtlinearitten mit Spikefrequenz-Adaptation und der Integration von Neuronpopulationen mit unterschiedlichen Antwortschwellen.

C2 Welche Mechanismen ermglichen die die Verschiebung von Kennlinien ber weite Intensittsbereiche?

Im ersten Teil der Arbeit wurden das Modell-Netzwerk und Feuerratenmodelle der Rezeptoren und des Interneurons definiert. Die Rezeptoren verfgen ber einen antwortgetriebenen Mechanismus von Spikefrequenz-Adaptation und verschieben ihre Kennlinien bei Vernderung der Hintergrundintensitt ber einen engen Bereich, knnen sich greren Vernderungen der Hintergrundintensitt jedoch nicht anpassen. Darin hneln sie auditorischen Rezeptoren von Heuschrecken und vermutlich Grillen, aber auch auditorischen Nervenfasern in Sugern. Verschiedene Mglichkeiten der Integration dieser Rezeptorpopulation wurden modelliert.

Modelle, die eine statische Nichtlinearitt im Modell-Interneuron in Kombination mit Spikefrequenz-Adaptation in den Rezeptoren und dem Interneuron enthielten, waren in der Lage die Verschiebung von Kennlinien ber grere Intensittsbereiche zu generieren. Zustzlich reproduzieren sie eine Reihe von Effekten, die in experimentell gemessenen Kennlinien beobachtet wurden, wie z.B. die Reduktion der Maximalantwort mit zunehmender Verschiebung sowie eine Verringerung der Steigung bei groen Verschiebungen. Diese Gruppe von Modellen ist dabei nicht auf eine Rezeptorpopulation mit unterschiedlichen Antwortschwellen angewiesen. Insbesondere wird die Steigung der Kennlinie des Interneurons nicht von der Steigung der Rezeptorkennlinien limitiert.

Im Gegensatz dazu konnte ein Modell, was selektiv diejenigen Rezeptoren verstrkt gewichtete, deren dynamischer Bereich im Bereich der aktuellen Hintergrundintensitt lag, zwar perfekte parallele Verschiebungen der Kennlinien ber weite Intensittsbereiche produzieren. Es bentigt jedoch Rezeptoren mit unterschiedlichen Antwortschwellen, die Steigung seiner Kennlinien ist von der Steigung der Rezeptorkennlinien limitiert und es reproduziert weder Unterschiede in der Breite des dynamischen Bereichs zwischen Onset und Steady State, noch die Abnahme der Maximalantwort von adaptierten Kennlinien mit zunehmender Verschiebung.

C3 Wie beeinflusst Adaptation die Informationsbertragung

Im zweiten Teil dieser Studie wurden die Modelle aus Teil 1 in Hinblick auf ihre Fhigkeit zur Intensittsunterscheidung in Abhngigkeit der Hintergrundintensitt und ihre Eigenschaften in der Kodierung zeitlich variabler Reize untersucht. Zur Quantifizierung der Intensittsunterscheidung wurden die Fisher-Informations-Funktionen aus den Kennlinien geschtzt. Hier zeigte sich, dass die Kennlinienverschiebung eine maximale Intensittsunterscheidung in der Nhe der aktuellen Hintergrundintensitt ermglicht, whrend Intensitten weiter abseits der Hintergrundintensitt kaum unterschieden werden knnen.

In den Antworten auf zeitlich variierende Reize zeigten sich Abweichungen von der Kodierung konstanter Reize. Einerseits zeigten alle Modelle mit Mechanismen zur Spikefrequenz-Adaptation eine Abhngigkeit der Verschiebung nicht nur vom Mittelwert der Intensitt sondern auch von deren Standardabweichung. Andererseits zeigten die Modelle, in denen die Rezeptoren adaptieren, eine Reduktion der Steigung der Kennlinien mit zunehmender Standardabweichung der Intensitt. Zur Quantifizierung der Kodierungseigenschaften fr zeitlich

variable Stimuli wurde die 'Mutual Information' zwischen Rausch-Stimuli und deren neuronalen Antworten geschtzt. Die Modelle, die eine Verschiebung der Kennlinien ber weite Intensittsbereiche generieren konnten, zeigten eine Prferenz fr bestimmte Standardabweichungen, whrend sie einen weiten Bereich von Mittelwerten gut kodierten.

Spikefrequenz-Adaptation trgt daher dazu bei, die Intensittsunterscheidung ber weite Intensittsbereiche hoch zu erhalten und Intensittsvernderungen bei unterschiedlichen Mittelwerten zu kodieren. Andererseits zeigte sich, dass antwortgetriebene Spikefrequenz-Adaptation zur Variabilitt neuronaler Antworten beitrgt, was die Die Intensittsdiskriminierung negativ beeinflussen kann.

C4 Fitten der Modelle an Daten zweier Grillen-Spezies

Die Kombination von Spikefrequenz-Adaptation und sttigender Nichtlinearitt im Interneuron funktionierte in zwei Varianten: Die Sttigung kann vor oder nach dem Adaptationsschritt im Intenneuron stattfinden. Beide Varianten generieren Kennlinien, die sich ber einen weiten Intensittsbereich verschieben. Sie unterscheiden sich allerdings in der Art, wie die Maximalfeuerrate mit zunehmender Verschiebung abnimmt. Bei Sttigung vor Adaptation (NL-A-Modell) zeigen die Kennlinien eine zunehmende Reduktion der Maximalfeuerrate fr alle Verschiebungen. Folgt die Sttigung der Adaptation im Interneuron (A-NL-Modell), nimmt die Maximalfeuerrate erst bei Hintergrundintensitten ab, die ausserhalb des Bereiches liegen, der von den Rezeptoren reprsentiert wird. hnliche qualitative Unterschiede wurden in den Kennlinien des AN1 zweier Grillenspezies beobachtet. Whrend die Maximalfeuerrate bei *Teleogryllus oceanicus* schnell abnimmt, bleibt sie bei *Gryllus bimaculatus* ber weite Bereiche konstant.

Beide Modelle wurden an Sets von Kennlinien beider Grillenspezies gefittet, um herauszufinden, ob tatschlich qualitativ unterschiedliche Modelle zur Erklrung ntig sind, oder ob ein einziges Modell bei entsprechenden Parametervernderungen die Daten beider Spezies reproduzieren kann. Weiterhin standen Kennlinien vom AN2 von *G. bimaculatus* zur Verfgung, die ebenfalls gefittet wurden, um die Vielseitigkeit der Modelle zu testen. Basierend auf dem RMSE unterschieden sich die beiden Modelle nicht in ihrer Fhigkeit die unterschiedlichen Datenstze zu reproduzieren. Allerdings ergaben die Fits der AN1-Kennlinien mit dem A-NL-Modell Werte fr die Strke der Rezeptoradaptation, die im Bereich experimentell beobachteter Werte lagen, whrend das NL-A-Modell unrealistisch starke Adaptation in den Rezeptoren bentigte. Die Fits zeigten vor allem die Bedeutung der Verteilung der Rezeptor-Antwortschwellen. Insbesondere wenn die Rezeptorpopulation klein ist, wie im Fall des AN2 angenommen, knnen einzelne Rezeptoren mit stark von den anderen abweichenden Antwortschwellen groen Einfluss auf die Form der Kennlinien ausben.

C5 Schlussfolgerungen und Ausblick

Die Ergebnisse dieser Arbeit zeigen, dass das Zusammenwirken von statischen Nichtlinearitten mit Spikefrequenz-Adaptation einer adaptiven Verschiebung von Kennlinien zugrunde

liegen knnte, wie sie in verschiedenen Sinnessystemen beschrieben wurde. Neben der Verschiebung der Kennlinien werden durch die Interaktion von Sttigung mit den Adaptationsmechanismen in den Neuronen des Netzwerks auch scheinbar komplexe Effekte reproduziert, wie eine Reduktion der Maximalfeuerrate mit zunehmender Verschiebung. Weiterhin sind diese Modelle weder auf eine Rezeptorpopulation mit heterogenen Antwortschwellen angewiesen, noch auf steile Rezeptorkennlinien. Offene Fragen betreffen vor allem die biophysikalische Realisierung der sttigenden Nichtlinearitt. Im AN1 der Grille ist die stark verstelte Morphologie des Interneurons eine mgliche Ursache fr diese Sttigung. Eine weitere Frage ist, wie die Art der Organisation der Rezeptorpopulation – homogen oder heterogen – die Intensittsdiskriminierung und die Kodierung zeitlich variabler Stimuli beeinflusst.

Bibliography

D. Albrecht, S. Farrar, and D. Hamilton. Spatial contrast adaptation characteristics of neurones recorded in the cat's visual cortex. *J Physiol*, 347(1):713–739, 1984.

M. Avissar, A. C. Furman, J. C. Saunders, and T. D. Parsons. Adaptation reduces spike-count reliability, but not spike-timing precision, of auditory nerve responses. *J Neurosci*, 27(24):6461–6472, 2007.

H. Barlow. Redundancy reduction revisited. *Network: Comp Neural Sys*, 12:241–253(13), 2001.

H. B. Barlow. Possible principles underlying the transformations of sensory messages. In W. Rosenblith, editor, *Sensory Communication*, pages 217–234. MIT Press, 1961.

H. B. Barlow and P. Földiák. Adaptation and decorelation in cortex. In R. Durbin, C. Miall, and G. Mitchison, editors, *The Computing Neuron*, pages 54–72. Addison-Wesley, 1989.

J. Benda. *Single neuron dynamics – models linking theory and experiment.* Phd thesis, Humboldt-Universtität zu Berlin, 2002.

J. Benda and R. Hennig. Spike-frequency adaptation generates intensity invariance in a primary auditory interneuron. *J Comput Neurosci*, 24:113–136, 2008.

J. Benda and A. V. M. Herz. A Universal Model for Spike-Frequency Adaptation. *Neural Comput*, 15(11):2523–2564, 2003.

J. Benda, M. Bethge, M. Hennig, K. Pawelzik, and A. V. M. Herz. Spike-frequency adaptation: Phenomenological model and experimental tests. *Neurocomputing*, 38-40:105–110, 2001.

J. Benda, A. Longtin, and L. Maler. Spike-Frequency Adaptation Separates Transient Communication Signals from Background Oscillations. *J Neurosci*, 25(9):2312–2321, 2005.

O. Bernander, C. Koch, and R. J. Douglas. Amplification and linearization of distal synaptic input to cortical pyramidal cells. *J Neurophysiol*, 72(6):2743–2753, 1994.

S. Beul. *Adaptation in the auditory interneurons AN1 and AN2 in Gryllus bimaculatus.* Bachelor thesis, Humboldt-Universtität zu Berlin, 2010.

A. Boccaccio, L. Lagostena, V. Hagen, and A. Menini. Fast adaptation in mouse olfactory sensory neurons does not require the activity of phosphodiesterase. *J Gen Physiol*, 128 (2):171–184, 2006.

A. Borst, M. Egelhaaf, and J. Haag. Mechanisms of dendritic integration underlying gain control in fly motion-sensitive interneurons. *J Comput Neurosci*, 2(1):5–18, 1995.

A. Borst, V. L. Flanagin, and H. Sompolinsky. Adaptation without parameter change: Dynamic gain control in motion detection. *Proc Nat Acad Sci*, 102(17):6172–6176, 2005.

N. Brenner, W. Bialek, and R. d. R. van Steveninck. Adaptive rescaling maximizes information transmission. *Neuron*, 26:695–702, 2000.

R. Brette and W. Gerstner. Adaptive exponential integrate-and-fire model as an effective description of neuronal activity. *J Neurophysiol*, 94(5):3637–3642, 2005.

D. A. Brown and P. R. Adams. Muscarinic suppression of a novel voltage-sensitive k+ current in a vertebrate neurone. *Nature*, 283(5748):673–676, 1980.

N. Brunel and J.-P. Nadal. Mutual information, fisher information, and population coding. *Neural Comput*, 10(7):1731–1757, 1998.

D. A. Burkhardt. Light adaptation and photopigment bleaching in cone photoreceptors in situ in the retina of the turtle. *J Neurosci*, 14(3):1091–1105, 1994.

M. E. Burns and D. A. Baylor. Activation, deactivation, and adaptation in vertebrate photoreceptor cells. *Ann Rev Neurosci*, 24(1):779–805, 2001.

P. C. Bush and T. J. Sejnowski. Effects of inhibition and dendritic saturation in simulated neocortical pyramidal cells. *J Neurophysiol*, 71(6):2183–2193, 1994.

M. Carandini and D. Ferster. A tonic hyperpolarization underlying contrast adaptation in cat visual cortex. *Science*, 276(5314):949–952, 1997.

F. S. Chance, S. B. Nelson, and L. F. Abbott. Synaptic Depression and the Temporal Response Characteristics of V1 Cells. *J Neurosci*, 18(12):4785–4799, 1998.

S. Chung, X. Li, and S. B. Nelson. Short-term depression at thalamocortical synapses contributes to rapid adaptation of cortical sensory responses in vivo. *Neuron*, 34(3): 437–446, 2002.

H. Clague, F. Theunissen, and J. P. Miller. Effects of adaptation on neural coding by primary sensory interneurons in the cricket cercal system. *J Neurophysiol*, 77(1):207–220, 1997.

B. Connors, M. Gutnick, and D. Prince. Electrophysiological properties of neocortical neurons in vitro. *J Neurophysiol*, 48(6):1302–1320, 1982.

A. Constanti and J. Sim. Calcium-dependent potassium conductance in guinea-pig olfactory cortex neurones in vitro. *J Physiol*, 387(1):173–194, 1987.

A. Crawford, M. Evans, and R. Fettiplace. Activation and adaptation of transducer currents in turtle hair cells. *J Physiol*, 419(1):405–434, 1989.

I. Dean, N. S. Harper, and D. McAlpine. Neural population coding of sound level adapts to stimulus statistics. *Nature Neurosci*, 8:1684 – 1689, 2005.

A. Dovzhenok and A. S. Kuznetsov. Exploring neuronal bistability at the depolarization block. *PloS one*, 7(8):e42811, 2012.

R. A. Eatock. Adaptation in hair cells. *Ann Rev Neurosci*, 23:285–314, 2000.

R. Eckert. *Tierphysiologie*. Georg Thieme Verlag, 2002.

M. Egelhaaf, J. Haag, and A. Borst. Processing of synaptic information depends on the structure of the dendritic tree. *NeuroReport*, 6(1):205–208, 1994.

G. Ehret, A. J. M. Moffat, and J. Tautz. Behavioral determination of frequency resolution in the ear of the cricket *Teleogryllus oceanicus*. *J Comp Phys A*, 148(2):237–244, 1982.

C. Enroth-Cugell and R. M. Shapley. Adaptation and dynamics of cat retinal ganglion cells. *J Physiol*, 233(2):271–309, 1973.

H. Esch, F. Huber, and D. W. Wohlers. Primary auditory neurons in crickets: Physiology and central projections. *J Comp Phys A*, 137(1):27–38, 1980.

A. L. Fairhall, G. D. Lewen, W. Bialek, and R. R. de Ruyter van Steveninck. Efficiency and ambiguity in an adaptive neural code. *Nature*, 412(6849):787–792, 2001.

H. E. Farris, A. C. Mason, and R. R. Hoy. Identified auditory neurons in the cricket *Gryllus rubens*: temporal processing in calling song sensitive units. *Hear Res*, 193(1):121–133, 2004.

P. Finlayson and M. Cynader. Synaptic depression in visual cortex tissue slices: an in vitro model for cortical neuron adaptation. *Exp Brain Res*, 106(1):145–155, 1995.

P. G. Finlayson and T. J. Adam. Excitatory and inhibitory response adaptation in the superior olive complex affects binaural acoustic processing. *Hear Res*, 103:1–18, 1997.

K. Fisch, T. Schwalger, B. Lindner, A. V. Herz, and J. Benda. Channel noise from both slow adaptation currents and fast currents is required to explain spike-response variability in a sensory neuron. *J Neurosci*, 32(48):17332–17344, 2012.

I. A. Fleidervish, A. Friedman, and M. J. Gutnick. Slow inactivation of na+ current and slow cumulative spike adaptation in mouse and guinea-pig neocortical neurones in slices. *J Physiol*, 493(Pt 1):83–97, 1996.

A. French. Action potential adaptation in the femoral tactile spine of the cockroach, periplaneta americana. *J Comp Phys A*, 155(6):803–812, 1984.

A. S. French. Two components of rapid sensory adaptation in a cockroach mechanoreceptor neuron. *J Neurophysiol*, 62(3):768–777, 1989.

A. S. French, U. Höger, S.-i. Sekizawa, and P. H. Torkkeli. Frequency response functions and information capacities of paired spider mechanoreceptor neurons. *Biol Cybern*, 85 (4):293–300, 2001.

D. J. Gibson, E. D. Young, and J. A. Costalupes. Similarity of dynamic range adjustment in auditory nerve and cochlear nuclei. *J Neurophysiol*, 53(4):940–958, 1985.

P. G. Gillespie and D. P. Corey. Myosin and adaptation by hair cells. *Neuron*, 19:955–8, 1997.

P. G. Gillespie and R. G. Walker. Molecular basis of mechanosensory transduction. *Nature*, 413:194–202, 2001.

T. Gollisch and A. V. M. Herz. Input-driven components of spike-frequency adaptation can be unmasked in vivo. *J Neurosci*, 24(34):7435–7444, 2004.

A. A. Grace, B. S. Bunney, H. Moore, and C. L. Todd. Dopamine-cell depolarization block as a model for the therapeutic actions of antipsychotic drugs. *Trends in Neurosci*, 20(1): 31–37, 1997.

R. Granit, D. Kernell, and G. Shortess. Quantitative aspects of repetitive firing of mammalian motoneurones, caused by injected currents. *J Physiol*, 168(4):911–931, 1963.

E. G. Gray. The fine structure of the insect ear. *Philosophical Transactions of the Royal Society of London. Series B, Biological Sciences*, pages 75–94, 1960.

B. Gustafsson and H. Wigström. Shape of frequency-current curves in cai pyramidal cells in the hippocampus. *Brain Res*, 223(2):417–421, 1981.

J. Haag, M. Egelhaaf, and A. Borst. Dendritic integration of motion information in visual interneurons of the blowfly. *Neurosci Let*, 140(2):173–176, 1992.

E. Hendrickson, J. Edgerton, and D. Jaeger. The capabilities and limitations of conductance-based compartmental neuron models with reduced branched or unbranched morphologies and active dendrites. *J Comput Neurosci*, 30(2):301–321, 2011.

R. Hennig, A. Franz, and A. Stumpner. Processing of auditory information in insects. *Microsc Res Tech*, 63(6):351–374, 2004.

R. M. Hennig. Ascending auditory interneurons in the cricket *Teleogryllus commodus* (walker): comparative physiology and direct connections with afferents. *J Comp Phys A*, 163(1):135–143, 1988.

K. J. Hildebrandt. *Neural adaptation in the auditory pathway of crickets and grasshoppers*. Phd thesis, Humboldt-Universtität zu Berlin, 2010.

K. J. Hildebrandt, J. Benda, and R. M. Hennig. Multiple arithmetic operations in a single neuron: The recruitment of adaptation processes in the cricket auditory pathway depends on sensory context. *J Neurosci*, 31(40):14142–14150, 2011.

K. G. Hill. Carrier frequency as a factor in phonotactic behaviour of female crickets (*Teleogryllus commodus*). *J Comp Phys A*, 93(1):7–18, 1974.

J. R. Holt and D. P. Corey. Two mechanisms for transducer adaptation in vertebrate hair cells. *Proc Nat Acad Sci*, 97(22):11730–11735, 2000.

G. Horseman and F. Huber. Sound localisation in crickets i. contralateral inhibition of an ascending auditory interneuron (an1) in the cricket *Gryllus bimaculatus*. *J Comp Physiol A*, 175:389–398, 1994.

F. Huber, T. Moore, and W. Loher. *Cricket behavior and neurobiology*. Cornell University Press, 1989.

A. Hudspeth and P. G. Gillespie. Pulling springs to tune transduction: adaptation by hair cells. *Neuron*, 12(1):1–9, 1994.

K. Imaizumi and G. S. Pollack. Neural coding of sound frequency by cricket auditory receptors. *J Neurosci*, 19(4):1508–1516, 1999.

K. Imaizumi and G. S. Pollack. Neural representation of sound amplitude by functionally different auditory receptors in crickets. *J Acoust Soc Am*, 109(3):1247–1260, 2001.

N. J. Ingham and D. McAlpine. Spike-frequency adaptation in the inferior colliculus. *J Neurophysiol*, 91(2):632–645, 2004.

N. J. Ingham and D. McAlpine. Gabaergic inhibition controls neural gain in inferior colliculus neurons sensitive to interaural time differences. *J Neurosci*, 25(26):6187–6198, 2005.

E. Javel. Long-term adaptation in cat auditory-nerve fiber responses. *J Acoust Soc Am*, 99: 1040, 1996.

M. Juusola and A. S. French. Adaptation Properties of Two Types of Sensory Neurons in a Spider Mechanoreceptor Organ. *J Neurophysiol*, 80(5):2781–2784, 1998.

E. R. Kandel, J. H. Schwartz, T. M. Jessell, et al. *Principles of neural science*, volume 4. McGraw-Hill New York, 2000.

J. Kang, J. R. Huguenard, and D. A. Prince. Voltage-gated potassium channels activated during action potentials in layer v neocortical pyramidal neurons. *J Neurophysiol*, 83(1): 70–80, 2000.

C. Koch and I. Segev. The role of single neurons in information processing. *Nature Neurosci*, 3:1171–1177, 2000.

L. E. Krueger. Reconciling fechner and stevens: Toward a unified psychophysical law. *Behav Brain Sci*, 12(02):251–267, 5 1989.

B. Lancaster and P. Adams. Calcium-dependent current generating the afterhyperpolarization of hippocampal neurons. *J Neurophysiol*, 55(6):1268–1282, 1986.

T. Lanthorn, J. Storm, and P. Andersen. Current-to-frequency transduction in ca1 hippocampal pyramidal cells: Slow prepotentials dominate the primary range firing. *Exp Brain Res*, 53(2):431–443, 1984.

S. Laughlin. A simple coding procedure enhances a neuron's information capacity. *Z Naturforsch C*, 36(9-10):910–912, 1981.

S. Laughlin. The role of sensory adaptation in the retina. *J Exp Biol*, 146(1):39–62, 1989.

S. B. Laughlin and R. C. Hardie. Common strategies for light adaptation in the peripheral visual systems of fly and dragonfly. *J Comp Physiol A*, 128(4):319–340, 1978.

T. Maddess and S. Laughlin. Adaptation of the motion-sensitive neuron h1 is generated locally and governed by contrast frequency. *Proc Roy Soc London B*, 225(1239):251–275, 1985.

D. V. Madison and R. A. Nicoll. Control of the repetitive discharge of rat ca 1 pyramidal neurones in vitro. *J Physiol*, 354(1):319–331, 1984.

Z. F. Mainen, N. T. Carnevale, A. M. Zador, B. J. Claiborne, and T. H. Brown. Electrotonic architecture of hippocampal ca1 pyramidal neurons based on three-dimensional reconstructions. *J Neurophysiol*, 76(3):1904–1923, 1996.

A. Mason and A. Larkman. Correlations between morphology and electrophysiology of pyramidal neurons in slices of rat visual cortex. ii. electrophysiology. *J Neurosci*, 10(5): 1415–1428, 1990.

B. J. May and M. B. Sachs. Dynamic range of neural rate responses in the ventral cochlear nucleus of awake cats. *J Neurophysiol*, 68(5):1589–1602, 1992.

D. A. McCormick, B. W. Connors, J. W. Lighthall, and D. A. Prince. Comparative electrophysiology of pyramidal and sparsely spiny stellate neurons of the neocortex. *J Neurophysiol*, 54(4):782–806, 1985.

M. D. McDonnell and N. G. Stocks. Maximally informative stimuli and tuning curves for sigmoidal rate-coding neurons and populations. *Phys Rev Lett*, 101:058103, 2008.

R. Moddemeijer. On estimation of entropy and mutual information of continuous distributions. *Signal Processing*, 16(3):233–246, 1989.

A. Moiseff and M. Konishi. Binaural characteristics of units in the owl's brainstem auditory pathway: precursors of restricted spatial receptive fields. *J Neurosci*, 3:2553–2562, 1983.

A. Moiseff, G. S. Pollack, and R. R. Hoy. Steering responses of flying crickets to sound and ultrasound: Mate attraction and predator avoidance. *Proc Nat Acad Sci*, 75(8): 4052–4056, 1978.

J.-P. Nadal and N. Parga. Nonlinear neurons in the low-noise limit: a factorial code maximizes information transfer. *Network: Comp Neural Sys*, 5:565–581, 1994.

E. Nadaraya. On estimating regression. *Theory of Prob and Appl*, 9:141–142, 1964.

M. Nelson, Z. Xu, and J. Payne. Characterization and modeling of p-type electrosensory afferent responses to amplitude modulations in a wave-type electric fish. *J Comp Physiol A*, 181(5):532–544, 1997.

H. Nocke. Physiological aspects of sound communication in crickets (*Gryllus campestris* l.). *J Comp Physiol A*, 80(2):141–162, 1972.

T. Nolen and R. Hoy. Initiation of behavior by single neurons: the role of behavioral context. *Science*, 226(4677):992–994, 1984.

T. Nolen and R. Hoy. Postsynaptic inhibition mediates high-frequency selectivity in the cricket teleogryllus oceanicus: implications for flight phonotaxis behavior. *J Neurosci*, 7 (7):2081–2096, 1987.

T. G. Nolen and R. R. Hoy. Phonotaxis in flying crickets. *J Comp Phys A*, 159(4):423–439, 1986.

B. J. O'Brien, T. Isayama, R. Richardson, and D. M. Berson. Intrinsic physiological properties of cat retinal ganglion cells. *J Physiol*, 538(3):787–802, 2004.

I. Ohzawa, G. Sclar, R. Freeman, et al. Contrast gain control in the cat visual cortex. *Nature*, 298(5871):266–268, 1982.

I. Ohzawa, G. Sclar, and R. D. Freeman. Contrast gain control in the cat's visual system. *J Neurophysiol*, 54(3):651–667, 1985.

B. P. Oldfield. Accuracy of orientation in female crickets *Teleogryllus oceanicus* (gryllidae): dependence on song spectrum. *J Comp Physiol A: Neuroethology, Sensory, Neural, and Behavioral Physiology*, 141(1):93–99, 1980.

C. J. Plack. *The sense of hearing*. Lawrence Erlbaum Associates Publishers, 2005.

G. S. Pollack and E. El-Feghaly. Calling song recognition in the cricket *Teleogryllus oceanicus*: comparison of the effects of stimulus intensity and sound spectrum on selectivity for temporal pattern. *J Comp Physiol A*, 171(6):759–765, 1993.

G. S. Pollack and R. R. Hoy. Temporal pattern as a cue for species-specific calling song recognition in crickets. *Science*, 204(4391):429–432, 1979.

A. V. Popov and A. M. Markovich. Auditory interneurones in the prothoracic ganglion of the cricket, *Gryllus bimaculatus*. *J Comp Physiol A*, 146(3):351–359, 1982.

S. A. Prescott and Y. De Koninck. Gain control of firing rate by shunting inhibition: roles of synaptic noise and dendritic saturation. *Proc Nat Acad Sci*, 100(4):2076–2081, 2003.

S. A. Prescott and T. J. Sejnowski. Spike-rate coding and spike-time coding are affected oppositely by different adaptation mechanisms. *J Neurosci*, 28(50):13649–13661, 2008.

A. Rees and A. R. Palmer. Rate-intensity functions and their modification by broadband noise for neurons in the guinea pig inferior colliculus. *J Acoust Soc Am*, 83:1488, 1988.

H. Reichert. *Neurobiologie*. Georg Thieme Verlag, 2000.

J. Reisert and H. R. Matthews. Adaptation of the odour-induced response in frog olfactory receptor cells. *J Physiol*, 519(3):801–813, 1999.

J. Rheinländer, K. Kalmring, A. V. Popov, and H. Rehbein. Brain projections and information processing of biologically significant sounds by two large ventral-cord neurons of *Gryllus bimaculatus* degeer (orthoptera, gryllidae). *J Comp Physiol*, 110(3):251–269, 1976.

W. A. Rosenblith and G. A. Miller. The threshold of hearing for continuous and interrupted tones. *J Acoust Soc Am*, 21(4):467–467, 1949.

J. S. Rothman, L. Cathala, V. Steuber, and R. A. Silver. Synaptic depression enables neuronal gain control. *Nature*, 457(7232):1015–1018, 2009.

M. V. Sanchez-Vives, L. G. Nowak, and D. A. McCormick. Cellular mechanisms of long-lasting adaptation in visual cortical neurons in vitro. *J Neurosci*, 20(11):4286–4299, 2000.

A. Sawczuk, R. K. Powers, and M. D. Binder. Spike frequency adaptation studied in hypoglossal motoneurons of the rat. *J Neurophysiol*, 73(5):1799–1810, 1995.

K. Schildberger. Temporal selectivity of identified auditory neurons in the cricket brain. *J Comp Physiol A*, 155(2):171–185, 1984. 10.1007/BF00612635.

K. Schildberger and M. Hörner. The function of auditory neurons in cricket phonotaxis. *J Comp Phys A*, 163(5):621–631, 1988.

K. Schildberger, D. W. Wohlers, B. Schmitz, H. U. Kleindienst, and F. Huber. Morphological and physiological changes in central auditory neurons following unilateral foreleg amputation in larval crickets. *J Comp Phys A*, 158(3):291–300, 1986. 10.1007/BF00603613.

D. M. Schneeweis and J. L. Schnapf. The photovoltage of macaque cone photoreceptors: Adaptation, noise, and kinetics. *J Neurosci*, 19(4):1203–1216, 1999.

P. Schwindt, W. Spain, and W. Crill. Long-lasting reduction of excitability by a sodium-dependent potassium current in cat neocortical neurons. *J Neurophysiol*, 61(2):233–244, 1989.

A. I. Selverston, H.-U. Kleindienst, and F. Huber. Synaptic connectivity between cricket auditory interneurons as studied by selective photoinactivation. *J Neurosci*, 5(5):1283–1292, 1985.

C. E. Shannon, W. Weaver, and R. E. Blahut. *The mathematical theory of communication.* Urbana: University of Illinois press, 1949.

R. Shapley and C. Enroth-Cugell. Visual adaptation and retinal gain controls. *Prog Retin Res*, 3:263–346, 1984.

T. O. Sharpee, H. Sugihara, A. V. Kurgansky, S. P. Rebrik, M. P. Stryker, and K. D. Miller. Adaptive filtering enhances information transmission in visual cortex. *Nature*, 439(7079): 936–942, 2006.

E. P. Simoncelli. Vision and the statistics of the visual environment. *Curr Opin Neurobiol*, 13(2):144 – 149, 2003.

S. G. Solomon, J. W. Peirce, N. T. Dhruv, P. Lennie, et al. Profound contrast adaptation early in the visual pathway. *Neuron*, 42(1):155–162, 2004.

S. S. Stevens. *Psychophysics: Introduction to its perceptual, neural, and social prospects*. Transaction Publishers, 1975.

J. F. Storm. Potassium currents in hippocampal pyramidal cells. In J. Z. J. Storm-Mathisen and O. Ottersen, editors, *Understanding the Brain Through the Hippocampus the Hippocampal Region as a Model for Studying Brain Structure and Function*, volume 83 of *Prog Brain Res*, pages 161 – 187. Elsevier, 1990.

J. Thorson, T. Weber, and F. Huber. Auditory behavior of the cricket - ii. simplicity of calling-song recognition in gryllus, and anomalous phonotaxisat abnormal carrier frequencies. *J Comp Phys A*, 146(3):361–378, 1982.

E. Todorov, A. Siapas, D. Somers, and S. Nelson. Modeling visual cortical contrast adaptation effects. In *Proceedings of the annual conference on Computational neuroscience*, pages 525–531. Plenum Press, 1997.

P. H. Torkkeli, S.-I. Sekizawa, and A. S. French. Inactivation of voltage-activated na+ currents contributes to different adaptation properties of paired mechanosensory neurons. *J Neurophysiol*, 85(4):1595–1602, 2001.

N. Ulanovsky, L. Las, D. Farkas, and I. Nelken. Multiple time scales of adaptation in auditory cortex neurons. *J Neurosci*, 24(46):10440–10453, 2004.

N. F. Viemeister. Auditory intensity discrimination at high frequencies in the presence of noise. *Science*, 221(4616):1206–1208, 1983.

N. F. Viemeister and S. P. Bacon. Intensity discrimination, increment detection, and magnitude estimation for 1-khz tones. *Hear Res*, 84:172–178, 1988.

G. S. Watson. Smooth regression analysis. *Sankhyā: Ind J Stat A*, pages 359–372, 1964.

M. Weckström, R. Hardie, and S. Laughlin. Voltage-activated potassium channels in blowfly photoreceptors and their role in light adaptation. *J Physiol*, 440(1):635–657, 1991.

B. Wen, G. I. Wang, I. Dean, and B. Delgutte. Dynamic range adaptation to sound level statistics in the auditory nerve. *J Neurosci*, 29(44):13797–13808, 2009.

Westerman, Larry A and Smith, Robert L. Rapid and short-term adaptation in auditory nerve responses. *Hear Res*, 15(3):249–260, 1984.

D. W. Wohlers and F. Huber. Intracellular recording and staining of cricket auditory interneurons (gryllus campestris l.,gryllus bimaculatus degeer). *J Comp Phys A*, 127(1): 11–28, 1978.

D. W. Wohlers and F. Huber. Processing of sound signals by six types of neurons in the prothoracic ganglion of the cricket *Gryllus campestris* l. *J Comp Phys A*, 146(2):161–173, 1982.

Selbständigkeitserklärung

Ich erkläre, dass ich die vorliegende Arbeit selbständig und nur unter Verwendung der angegebenen Literatur und Hilfsmittel angefertigt habe.

_____

(18. Juli 2013, Ulrike Ziehm)